Fbxl13 regulates centrosome homeostasis and migration through ubiquitin mediated proteolysis

A thesis submitted for the degree of Doctor of Philosophy

By

ELLA SUI LING FUNG

January 2017

St Anne's College

Oxford Institute for Radiation Oncology
Department of Radiation Oncology and Biology
University of Oxford

Supervised by:

Dr Vincenzo D'Angiolella
Dr Timothy Humphrey

CANCER RESEARCH UK | MRC Medical Research Council
OXFORD INSTITUTE FOR RADIATION ONCOLOGY

Croucher Foundation
裘槎基金會

Acknowledgements

This thesis is dedicated to my family. Their selfless support from afar has been more consistent than my calls or visits ever were, which always fills me with guilt! “When are you coming back?” was a common refrain, and being apart is never easy, but their support encouraged me to make the time away all the more worthwhile. We all know how special the love of a grandparent is. I particularly need to thank my parents, for supporting emotionally and often financially my life’s worth of education that culminates in this thesis. I also need to thank Yu Hui Kang for his endless patience while his wife-to-be kept (mis?)prioritising work over our time together, and writing chapters instead of wedding invitations. I am blessed and secretly relieved that even after seeing me at my worst, he married me anyway.

The boss, Dr Vincenzo D’Angiolella! Vincenzo, you have contributed so much to my personal and scientific development over these past three years, and for this I will always be grateful. Your passion hasn’t wavered all these years since the lab was just unpacking itself from cardboard boxes, and I think this has been the best part of learning from you. It’s infectious! To care deeply and be invested were not on our project aims, but we hands down nailed those first, and that was most important. Thank you for all the times you’ve listened and fathered me through failed experiments, bike thefts, second year blues, and even marriage prep. For everything, you have my utmost gratitude!

I am also indebted to all my group members, past and present, who have made the lab such a colourful place. In particular, I couldn’t have possibly accomplished anything near what I have without the support of Dr Madalina Raducu. Madalina, thank you for always making time for me, and being the best role model for work ethic (and LAUGH) I could have asked for. It wouldn’t have been the same without you! I also need to thank Dr Ioanna Mavrommatis, Dr Judith Nicholson for her reality checks, and Dr Hongbin Yang, whose arrival was the motivation epipen in my last months at the bench.

And of course, a shout-out to all the other friendly faces: the tissue culture regulars (Dr Sovan Sarkar I’m looking at you), the microscopy regulars (Leanne Bradley, Dr Xianning Lai), the facilities angels, the Rammies, the takeaway regulars, the ground floor Asians, Maria and Ihor, my second family at St Ebbe’s Church, and the flatmate (Poppy Roworth ☺). I will always think of you fondly!

And so, I thank the Oxford Institute for Radiation Oncology for giving me this priceless opportunity. Furthermore, I would like to thank our collaborators Professor Erich Nigg for providing the Cep152 and Cep192 constructs, Professor Laurence Pelletier for providing the Cep192 antibody, and Professor Benedikt M Kessler for the mass spectrometry analysis service provided. Finally, none of this would have been possible without the financial support of the Medical Research Council (MRC) and Cancer Research UK (CRUK) for this project, and the Croucher Foundation for my tuition fees.

Abstract

Fbxl13 regulates centrosome homeostasis and migration through ubiquitin mediated proteolysis

Oxford Institute for Radiation Oncology, Department of Radiation Oncology and Biology
St Anne's College, University of Oxford

ELLA SUI LING FUNG

Fbxl13 (F-box and leucine-rich repeat protein 13) is an orphan F-box protein. F-box proteins are a family of substrate-targeting specificity factors for the SCF superfamily of E3 ubiquitin ligases. Since their discovery, many F-box proteins have been shown to have oncogenic and tumour suppressive roles. The importance of Fbxl13 itself in tumourigenesis is reflected in several genome-wide shRNA screens. Fbxl13 depletion in human cancer cells correlates with increased ionising radiation sensitivity and increased genomic instability. Furthermore, Fbxl13 depletion reduces proliferation in mouse embryonic epidermis. Conversely, Fbxl13 amplification is frequently observed in several cancer patient cohorts. However, the main function of Fbxl13 is unknown and its biochemical mechanism of action remains uncharacterised. The aim of this study was to identify the interactors, substrates, and functions of Fbxl13, in order to elucidate its role in tumourigenesis. In this study, I identify and validate Fbxl13 interactors Centrin-2, Centrin-3, Cep152, and Cep192. I show that Fbxl13 is enriched at the centrosome, and present evidence that Fbxl13 targets Cep192-3 for ubiquitin mediated proteolysis. In line with this, Fbxl13 overexpression downregulated centrosomal Cep192 and γ-tubulin, and disrupted the microtubule nucleation activity at the centrosome. Finally, Fbxl13 amplification in U2OS cells is associated with increased cell motility. Thus, we propose that Fbxl13 is a novel regulator of centrosome microtubule nucleation activity.

Table of Contents

List of Figures

List of Tables

List of Equations

Abbreviations

γ-TuRC	γ-tubulin ring complex
aa	amino acid
AEBSF	4-(2-Aminoethyl)benzenesulfonyl fluoride hydrochloride
APC/C	anaphase promoting complex/cyclosome
ATM	ataxia telangiectasia mutated
ATP	adenosine triphosphate
ATR	ataxia-telangiectasia and Rad3-related
bp	base pairs
BSA	bovine serum albumin
°C	degrees centigrade
CDK	cyclin dependent kinase
Cent2	centrin-2
Cent3	centrin-3
Cep152	centrosomal protein 152 kDa
Cep192	centrosomal protein 192 kDa
CHX	cycloheximide
CP110	Centriolar coiled-coil protein of 110 kDa
CPAP	centrosomal P4.1 associated protein
Cul	Cullin
CV	column volume
DAPI	4',6-diamidino-2-phenylindole
DMEM	Dulbecco's modified Eagle medium
DMSO	dimethylsulphoxide
DNA	deoxyribonucleic acid
dNTP	deoxynucleotide triphosphate
DTT	dithiothreitol
DUB	deubiquitinase
E-64	[N-(trans-Epoxysuccinyl)-L-leucine 4-guanidinobutylamide]
E coli	*Escherichia coli*
EGFR	epidermal growth factor receptor
FACS	fluorescence activity sorting assay
FBS	foetal bovine serum
FbxI13	F-box and leucine-rich repeat protein 13
GCP	γ-tubulin complex proteins
GFP	green fluorescent protein
GST	Glutathione S-transferase
Gy	Gray
h	hours
HECT	homologous to the E6AP carboxyl terminus
HU	hydroxyurea
IgG	immunoglobulin G
IgG_{LC}	immunoglobulin G light chain
IF	immunofluorescence
IPTG	β-D-1-thiogalactopyranoside
IR	ionizing radiation
K	lysine
kDa	kilo Dalton
LB	Luria-Bertani broth
LRR	leucine-rich repeats

mins	minutes
M	molar
MTOC	microtubule organising centre
NAE	NEDD8-activating enzyme
NEM	N-ethylmaleimide
Nlp	Ninein-like protein
Noco	nocodazole
p	phosphorylated
PBS	phosphate buffered saline
PCM	pericentriolar matrix
PCNA	proliferating cell nuclear antigen
PCR	polymerase chain reaction
PEI Max	Polyethylenimine HCl Max
PI	propidium iodide
Plk4	Polo-like kinase 4
PMSF	phenylmethylsulfonyl fluoride
Polybrene	Hexadimethrine bromide
PReM	phospho-regulated multimerisation domain
PVDF	polyvinylidene fluoride
px	pixel
qPCR	quantitative real-time PCR
RBR	ring between ring
rcf	relative centrifugal force
RING	really interesting new gene
RNA	ribonucleic acid
RNR	ribonucleotide reductase
RRM2	ribonucleotide reductase regulatory subunit M2
rtPCR	reverse transcription PCR
S	serine
SAS-6	spindle assembly 6 homolog
SCF	Skp-Cullin-F-box
SDS	sodium dodecyl sulphate
Skp2	S-phase kinase-associated protein 2 (Fbxl1)
STIL	SCL/TAL1 interrupting locus
T	threonine
TAE buffer	Tris base, acetic acid, and EDTA buffer
Tet	tetracycline
Ub	ubiquitin
USP3	ubiquitin specific protease 3

1 Introduction

1.1 Ubiquitylation

Ubiquitylation is the covalent addition of the small molecule ubiquitin onto a target protein in the form of ubiquitin monomers or polyubiquitin chains. The type of ubiquitylation determines substrate outcome, which includes altered protein stability, protein-protein interactions, subcellular localisation, and protein activity. The large repertoire of both substrates and ubiquitin chain types makes this pathway highly diverse. This is reflected in the ubiquitin system, which has developed attributes to ensure specificity of the ubiquitylation process. Ubiquitylation is also reversible, and can be removed by deubiquitinating enzymes (DUBs). Thus, the ubiquitin system is a powerful intracellular tool, used to regulate signal transduction, cell cycle progression, the circadian rhythm, and many other biological processes.

1.1.1 The ubiquitylation process

Ubiquitin is a 76 amino-acid protein. It was identified as a polypeptide able to stimulate ATP-dependent proteolysis in reticulocyte lysates (Ciehanover et al., 1978), and so named due to its abundance and high conservation (Wilkinson et al., 1980). Indeed, in humans, it is estimated that HeLa cells have a total of ~8,200,000 ubiquitin proteins per cell, just over half the number of tubulin-β proteins per cell (~15,300,000)(Kulak et al., 2014). Altogether, human ubiquitin is encoded from four genes: UbB, UbC, Uba52, and Uba80 (Baker and Board, 1987; Wiborg et al., 1985).

Ubiquitin is used to covalently modify ~1000 different substrate proteins in mammalian cells (Clague et al., 2015) through covalent attachment to substrate lysine residues. This process occurs through the Ubiquitin System, which comprises all proteins directly involved in ubiquitin activation and ligation. This system is highly conserved from yeast to mammals, and is central to many intracellular processes. Indeed, the Ubiquitin System is estimated to account for ~1.3% of total protein content in HeLa cells (Clague et al., 2015; Kulak et al., 2014). It is composed of a cascade of three enzymes: the E1 ubiquitin activating enzyme, E2 ubiquitin conjugating enzyme, and E3 ubiquitin ligase complex (Figure 1.1).

Firstly, ubiquitin is activated by E1 ubiquitin activating enzyme in an ATP-dependent manner, through the generation of a high-energy thioester linkage between the C terminal glycine residue of ubiquitin and the E1 cysteine active site. Following ubiquitin binding, the E1 enzyme undergoes conformational changes that reveal cryptic E2 binding sites (Lee and Schindelin, 2008). This allows the E1-Ub complex to interact with the E2 conjugating enzyme, prompting the transfer of ubiquitin from the E1 to the E2. This involves the formation of a new thioester linkage between the C terminal glycine residue of ubiquitin and the E2 cysteine active site (trans-thiolation). Once ubiquitin is transferred from the E1, its binding affinity for the E2 is lowered, facilitating its release (Lee and Schindelin, 2008). This is important, as the E1 and E3 binding surfaces of the E2 overlap. Following E1 release, the E2-Ub complex is then able to bind to the E3 ubiquitin ligase. The E3 ligase is responsible for bringing together the E2-Ub and the substrate, which is bound through the E3's substrate-targeting domain. Depending on the family of E3, the mechanism of ubiquitin transfer to the substrate differs. Some E3 ubiquitin ligases (the HECT and RBR families) also contain active cysteines, and receive the active

ubiquitin from the E2 prior to substrate ubiquitylation (reviewed in Berndsen and Wolberger (2014)). Other E3 ubiquitin ligases (RING family) are unable to receive ubiquitin, and merely act as a scaffold to bring the E2-Ub into proximity with the substrate (reviewed in Berndsen and Wolberger (2014)). In both cases, the ubiquitin then forms a covalent isopeptide bond with the substrate. This occurs between the carboxyl group on the C terminal glycine of ubiquitin, and the ε-amino group of a lysine residue on the substrate. The addition of a single ubiquitin moiety to a substrate is known as monoubiquitylation. Successive rounds of substrate ubiquitylation can also occur (polyubiquitylation). Lysine residues of ubiquitin can also serve as ubiquitin acceptor residues, forming polyubiquitin chains on a substrate. Other acceptor lysine residues on the substrate may also be ubiquitylated, resulting in multiple monoubiquitylations.

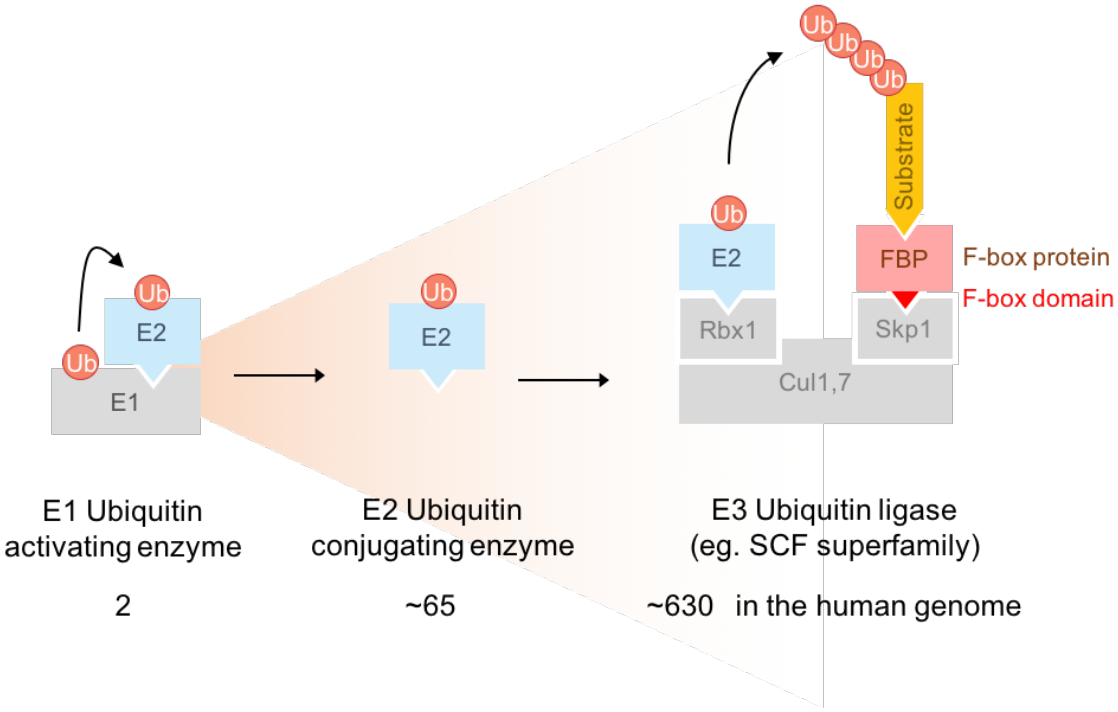

Figure 1.1 The Ubiquitin System

The Ubiquitin System is comprised of three enzymes: the E1 ubiquitin activating enzyme (left), the E2 ubiquitin conjugating enzyme (middle), and the E3 ubiquitin ligase complex (right). These activate ubiquitin (red) and transfer it to a specific substrate (yellow). The E3 ubiquitin ligase is responsible for bringing the active ubiquitin on the E2 in proximity with a substrate. The E3 ubiquitin ligase confers substrate selectivity to the Ubiquitin System. The SCF ubiquitin ligase, shown here, targets substrates through an F-box protein (red). The F-box domain recruits Skp1, which is bound to the Cullin (Cul1,7) scaffold. This scaffold recruits the E2 enzyme via Rbx1. The cascade is hierarchical, with the approximate number of genes encoding each shown (Clague et al., 2015). Figure adapted from Deshaies and Joazeiro (2009).

1.1.2 Generating functional diversity in the ubiquitin system

The ubiquitin system is hierarchical. The relative protein abundance of the E1, E2, and E3 complexes has a 1:3:2 ratio (Clague et al., 2015; Kulak et al., 2014). However, the numbers of genes encoding the E1, E2 and E3 enzymes has a ratio of approximately 2:65:630 (Clague et al., 2015). It is through the diversity of E2 and E3 complexes that the ubiquitin system can generate a broad functional diversity.

1.1.2.1 E1 ubiquitin activating enzymes

The human genome encodes 2 E1 enzymes (Ube1 and Uba6) which activate ubiquitin for all ubiquitin-requiring processes in the cell (Jin et al., 2007). Although they are the least diverse of the ubiquitin cascade enzymes, E1s are amongst the most abundant proteins in the cell: Ube1 is among the top 2% abundant proteins in HeLa cells (~3,000,000 per cell) (Clague et al., 2015). It is thought that Ube1 and Uba6 are differentially regulated. This is because in proliferating cells, effectively all Ube1 is charged with ubiquitin, and migrates at a higher molecular weight (Jin et al., 2007). In comparison, only 50% of Uba6 is charged with ubiquitin (Jin et al., 2007). Additionally, Ube1 and Uba6 were shown to have distinct specificities against a panel of E2 conjugating enzymes, and were able to charge some E2s with ubiquitin, and not others (Jin et al., 2007).

1.1.2.2 E2 ubiquitin conjugating enzymes

The human genome encodes for 35 ubiquitin conjugating enzymes. Together, these are in a 3-fold excess of the E1 enzymes (Clague et al., 2015). The E2 has a higher affinity for E1-Ub than E3 enzymes, which is advantageous as it prevents un-conjugated E2s from binding to E3s. Indeed, effectively all E2s are ubiquitin-conjugated in cells at any given time (Jin et al., 2007; Soucy et al., 2009).

E2 conjugating enzymes have emerged as the key regulators of ubiquitin chain assembly, with preferential E2s governing initiation and elongation (Ye and Rape, 2009). For example, yeast Ubc4 preferentially initiates ubiquitin chains when incubated with yeast APC/C (E3) and substrates, whereas Ubc1 preferentially extends K48-linked ubiquitin chains (Rodrigo-Brenni and Morgan, 2007). It is likely that human E2 conjugating enzymes have a similar preference: for the human E3 ligase Brca1, several E2s only participate in chain initiation (monoubiquitylation; Ube2w and Ube2e2), whereas others participate in chain elongation (Ube2k) (Christensen et al., 2007). It is thought that the distinction between E2 activities lies in their structure. For example, most E2s involved in ubiquitin chain elongation also contact the pre-existing chain, resulting in high chain specificity (reviewed in Ye and Rape (2009)). Additional functional diversity is generated by E2s through ubiquitin chain length and topology regulation, reviewed in Ye and Rape (2009). In this way, E2s play a pivotal role in determining the outcome of substrate ubiquitylation.

1.1.2.3 E3 ubiquitin ligase complex

The human genome encodes for >630 E3 ubiquitin ligases (Deshaies and Joazeiro, 2009). The E3 ubiquitin ligase complex is therefore the most diverse arm of the ubiquitin system. These are categorised into three groups based on conserved structural domains and mechanism of ubiquitin transfer: the Homology to E6AP C Terminus (HECT) family, the Really Interesting New Gene (RING) family, and the RING-between-RING (RBR) family. E3 ubiquitin ligases are characterised by their high substrate specificity, with each E3 targeting a unique pool of substrates. In this way, the ubiquitin system influences a wealth of intracellular pathways.

Several E3 ubiquitin ligases form large multiprotein complexes, and further expand their functional diversity by using interchangeable substrate-binding subunits. This can be seen in the anaphase promoting complex/cyclosome (APC/C), which targets different substrate pools through two adaptors, Cdc20 and Cdh1 (reviewed in Sivakumar and Gorbsky (2015)). The sequential degradation of first Cdc20 substrates and then Cdh1 substrates has a crucial role in regulating the anaphase to telophase transition in mitosis. In addition to the APC/C, another class of multi-subunit E3 ubiquitin ligases are the cullin-RING E3 ubiquitin ligases. These can be subdivided based on the cullin protein in the E3 ligase backbone, which assembles with different substrate adaptors and E2 enzyme adaptors. The largest and best characterised of these families is the Skp1-Cullin-F-box (SCF) superfamily of E3 ubiquitin ligases. SCF ubiquitin ligases can utilise 69 different substrate adaptors known as F-box proteins (reviewed in Cardozo and Pagano (2004)). The regulation of these substrate recognition subunits allows for high-resolution, spatio-temporal regulation of ubiquitin ligase activity.

Skp1-Cullin-F-box (SCF) E3 ubiquitin ligases

SCF E3 ubiquitin ligases are multi-subunit complexes composed of Cullin (Cul1,7), Skp1, Rbx1, and an F-box protein (Figure 1.1, right) (reviewed in Cardozo and Pagano (2004)). The cullin forms the backbone of the SCF complex. Through Rbx1, the backbone recruits the E2 conjugating enzyme. Through Skp1, it recruits an F-box protein. The F-box protein contains the substrate recognition domain, and confers substrate specificity to the entire SCF complex.

The human genome encodes for 69 human F-box proteins, characterised by the F-box domain required for Skp1 binding (Cenciarelli et al., 1999; Jin et al., 2004;

Winston et al., 1999). F-box proteins are then sub-categorised into three groups based on their C terminal domain, or substrate recognition domain. Fbxw proteins are characterised by WD-40 repeats; Fbxls are characterised by leucine-rich repeats (LRR); Fbxos encompass other repeats. Through these variable C terminal regions, each F-box protein targets different substrate pools. Several F-box proteins have been identified as crucial regulators of oncogenic pathways. For example, Fbxl17 is overexpressed in medulloblastoma and targets a well-known tumour suppressor, Sufu, for ubiquitin mediated proteolysis (Raducu et al., 2016). Another example is Fbxl1 (Skp2), which degrades key suppressors of cell cycle progression, such as the CDK (cyclin dependent kinase) inhibitors p21 and p27 (Carrano et al., 1999; Yu et al., 1998). Due to the specificity and functional importance of F-box proteins, they represent molecular targets for cancer therapy. Indeed, inhibitors of F-box proteins have been developed such as Compound 25 (for Skp2/Fbxl1) and UB-036 (for β-TrCP/Fbxw1), reviewed in Skaar et al. (2014). However, out of 69 F-box proteins, only ~20 have known substrates and/or functions (Skaar et al., 2009).

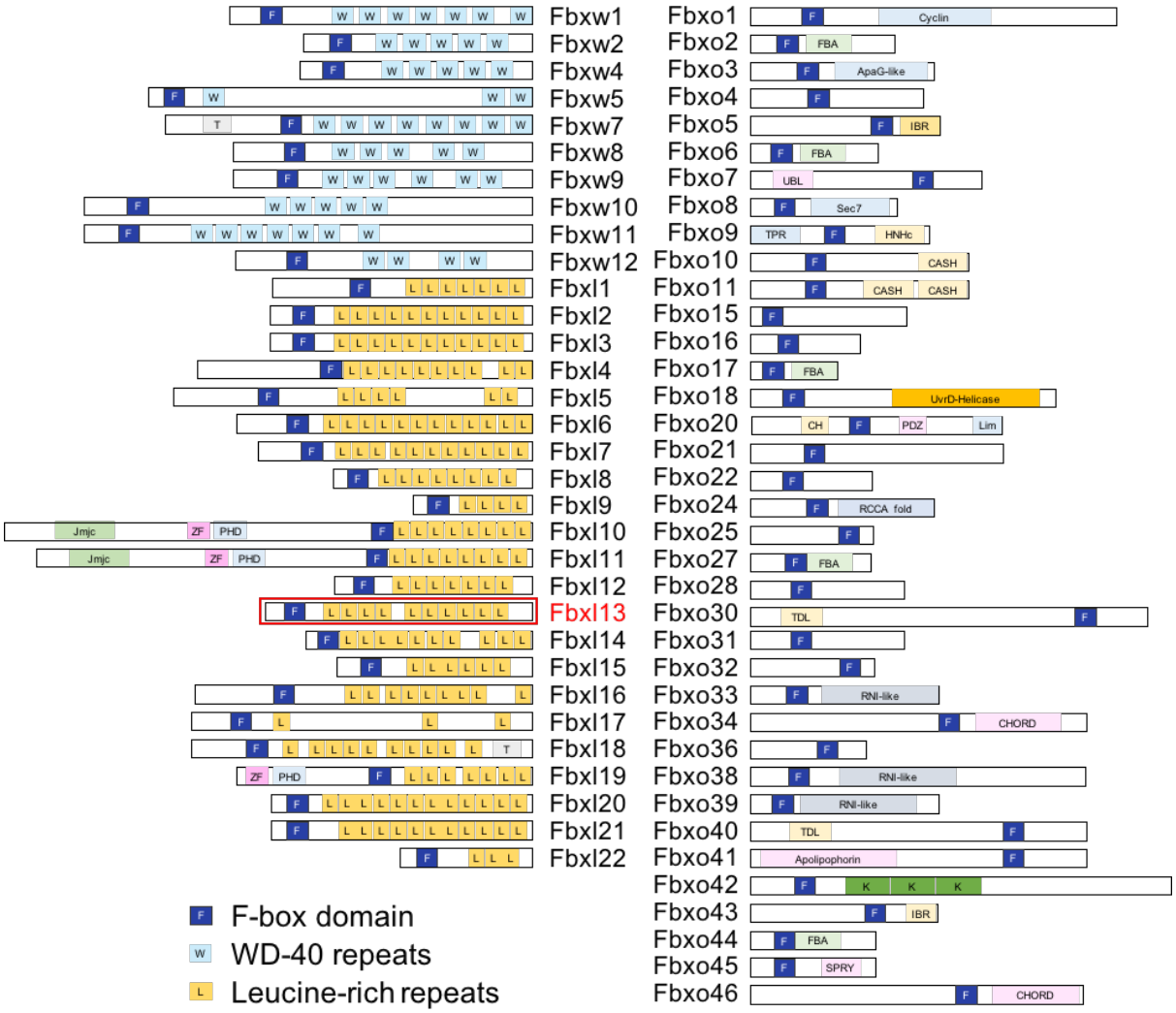

Figure 1.2 The human F-box proteins

F-box proteins are the substrate-selectivity factor of SCF (Skp-Cullin-F-box) E3 ubiquitin ligases. The human genome encodes for 69 putative F-box proteins, which were identified by their F-box domain (dark blue). This domain interacts with Skp1 to recruit the Cullin backbone and form a fully functional E3 ubiquitin ligase. F-box proteins are categorised into three groups based on their C terminal composition: 10 Fbxws (WD-40 repeats), 22 Fbxls (leucine-rich repeats), and 37 Fbxos (other repeats). These variable C terminal repeats are used to target different substrate pools for ubiquitylation. Only one third of F-box proteins have known substrates and/or functions at the time of writing. The subject of this study is Fbxl13 (red). Figure adapted from Jin et al. (2004).

1.1.2.4 Deubiquitination

Ubiquitylation is a reversible modification. The removal of ubiquitin from substrates is termed deubiquitination, a highly specific process catalysed by deubiquitinating enzymes (DUBs), reviewed in Reyes-Turcu et al. (2009). The ability of ubiquitylated substrates to be further regulated by DUBs adds a layer of complexity to the ubiquitin system. DUBs cleave the isopeptide bond between ubiquitin and substrate, or ubiquitin and ubiquitin. Interestingly, the total number of DUB proteins in the cell is similar to the number of E2 conjugating enzymes (~10,000,000) (Clague et al., 2015; Kulak et al., 2014), and are encoded by 80 genes in the human genome. The activity of these DUBs is highly regulated. For example, DUBs have specificity for both ubiquitin chain-linkages as well as substrates. Additionally, most DUBs have cryptic catalytic sites. Only when the DUB is bound to both substrate-ubiquitin does it undergo conformational rearrangements to reveal these cryptic sites, and permit deubiquitinase activity. Strict regulation of DUB activity is crucial, as deubiquitination is involved in cellular processes such as signal transduction, DNA damage repair, and chromatin remodelling.

For instance, the DUB USP3 (ubiquitin specific protease 3) is a chromatin modifier involved in the downregulation of DNA damage repair signalling. Following DNA damage resolution, USP3 deubiquitinates histones H2A and H2AX to switch off the ubiquitin mediated signalling of DNA double strand break repair (Nicassio et al., 2007). DUBs are also important in ubiquitin recycling. Three DUBs are associated with the 19S proteasome lid (PSMD13/POH1, UCHL5, and USP13), above the opening to the 26S proteasome core complex where proteolysis takes place (Yao and Cohen, 2002). Here, they intercept incoming substrates modified with ubiquitin, and release ubiquitin chains. This serves two functions: firstly, to

facilitate substrate unfolding into the 26S proteasome channel, and secondly, to prevent the proteolysis of ubiquitin along with the substrate (Yao and Cohen, 2002). The timing of DUB activity is also important. It has been suggested that if the deubiquitination of proteasome-bound substrates outpaces their proteolysis, the substrate may be freed from proteolysis (reviewed in Finley (2009)).

1.1.3 Cellular role of ubiquitylation

1.1.3.1 The ubiquitin code

Protein ubiquitylation can alter protein stability, protein-protein interactions, localisation, or activity. The outcome of ubiquitylation is signalled by the composition of the polyubiquitin chain, and is known as the ubiquitin code, reviewed in Komander and Rape (2012).

Ubiquitin can be extended into polyubiquitin chains between 2 to 10 ubiquitin molecules long. Ubiquitin can polymerise through its C terminal glycine residue and one of seven lysines: K6, K11, K27, K29, K33, K48, and K63. Different E2-E3 ligase complexes can polymerise ubiquitin chains of different linkages and lengths, or in some cases, on secondary sites on the substrate, which can signal for degradation and/or serve as secondary signals (Kerscher et al., 2006; 2012; Pickart and Eddins, 2004; Zhou et al., 2014).

The lysine used to polymerise ubiquitin chains determines substrate outcome. This signal is transduced by ubiquitin readers, which distinguish between polyubiquitin chains (reviewed in Komander and Rape (2012)). One distinguishing feature is the distance between ubiquitin molecules in the chain. For example, structural analyses revealed that K48-linked chains are compacted in a “closed” structure, whereas K63-linked chains are extended in an “open” structure (Figure

1.3) (Tenno et al., 2004). Ubiquitin chain readers can therefore distinguish between the two by introducing a spacer of defined length between its ubiquitin binding domains (UBDs). Indeed, it has been shown that Rap80 contains a longer spacer and recognises K63-linked chains, whereas Ataxin-3 contains a shorter spacer and recognises K48-linked chains (Sims and Cohen, 2009). Swapping these linkers also swapped their chain-binding specificities, demonstrating that ubiquitin chain recognition was determined by linker length (Sims and Cohen, 2009).

It is also becoming increasingly clear that the ubiquitin code is highly complex (reviewed in Komander and Rape (2012)). Polyubiquitin chains can be homogenous, containing the same linkage, or mixed, with alternating lysine linkages with each successive ubiquitin molecule. Ubiquitin chains can also be branched: it is possible for one ubiquitin molecule to be modified by two ubiquitin molecules on different lysine residues. The function of these diverse polyubiquitylation chains has yet to be characterised. However, monoubiquitylation and several homologous chain types have been well characterised, and each trigger distinct outcomes in the cell (Figure 1.3).

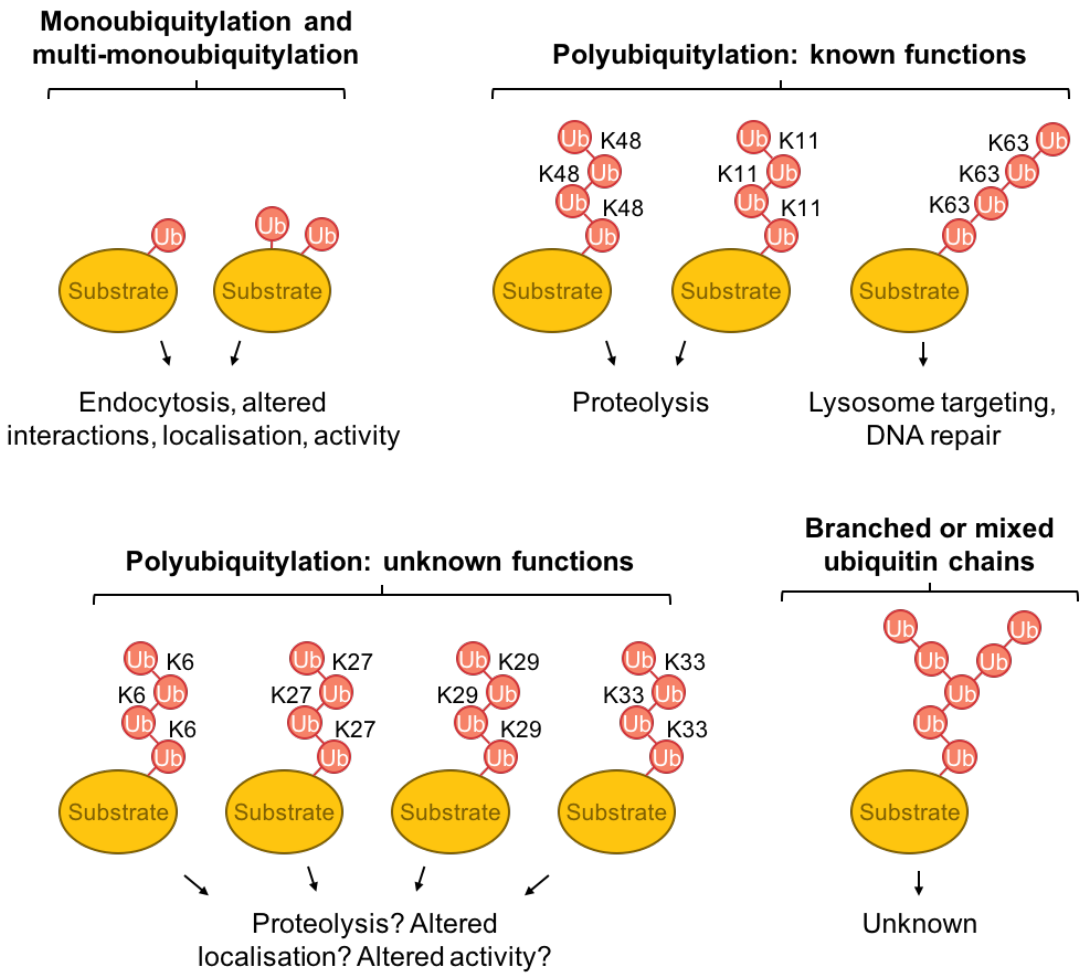

Figure 1.3 The ubiquitin code

Various types of ubiquitin chain and their known outcomes. Ubiquitin is highlighted in red, and the substrate in yellow. The ubiquitin chain type is labelled according to the lysine residue used to extend the polyubiquitin chain. Figure adapted from Ye and Rape (2009).

1.1.3.2 Protein stability

It is well established that ubiquitylation can result in degradation by the 26S proteasome. Indeed, this is the pathway in which ubiquitin was first characterised (Ciechanover et al., 1980; Wilkinson et al., 1980). Proteolysis is primarily signalled by K48 and K11 polyubiquitin linkages of more than 4 ubiquitin molecules (Chau et al., 1989; Matsumoto et al., 2010). This is the major intracellular pathway that regulates controlled, targeted protein degradation. The degradation of signalling activators or inhibitors allows irreversible switches in the cell. For this reason, ubiquitin mediated proteolysis is often found in the regulation of unidirectional cellular processes, such as cell cycle regulation, signal transduction, and circadian rhythm. Indeed, during mitotic progression, the APC/C targets multiple substrates such as securin, Cyclin B1, and Aurora A for ubiquitin mediated proteolysis via K11-linked polyubiquitin chains (Matsumoto et al., 2010). The cullin-RING superfamily has been estimated to account for ~20% of all ubiquitin mediated proteolysis in the cell (Soucy et al., 2009).

Ubiquitylation has also been observed to regulate lysosomal degradation, which is frequently triggered by monoubiquitylation or K63-linked ubiquitin chains (reviewed in Mukhopadhyay and Riezman (2007)). Lysosomal degradation is the pathway in which membrane proteins are degraded, following endocytosis and sorting to the lysosome. In this way, lysosomal degradation is commonly used for receptor downregulation. For example, EGFR (epidermal growth factor receptor) is endocytosed and targeted for K63-linked ubiquitylation, resulting in its lysosome targeting (Huang et al., 2006a). Instead, EGFR deubiquitination by either USP80 or AMSH allows it to be trafficked back to the plasma membrane and recycled (Mizuno et al., 2005).

1.1.3.3 Protein-protein interaction

Substrate ubiquitylation can also generate novel binding regions to recruit protein interactors. This has been observed following both monoubiquitylation and K63-linked chains. For example, the DNA polymerase processivity factor PCNA (proliferating cell nuclear antigen) is monoubiquitylated following DNA damage. This recruits translesion synthesis polymerases (Y family polymerases) to stalled replication forks for DNA damage repair (Bienko et al., 2005). Y family polymerases contain two conserved ubiquitin binding domains, which facilitate binding to monoubiquitylated PCNA. In line with this, deletion of either ubiquitin binding domain sensitises cells to ultraviolet irradiation (Bienko et al., 2005). Thus, PCNA ubiquitylation recruits crucial DNA damage repair factors to prevent stalled replication fork collapse. Following DNA damage resolution, PCNA is deubiquitylated by USP1, facilitating the switch to normal DNA synthesis (Huang et al., 2006b).

Similarly, the E3 ubiquitin ligase RNF8 is recruited to sites of DNA damage by MDC1 (mediator of damage checkpoint 1). Here, it acts with the E2 conjugating enzyme UBC13 to ubiquitylate histones H2A and H2AX with K63-linked chains (Huen et al., 2007; Mailand et al., 2007). Interestingly, UBC13 is the only known E2 conjugating enzyme to polymerise K63-linked chains. This signal is then recognised by a second E3 ubiquitin ligase, RNF168, which binds UBC13 and ubiquitylates neighbouring H2A and H2AX histones (Doil et al., 2009). This further propagates the K63-linked signal at the site of DNA damage in a positive feedback loop (Doil et al., 2009). Repair factors are then recruited to these sites, such as the ubiquitin chain reader Rap80, which complexes with Brca1 (Sims and Cohen, 2009).

1.1.3.4 Subcellular localisation

By inducing conformational changes, ubiquitylation can reveal substrate localisation signals and induce localisation changes. One prominent example of this is the monoubiquitylation of p53 by MDM2. Whereas polyubiquitylation of p53 by MDM2 signals for its proteolysis, monoubiquitylation reveals a cryptic p53 nuclear export signal (Carter et al., 2007). This results in its dissociation from MDM2, and relocation to the cytoplasm. The cause behind this switch in MDM2 activity is unclear, however it has been shown that high levels of MDM2 favour p53 polyubiquitylation, whereas low levels favour p53 monoubiquitylation (Li et al., 2003). p53 downregulation by either mono- or poly-ubiquitylation is inhibited by the deubiquitinating enzyme USP10. Following DNA damage, USP10 is activated by ATM phosphorylation, and deubiquitinates p53. This both prevents p53 proteasome degradation, and induces p53 re-import to the nucleus (Yuan et al., 2010).

1.1.3.5 Protein activity

Less frequently, ubiquitylation can also alter substrate activity. This occurs for the transcription factor NF-κB. This transcription factor exists as an inactive precursor, NF-κB1 (p105). Monoubiquitylation by $SCF^{\beta TRCP}$ targets p105 for partial proteolysis of its C terminal, resulting in an active NF-κB subunit (p50) (Kravtsova-Ivantsiv and Ciechanover, 2015). The exact mechanism behind this partial proteolysis is unknown.

1.1.4 Substrate recognition

E3 ubiquitin ligases recognise specific binding domains on substrates (degrons). In many cases, the binding of E3 ubiquitin ligases to substrates can be triggered by post-translational modifications of these degrons, ensuring timely ubiquitylation. In

this way, multiple layers of binding regulation increase the stringency of substrate recognition.

1.1.4.1 Phospho-degrons

One of the best characterised forms of substrate recognition is phosphorylation. Here, degron phosphorylation is required for E3 ubiquitin ligase recognition. This often occurs in signal transduction. For example, in the Wnt signalling pathway, the transcription factor effector β-catenin is regulated by the E3 ubiquitin ligase β-TrCP (Fbxw1) (Hart et al., 1999). In the absence of signal transduction, β-catenin is degraded by β-TrCP to prevent the transcription of Wnt responsive genes. In this case, β-catenin degradation is stimulated by the sequential activity of two kinases: CK1α (casein kinase Iα) and GSK-3 (glycogen synthase kinase 3) (Hart et al., 1998; Liu et al., 2002). CKIα is a “priming” kinase, and its phosphorylation of β-catenin at S45 precedes and is required for subsequent GSK-3 recognition of T41, S37, and S33 (Liu et al., 2002). β-catenin S33 and S37 phosphorylation are in turn required for recognition and ubiquitylation by β-TrCP (Liu et al., 2002). The requirement of a priming phosphorylation prior to degron phosphorylation adds a layer of stringency to prevent aberrant β-catenin degradation.

1.1.4.2 Regulated degron access

E3 ubiquitin ligase access to the substrate degron may also be regulated by post-translational modifications outside of the degron. This is seen in the SCF^{Fbxo1} (or $SCF^{Cyclin\ F}$) targeting of RRM2 (ribonucleotide reductase regulatory subunit M2). RRM2 phosphorylation by CDKs at T33 (outside of the degron) is required for Cyclin F binding to the RRM2 degron. It is possible that T33 phosphorylation triggers conformation changes that reveal a cryptic degron (D'Angiolella et al., 2012).

1.1.4.3 Cofactor dependent degrons

Substrate recognition by E3 ubiquitin ligases can also be regulated by cofactors. This is exemplified by the cyclin-dependent kinase inhibitor p27. In late G1, p27 is degraded by $SCF^{Skp2/Fbxl1}$ in order for Cyclin-CDK activity to drive cells into S phase. However, $SCF^{Skp2/Fbxl1}$ is unable to bind p27 directly. Its interaction is mediated by a cofactor, Cks1 (CDK subunit 1), which induces conformational changes in p27 to increase its binding affinity to $SCF^{Skp2/Fbxl1}$ (Ganoth et al., 2001; Spruck et al., 2001). It is thought that this restricts $SCF^{Skp2/Fbxl1}$-mediated p27 degradation to the G1/S transition, where Cks1 levels are highest (Spruck et al., 2001).

1.1.4.4 Phospho-inhibition of degrons

Degron modifications can also inhibit E3 ubiquitin ligase binding. In one such example, the phosphorylation of the Cdt2 degron at T464 prevents SCF^{Fbxo11} binding and subsequent degradation (Rossi et al., 2013). Cdt2 regulation is crucial for cell cycle progression, as it downregulates the replication initiation factor Cdt1. Indeed, Cdt2 phosphorylation was shown to be CDK dependent, suggesting that its degradation is blocked in proliferating cells (Rossi et al., 2013). A stable, phospho-mimic of Cdt2 (T464D) resulted in delayed mitotic exit (Rossi et al., 2013). In such cases, the coordinated activity of E3 ubiquitin ligases and CDKs ensures that ubiquitylation events are tethered to the cell cycle.

1.1.4.5 Domain-based recognition

Finally, some E3 ubiquitin ligases target substrates through larger domains, and not short stretches of amino acids. This is seen for SCF^{Fbxl3}, which utilises its leucine-rich repeats to target the surfaces of Cry1 and Cry2 (cryptochrome 1 and 2) (Busino et al., 2007). The recognition of Cry1 and Cry2 then lead to their ubiquitin

mediated proteolysis (Busino et al., 2007; Godinho et al., 2007). This is crucial for the oscillation of the circadian rhythm, as Cry1 and Cry2 negatively repress Clock-Bmal1, a transcription factor which drives the start of the circadian clock (Busino et al., 2007; Godinho et al., 2007). As Fbxl3 levels do not oscillate, it is envisaged that post-translational modifications stimulate surface recognition of Cry1 and Cry2 by SCF^{Fbxl3} (Busino et al., 2007).

1.1.5 Ubiquitylation in cancer

As we have seen, the ubiquitin system is a diverse regulatory pathway involved in many crucial cellular functions – such as cell cycle progression, apoptosis, receptor downregulation, DNA damage signalling and repair, and dNTP pool regulation – as determined by the substrate-specificity of the E3 ubiquitin ligase. For this reason, E3 ubiquitin ligases are often implicated in tumourigenesis. Recent studies have elucidated their role as both cell proliferation agonists *and* antagonists, and their potential as targets for anticancer therapies (reviewed in Hoeller and Dikic (2009)).

1.1.5.1 Tumour suppressor roles of E3 ubiquitin ligases

E3 ubiquitin ligases commonly regulate signal transduction, for example in cell proliferation. One of the best characterised E3 ubiquitin ligases involved in tumour suppression is SCF^{Fbxw7} (reviewed in Welcker and Clurman (2008)). The F-box protein Fbxw7 has been shown to target many oncogenes for ubiquitin mediated proteolysis. For example, Fbxw7 was first found to degrade Cyclin E (Koepp et al., 2001; Strohmaier et al., 2001). Cyclin E promotes progression through the G1/S boundary, and DNA replication initiation. Correspondingly, the loss of Fbxw7 was associated with extremely high Cyclin E levels and genomic instability (Strohmaier

et al., 2001). Fbxw7 was later found to target many other proto-oncogenes for ubiquitin mediated proteolysis: c-Myc (transcription factor for cell proliferation), c-Jun (transcription factor for cell proliferation), SREBP (sterol regulatory element binding protein; transcription factor for membrane synthesis and lipid metabolism), Notch (transcription factor for cell proliferation and prevents differentiation), and PS1 (presinilin; a Notch signal transducer) (reviewed in Welcker and Clurman (2008)). In all cases, substrate recognition is dependent on dual-phosphorylation of the Fbxw7 degron. Strikingly, stabilising mutations that impair Fbxw7-substrate binding are commonly found at these degrons, and are frequently found in cancer. For example, the c-Myc T58 region is commonly mutated in Burkitt's lymphoma, and results in increased stability (Gregory and Hann, 2000). On average, Fbxw7 is mutated in 6% of all cancers, including 30% of all leukaemias and 4-15% of gastrointestinal cancers (pancreatic, gastric, colon) (Welcker and Clurman, 2008). Therapies targeting the Fbxw7 pathway are undergoing development, with a focus on Fbxw7 substrates such as Myc and Notch (reviewed in Welcker and Clurman (2008)).

1.1.5.2 Oncogenic roles of E3 ubiquitin ligases

E3 ubiquitin ligases are also commonly oncogenic. One such ligase is SCF^{Fbxl17}, which targets the tumour suppressor Sufu for ubiquitin mediated proteolysis (Raducu et al., 2016). Sufu is a suppressor of the Hedgehog signalling pathway, and acts by sequestering downstream Gli transcription factors. The SCF^{Fbxl17}-mediated ubiquitylation of Sufu facilitates Gli release and activation of Hedgehog target genes including Myc, Cyclin D, and Bcl-2 (Raducu et al., 2016). Thus, tumours overexpressing Fbxl17 show increased proliferation rates and are associated with poor prognosis (Raducu et al., 2016).

Another E3 ubiquitin ligases that regulates cell proliferation is Efp (oestrogen-inducible RING finger protein). Efp is a target gene of oestrogen receptors, and promotes cell proliferation by targeting 14-3-3σ for proteolysis (Urano et al., 2002). 14-3-3σ is a p53 effector that normally arrests cells at the G2/M transition by sequestering Cyclin B and Cdc2 to the nucleus to prevent mitotic entry (Chan et al., 1999; Hermeking et al., 1997). Thus, by degrading 14-3-3σ, Efp overcomes the G2/M checkpoint. However, in breast cancer, Efp is commonly upregulated and associated with poor prognosis. Indeed, MCF7 cells (a breast cancer cell line) overexpressing Efp can generate tumours in ovariectomised mice, in the absence of oestrogen, whereas control MCF7 cells cannot (Urano et al., 2002). It has therefore been proposed that Efp is involved in the switch from oestrogen-dependence to oestrogen-independence in breast cancer proliferation. This switch is a crucial point for patients, as oestrogen-independence limits available treatments: such tumours are chemoresistant to treatments that rely on oestrogen, such as Tamoxifen (reviewed in Nalepa and Harper (2003)).

1.2 Centrosomes

Centrosomes are the microtubule organising centres (MTOC) of animal cells. They consist of a pair of orthogonally arranged centrioles embedded in pericentriolar matrix (PCM), and regulate the geometry of microtubule arrays in the cell. In this way, centrosomes regulate crucial processes such as cell shape, cell polarity, cell motility, intracellular trafficking, and chromosome segregation (reviewed in Doxsey et al. (2005)). In recent years, the architecture and symmetry of the centrosome has been elucidated in detail due to the rise of super-resolution microscopy techniques.

1.2.1 Centrosome structure

Prior to duplication, one centrosome consists of two orthogonally arranged centrioles, linked at their base, embedded in a highly organised network of scaffold proteins known as the pericentriolar matrix (PCM) (Figure 1.4). The younger centriole (assembled in the previous cell cycle) is known as the daughter centriole, whereas the older is the mother centriole. Centrioles are polarised along their length, with the base referred to as the proximal end, and the tip as the distal end. The mother uniquely possesses distal and sub-distal appendage proteins (Figure 1.4) (Paintrand et al., 1992). In differentiated cells, the mother is anchored to the plasma membrane by these appendages for ciliogenesis (Graser et al., 2007). Both the centrioles and PCM are highly organised.

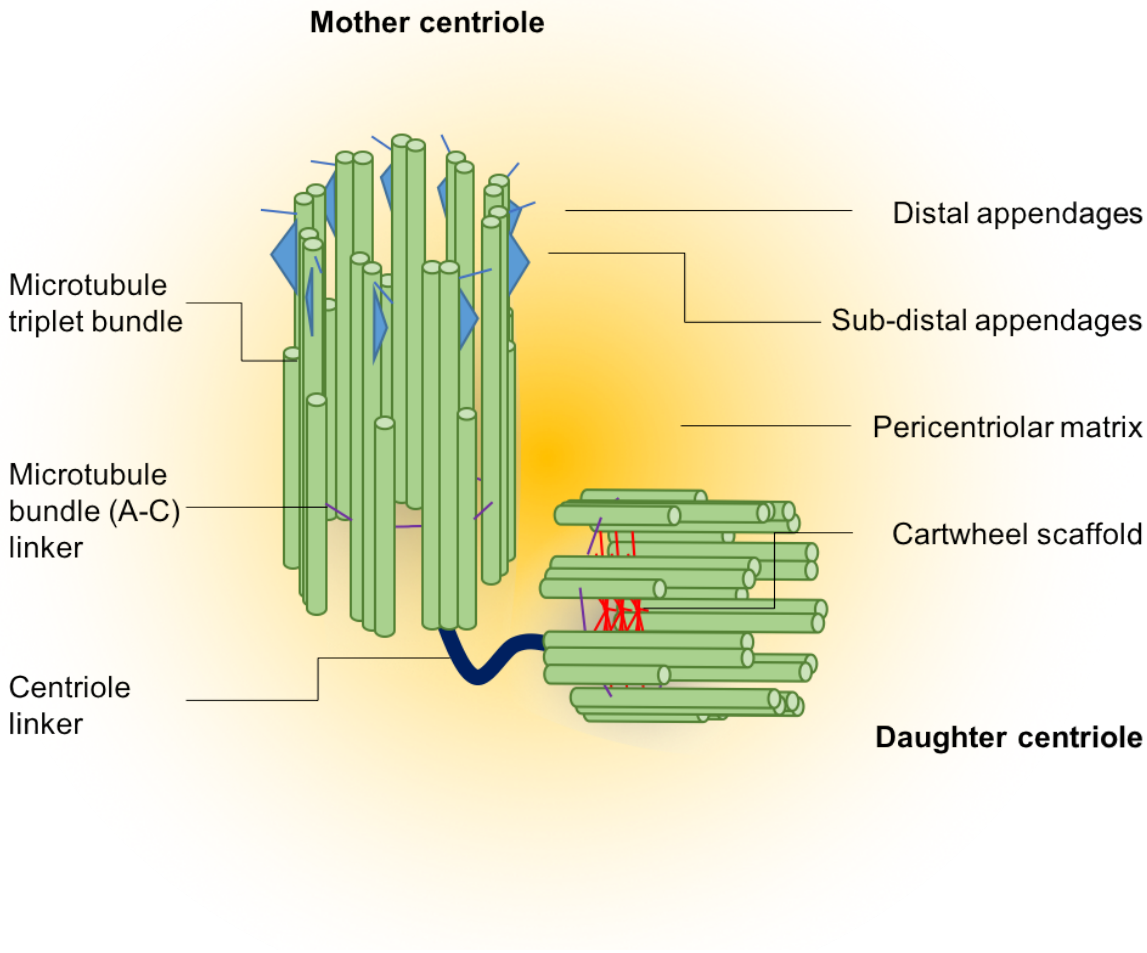

Figure 1.4 Centrosome structure

A simplified diagram of the vertebrate centrosome. Each centrosome comprises two centrioles, a mother and a daughter, embedded in pericentriolar matrix. Each centriole is a cylindrical, microtubule-based structure with nine-fold symmetry, measuring only 250 nm in diameter and 150-500 nm in length. The microtubules are arranged in triplet bundles (green), which fan away from the central lumen, clockwise when viewed from the distal end. The outermost microtubule in each bundle is ~30% shorter than the other two. During centriole duplication, the daughter centriole is stabilised by a cartwheel scaffold (red) in its lumen. The mother and daughter centrioles are linked by a proteinaceous linker, which is dissolved during centrosome separation. The mother centriole uniquely has distal and sub-distal appendages. Figure adapted from Pihan (2013).

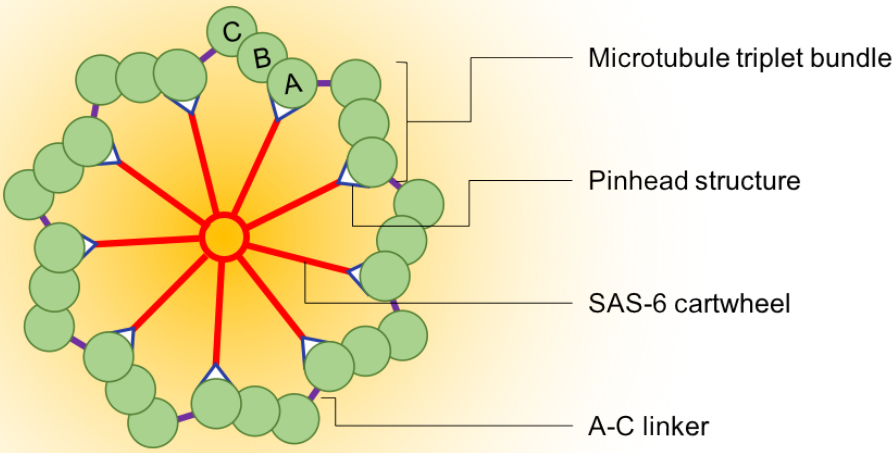

Figure 1.5 Centriole structure

The vertebrate centriolar wall in cross-section, viewed from the distal end. Nine bundles of microtubules (green) are organised around a central cartwheel composed of SAS-6 (red). Each cartwheel spoke ends in a pinhead structure (blue) associated with microtubule A of a triplet bundle. Microtubules B and C fan away from the central lumen in a clockwise manner. Each microtubule bundle is linked with its neighbour, via an A-C microtubule linker (purple). Figure adapted from Winey and O'Toole (2014).

1.2.1.1 Centrioles

Each centriole is a cylindrical, microtubule-based structure with nine-fold symmetry, measuring only 250 nm in diameter and between 150-500 nm in length (reviewed in Winey and O'Toole (2014)). The centriolar walls of the vertebrate centrosome are comprised of nine microtubule triplet bundles (Figure 1.4). In cross-section, the microtubule triplet bundles are arranged in a slanted configuration, fanning away from the central lumen (Figure 1.5). When viewed from the distal end, they are arranged in a clockwise manner (Paintrand et al., 1992).

Each triplet bundle consists of three interlinked microtubules. The microtubule positioned closest to the central lumen (microtubule A) has the typical microtubule composition of 13 α- and β-subunit protofilaments (Li et al., 2012). However, the other two microtubules in the triplet bundle diverge from the typical microtubule structure. The following microtubule (B) has 10 protofilaments, and shares 3 protofilaments with triplet A to complete the 13 protofilaments found in a typical microtubule. In the same way, the third microtubule (C) also shares three protofilaments with microtubule B. It is proposed that this unique arrangement of protofilaments is facilitated by minor tubulin isoforms δ and ε, which are predominantly present in species with triplet microtubules (reviewed in Winey and O'Toole (2014)). However, exceptions exist, as Drosophila lack these tubulin isoforms despite forming triplet microtubules in certain tissues.

It was previously thought that the nine-fold radial symmetry of the centriole derives from a cartwheel scaffold found at the base of growing daughter centrioles (Guichard et al., 2010). In human cells, this scaffold is formed by the SAS-6 protein. SAS-6 proteins self-assemble to form a distinctive cartwheel structure with nine-fold

radial symmetry, with a central hub of 23 nm, and nine spokes radiating outwards (Kitagawa et al., 2011; van Breugel et al., 2011). Each spoke ends in a pinhead structure, composed of Cep135, CPAP, and STIL (Cottee et al., 2013). This pinhead structure serves as an adaptor between a cartwheel spoke and microtubule A of the centriolar wall (Figure 1.5). Depletion of SAS-6, other cartwheel components, or disruption of the cartwheel symmetry impaired daughter centriole formation or led to daughter centrioles with defective symmetry (Cottee et al., 2013; Lin et al., 2013; Nakazawa et al., 2007; Vulprecht et al., 2012). It was therefore proposed that the SAS-6 cartwheel templated procentriole formation (the scaffold model). However, it was observed that a fraction of SAS-6 null or mutant cells still formed wildtype centrioles, challenging the scaffold model (Hilbert et al., 2016; Nakazawa et al., 2007). Indeed, when Hilbert et al. engineered a range of SAS-6 mutants that formed cartwheel structures with 5-fold to 10-fold symmetry, they found that these mutants still yielded centrioles with 9-fold symmetry. However, these centrioles are often shorter (30% shorter) and disorganised at the distal end (Hilbert et al., 2016). Thus, the current view is that the cartwheel and centriolar wall form in parallel and stabilise one another (the interdependence model) (Hilbert et al., 2016). Following anaphase, SAS-6 and STIL are both targeted for proteolysis by APC/C^{Cdh1}, and the cartwheel structure is dissolved (Arquint and Nigg, 2014; Strnad et al., 2007).

Once assembled, the centriole is extremely stable. Whereas cytoskeletal microtubules are easily depolymerised into α- and β-tubulin monomers by cold shock, centrioles persist. The centriolar wall is strengthened by linkages between each microtubule triplet bundle (Figure 1.5). These are called A-C linkers, as they are formed between microtubule A and C of neighbouring triplets (Paintrand et al., 1992). It is also thought that post-translational modifications contribute to the

stability of centriolar microtubules, such as glutamylation (reviewed in Wloga and Gaertig (2010)). Electron microscopy in lower eukaryotes such as *C. reinhardtii* has also revealed additional protein structures that may contribute to basal body stability, such as Y-shaped linkers between microtubules A and B, and filaments inside the distal lumen of microtubule C (Li et al., 2012). The molecular components of these complexes have yet to be identified. It also remains to be seen whether similar structures are found in higher eukaryote centrioles.

1.2.1.2 Pericentriolar matrix

Centrioles are embedded in a scaffold of proteins called the pericentriolar matrix (PCM). The PCM is the main microtubule organising component of the centrosome. Although previously thought to be an amorphous cloud of proteins, it has become clear from super-resolution microscopy techniques in recent years that the interphase PCM is highly organised in concentric layers (reviewed in Lüders (2012)).

The PCM is organised around the mother centriole. Super-resolution microscopy has revealed that interphase PCM proteins have distinctive localisation patterns, often in concentric rings of discrete size. By measuring the radius of these rings, it has been possible to separate proteins into inner, intermediate, and outer layers of the PCM. For example, the inner PCM layer contains Cep152, Cep192, and NEDD1 (diameter ~300 nm) (Lawo et al., 2012; Sonnen et al., 2012). These proteins form the PCM core, and are crucial for both centriolar duplication (Cep152 and Cep192) and microtubule nucleation activity (Cep192 and NEDD1). The intermediate layer contains PCM components such as γ-tubulin (diameter ~400 nm), and the outer layer contains CDK5RAP2 and pericentrin (diameter ~500-600 nm), components

which are expanded upon entry into mitosis in a Cep192-dependent process termed centrosome maturation (Khodjakov and Rieder, 1999; Lawo et al., 2012; Sonnen et al., 2012). Interestingly, the discrete layers of the interphase PCM are lost upon its dramatic expansion during this process.

1.2.2 Centrosome duplication

For each daughter cell to receive one centrosome following mitosis, the centrosome must undergo duplication. Centrosome duplication is a highly conserved process, with a core pathway derived from the last common eukaryotic ancestor (Carvalho-Santos et al., 2010). The centrosome duplication pathway is tethered to the cell cycle to ensure that it only occurs once per cell cycle. As with DNA replication, centrosome duplication of more than once per cycle can have deleterious effects. Indeed, centrosome reduplication results in centrosome amplification, which is correlated with genomic instability and cancer progression (reviewed in Godinho and Pellman (2014)). Centrosome under-duplication is also deleterious, resulting in daughter cells that lack centrosomes, which leads to mitotic delay and genomic instability. In fact, animal cells that lack centrosomes undergo a p53-dependent G1 arrest to prevent the propagation of this problem (Wong et al., 2015).

The centrosome cycle contains three main stages that will be discussed here: procentriole formation, centrosome maturation, and centriole disengagement (reviewed in Fırat-Karalar and Stearns (2014)).

1.2.2.1 Procentriole formation

In G1, a procentriole begins to form on each of the two existing centrioles. This process is driven by Cep192 and Cep152 (Cizmecioglu et al., 2010; Hatch et al.,

2010; Kim et al., 2013; Sonnen et al., 2013). Cep192 is localised in close proximity to the centriolar wall throughout the cycle (Sonnen et al., 2013). Upon G1 entry, Cep152 independently localises to the proximal end of the centriolar wall (Sonnen et al., 2013). Together, Cep152 and Cep192 are both required for the recruitment and downstream activation of Plk4, a polo-like kinase required for centriole formation (Bettencourt-Dias et al., 2005; Habedanck et al., 2005; Kim et al., 2013; Sonnen et al., 2013). The concentration of Plk4 at centrosomes results in its full activation through trans-autophosphorylation (Lopes et al., 2015). Cep152 and Cep192 initially recruit Plk4 around the base of the mother centriole (Sonnen et al., 2013). As G1 progresses, the ring of Plk4 at the proximal base of the mother centriole breaks symmetry, and is localised into a single point which marks the subsequent site of procentriole formation (Sonnen et al., 2012). How Plk4 localisation breaks symmetry remains unknown, although the switch coincides with the presence of centriolar STIL (SCL/TAL1-interrupting locus protein) (Ohta et al., 2014).

At the site of centriole duplication, Plk4 phosphorylates STIL (Curtiss et al., 2005; Dzhindzhev et al., 2010; Ohta et al., 2014). This allows STIL to interact more efficiently with the cartwheel component SAS-6, and recruit SAS-6 to the site of centriole duplication for stable procentriole formation (Dzhindzhev et al., 2010; Ohta et al., 2014). Together, STIL and SAS-6 recruit CPAP (centrosomal P4.1 associated protein) and Cep135 to the pinhead structure at the spokes of the cartwheel. Here, CPAP and Cep135 associate the cartwheel to the centriolar wall (via microtubule triplet A) to promote centriolar elongation and stability (Lin et al., 2013; Tang et al., 2009; Tang et al., 2011).

1.2.2.2 Centrosome maturation

In mitosis, the PCM expands to increase the microtubule nucleation activity for sufficient bipolar spindle formation (centrosome maturation) (Khodjakov and Rieder, 1999). This is achieved by enriching γ-tubulin, which together with five GCPs (γ-tubulin complex proteins) and NEDD1 forms the γ-TuRC (γ-tubulin ring complex). The γ-TuRC nucleates microtubule assembly by serving as a template for α- and β-tubulin protofilaments (Khodjakov and Rieder, 1999; Moritz et al., 1995).

In vertebrate cells, centrosome maturation is driven by Cep192 (Gomez-Ferreria et al., 2007; Zhu et al., 2008). Cep192 recruits Plk1 and Aurora A to the centrosome in a cooperative fashion, resulting in their activation (Joukov et al., 2014; Meng et al., 2015). Plk1 then phosphorylates both Cep192 and NEDD1, a γ-TuRC component that independently localises to the centrosome, to generate γ-tubulin binding sites (Gomez-Ferreria et al., 2012; Joukov et al., 2014; Lüders et al., 2006). The loss of either Cep192 or NEDD1 results in reduced γ-tubulin recruitment to the centrosome, and defective spindle formation (Gomez-Ferreria et al., 2007; Gomez-Ferreria et al., 2012; Joukov et al., 2014; Zhu et al., 2008).

In *D. melanogaster*, it has been shown that the PCM expands in a highly orchestrated fashion (Conduit et al., 2014a). Here, mitotic Plk1 phosphorylates the PCM protein centrosomin (CDK5RAP2 in humans) at a phospho-regulated multimerisation (PReM) domain. This allows centrosomin to multimerise and form a scaffold, expanding the PCM outwards (Conduit et al., 2014a). The expansion of the PCM involves a positive feedback loop between centrosomin and Spd2 (Cep192 in humans), which recruit one another (Conduit et al., 2014b). It is speculated that a similar mechanism underlies centrosome maturation in vertebrate cells.

1.2.2.3 Centriole disengagement

Following centriole duplication, the new mother and daughter centrioles are held together at their proximal ends by a proteinaceous linker in a tightly opposed arrangement (engaged). Upon mitotic exit, the newly formed daughter centriole disengages from the mother centriole, and they are held loosely together by a flexible protein linker (Bahe et al., 2005).

The importance of centriole disengagement can be seen in cells where centriole disengagement is blocked. In this case, centrosomes duplication is impaired (Tsou et al., 2009). On the other hand, ectopic centriole disengagement is accompanied with centrosome reduplication (Loncarek et al., 2010). Centriole disengagement is therefore an essential licensing step to permit the next round of centriole duplication.

Thus far, two key cell-cycle regulated proteins have been found to mediate centriole disengagement: separase and Plk1 (Lee and Rhee, 2012; Tsou and Stearns, 2006; Tsou et al., 2009). Separase is a protease active in anaphase, and plays a prominent role in sister chromatid separation by cleaving cohesion rings. Its activity is restricted to anaphase through inhibition by Cyclin B and securin. It was observed that separase is also able to localise at the centrosome, and that separase-dependent cleavage of pericentrin-B is necessary for centriole disengagement (Lee and Rhee, 2012). Conversely, a non-cleavable mutant of pericentrin-B prevented centriole disengagement (Lee and Rhee, 2012). However, these centrioles did not remain engaged over time even in separase null cells, suggesting that separase-independent mechanisms also regulate centriole disengagement (Tsou et al., 2009). A high throughput pharmacologic inhibitor screen revealed this other mechanism to be Plk1 dependent (Tsou et al., 2009).

Plk1 is required in early mitosis for centriole disengagement, and double depletion of both Plk1 and separase completely abolishes centriole disengagement (Tsou et al., 2009).

1.2.3 Centrosomes and microtubule nucleation

The microtubule cytoskeleton plays a central role in the organisation of eukaryotic cells. Microtubules themselves are highly dynamic polymers comprised of α-tubulin and β-tubulin subunits, and constantly undergo cycles of polymerisation and depolymerisation in the cell. Microtubules originate from microtubule organising centres (MTOCs) which favour tubulin polymerisation. In the vertebrate cell, the major MTOC is the centrosome, although acentrosomal microtubule nucleation sites such as the Golgi apparatus or chromosomes also exist. Microtubule nucleation at these sites is promoted by the γ-tubulin ring complex (γ-TuRC). This complex consists of γ-tubulin and five GCP proteins, and acts as a template for α-tubulin and β-tubulin subunits to polymerise into 13-fold symmetry tubules (reviewed in Kollman et al. (2011)). Thus, regulation of the γ-TuRC is fundamental to the dynamic organisation of the microtubule cytoskeleton in response to cell cycle changes and signalling.

It is known that Cep192 promotes the microtubule-nucleation capacity of the mitotic centrosome during centrosome maturation (Gomez-Ferreria et al., 2007; Zhu et al., 2008), as described above. Cep192 has also been shown to recruit γ-tubulin at the interphase centrosome, although this pathway is less well defined, and the mechanism of γ-tubulin recruitment is unclear (O'Rourke et al., 2014). Whereas in mitosis, Plk1 generates a phospho-recognition domain on Cep192 for γ-tubulin, the

interphase centrosome lacks Plk1, and it is unclear whether Cep192 directly recruits γ-tubulin in a similar fashion.

The importance of MTOC activity can be seen in recent studies where microtubule nucleation is deregulated. This can occur following the overexpression of microtubule nucleation factors, or centrosome amplification. For example, Godinho et al. observed that centrosome amplification in non-transformed MCF10A cells resulted in loss of cell-cell adhesion, mammosphere integrity, and oncogene-like induction of invasive protrusions (Godinho et al., 2014). Strikingly, these oncogenic phenotypes were rescued following Cep192 depletion, demonstrating that they were dependent on the increased microtubule nucleation activity of the extra centrosomes. Godinho et al. found that the increased centrosome microtubules resulted in increased Rac1 activation at the plasma membrane, resulting in actin cytoskeleton reorganisation.

On the other hand, ectopic suppression of MTOC activity is also undesirable. Nlp (Ninein-like protein) is a centrosomal protein that suppresses microtubule nucleation and release (Schnerch and Nigg, 2016). Schnerch et al. found that Nlp overexpression also causes oncogenic aberrations using the same non-transformed MCF10A model system as Godinho et al., including loss of cell-cell adhesion, cell polarisation, and mammospheres architecture. Furthermore, Nlp is also commonly amplified in breast tumours (Schnerch and Nigg, 2016). Thus, it is coming to light that MTOC activity must be maintained at steady-state levels to prevent deleterious effects.

1.2.4 Centrosome regulation by ubiquitylation

Ubiquitylation is a crucial regulatory tool found in most intracellular pathways. It is unsurprising, therefore, that ubiquitylation is also involved in centrosome regulation. The centrosome duplication pathway is known to be regulated by ubiquitylation at multiple steps.

1.2.4.1 Plk4 ubiquitylation

Robust centriole duplication is dependent on tightly regulated levels of Plk4, the master kinase that drives procentriole formation. Indeed, overexpression of Plk4 results in the formation of multiple daughter centrioles at the base of the mother centriole, creating a striking rosette phenotype (Bettencourt-Dias et al., 2005; Habedanck et al., 2005). Under normal conditions, the levels of Plk4 are regulated via ubiquitin mediated proteolysis. Here, Plk4 auto-phosphorylates itself, creating a phospho-degron recognised by $SCF^{\beta\text{-}TrCP}$ (Cunha-Ferreira et al., 2009; Holland et al., 2010; Rogers et al., 2009). This creates a negative feedback loop in which Plk4 is self-limiting, and serves as a mechanism to prevent aberrant procentriole formation. Interestingly, a second E3 ubiquitin ligase, Mib1, has been proposed to regulate Plk4 levels: Mib1 silencing results in further centriole overduplication, but only when Plk4 levels are already overexpressed (Čajánek et al., 2015). For this reason, it has been suggested that Mib1 is a failsafe mechanism to regulate ectopic Plk4 levels. In contrast, β-TrCP silencing results in centriole overduplication in normal cells, and has therefore been suggested to regulate steady-state Plk4 levels (Čajánek et al., 2015).

1.2.4.2 SAS-6 ubiquitylation

The cartwheel protein SAS-6 is cell cycle regulated, and targeted for ubiquitin mediated proteolysis by both APC/C^{Cdh1} and SCF^{Fbxw5} (Puklowski et al., 2011; Strnad et al., 2007). In turn, SCF^{Fbxw5} activity is inhibited by Plk4 phosphorylation at S151 (Puklowski et al., 2011). This means that upon G1 entry, Plk4 becomes activated, inhibiting SCF^{Fbxw5} activity, and allowing SAS-6 levels to accumulate for centriole duplication. Following centriole duplication, Plk4 activity falls, and SCF^{Fbxw5} limit SAS-6 levels to prevent centriole overduplication (Puklowski et al., 2011). Finally, upon entry into mitosis, Fbxw5 is targeted for ubiquitin mediated proteolysis by both APC/C^{Cdc20} and APC/C^{Cdh1}, allowing SAS-6 to re-accumulate for the following cell cycle (Puklowski et al., 2011). APC/C^{Cdh1} also suppresses Fbxw5 levels during G1.

1.2.4.3 CP110 ubiquitylation

Centrioles are capped by CP110 (Centriolar coiled-coil protein of 110 kDa) (Chen et al., 2002). CP110 levels are limiting for centriole duplication: its depletion disrupts centriole duplication under normal conditions, and following either hydroxyurea-treatment or Plk4 overexpression (Chen et al., 2002; Kleylein-Sohn et al., 2007). Indeed, CP110 levels are highest in S-phase (Chen et al., 2002). It has been shown that in G2 and M phases, CP110 is targeted for ubiquitin mediated proteolysis by the F-box protein Cyclin F (or Fbxo1) (D'Angiolella et al., 2010). The depletion of Cyclin F leads to CP110 accumulation and centriole overduplication, in a CP110 dependent manner (D'Angiolella et al., 2010). CP110 ubiquitylation is countered by USP33 (ubiquitin specific protease 33), which deubiquitylates CP110 to prevent its proteolysis in S/G2 phase (Li et al., 2013). USP33 overexpression also results in

CP110 accumulation and centriole overduplication, consistent with Cyclin F depletion phenotypes (Li et al., 2013).

1.3 Project aims

The specificity of F-box proteins and their involvement in tumour progression have made them attractive and successful targets for anti-cancer treatments (reviewed in Skaar et al. (2014)). As two thirds of F-box proteins remain completely uncharacterised, there is still much work to be done.

Recent genome-wide screens have further implicated the F-box family in various oncogenic processes. In particular, the orphan protein Fbxl13 (F-box and leucine-rich repeat protein 13) has been identified in several screenings. For example, when silenced with shRNAs, Fbxl13 was found to sensitise U2OS cells to IR (Hurov et al., 2010). In line with this, Fbxl13 depletion also resulted in increased genomic instability in HeLa cells as measured with γH2AX foci (Paulsen et al., 2009). Together, these screens suggest that Fbxl13 may have an oncogenic function. Indeed, a genome-wide shRNA screen in mice found that Fbxl13 depletion reduces proliferation in mouse embryonic epidermis (Beronja et al., 2013). Finally, an online repository of cancer patient cohorts also shows that Fbxl13 is frequently amplified in several solid tumour cohorts, such as breast cancer (20%), non-epithelial prostate cancer (20%), head and neck cancer (10%), and oesophageal cancer (10%) (cBioPortal). For these reasons, we believe that Fbxl13 has an important function in cell physiology.

The study in this thesis therefore aims to characterise the substrates of Fbxl13, to understand its biological function, and investigate its potential mechanism of action in tumour progression. These aims were guided by the following questions:

1. What are the interactors of Fbxl13?

2. Of these interactors, which could be substrates of Fbxl13?
3. For identified substrates, what is the outcome of Fbxl13-mediated ubiquitylation?
4. What is the downstream function of Fbxl13-mediated substrate ubiquitylation?
5. Given the implications of Fbxl13 in cancer, does deregulation of the Fbxl13-substrate pathway result in oncogenic processes?

2 Materials and Methods

2.2 Materials

2.2.1 General laboratory and cell culture reagents

Cell culture media was supplied by Corning and cell culture plastics were obtained from Greiner Bio-One. General laboratory reagents and chemicals used are detailed in Table 2.1.

Table 2.1 Chemicals and cell culture reagents

Name	Producer or UK distributor
Acetic acid	Sigma-Aldrich
Agarose	Invitrogen/Life Technologies
β-mercaptoethanol	Sigma-Aldrich
Betaine	Sigma-Aldrich
BSA (bovine serum albumin)	Sigma-Aldrich
DMEM (Dulbecco's modified Eagle medium)	Corning
DMSO (dimethylsulphoxide)	Sigma
DNase I	Qiagen
Ethanol	Sigma-Aldrich
Ethidium bromide	Sigma-Aldrich
FBS (foetal bovine serum)	Sigma-Aldrich
Glycine	Thermo Fisher Scientific
HiPerfect	Qiagen
Laemmli buffer	Invitrogen/Life Technologies
LB (Luria-Bertani broth)	Sigma-Aldrich
Lipofectamine 2000	Invitrogen/Life Technologies
Methanol	Thermo Fisher Scientific
NEM (N-ethylmaleimide)	Sigma-Aldrich
Nocodazole	Cayman Chemicals
Nonidet P-40	Sigma-Aldrich
Paraformaldehyde	VWR

PBS (phosphate buffered saline)	Sigma-Aldrich
PEI (Polyethylenimine HCl) Max	Polysciences
PMSF (phenylmethylsulfonyl fluoride)	Sigma-Aldrich
Protease inhibitor cocktail (mammalian)	Roche
ProLong® Gold Anti-Fade	Invitrogen/Life Technologies
PI (propidium iodide)	Sigma-Aldrich
SDS (sodium dodecyl sulphate)	BioRad
SYBR® Green	Applied Biosystems
Tetracycline-free FBS	Clontech
Thymidine	Sigma-Aldrich
Triton X-100	Sigma-Aldrich
Tween 20	Thermo Fisher Scientific
X-tremeGENE HP	Roche

2.2.2 Antibodies

Table 2.2 Primary Antibodies used for Western blotting

Name	Species	Clone ID	Dilution	Reference
Cyclin B	Mouse	V152	1:5000	Invitrogen/Life Technologies, AHF0052
Centrin-2	Rabbit	-	1:1000	Santa Cruz, SC27793
Centrin-3	Mouse	SS12	1:1000	Santa Cruz, SC100933
Cep192	Rabbit	-	1:1000	Prof L Pelletier, Gomez-Ferreria et al. (2014)
Flag	Rabbit	-	1:1000	Sigma-Aldrich, F7425
Fbxl13	Rabbit	-	1:5000	Aviva, OAAB12542
GAPDH	Mouse	GA1R	1:2000	Invitrogen/Life Technologies, MA5-15738
HA	Mouse	IgG3	1:1000	Millipore, 05-904
p-Histone H3 (S10)	Rabbit	-	1:1000	Millipore, 06-570
Myc	Mouse	9B11	1:1000	Cell Signalling Technology, 2276

Table 2.3 Secondary Antibodies used for Western blotting

Name	Dilution	Reference
HRP Goat Anti-Mouse IgG (H+L)	1:10,000	Invitrogen/Life Technologies, 62-6520
HRP Goat Anti-Rabbit IgG (H+L)	1:10,000	Invitrogen/Life Technologies, 65-6120
HRP Chicken Anti-Protein-A/G	1:5000	Thermo Fisher Scientific, 11829240

Table 2.4 Antibodies used for immunofluorescence

Name	Species	Clone ID	Dilution	Reference
Primary antibodies				
γ-Tubulin	Mouse	GTU-88	1:5000	Sigma, T5326
γ-Tubulin	Rabbit	-	1:2000	Sigma, T5192
Cep152	Rabbit	-	1:300	Bethyl, A310-901A
Cep192	Rabbit	-	1:300	Prof L Pelletier, Gomez-Ferreria et al. (2014)
Centrin-3	Mouse	SS12	1:300	Santa Cruz, SC100933
Secondary/conjugated antibodies				
Alexa Fluor 488 Donkey Anti-Rabbit IgG			1:500	Invitrogen/Life Technologies
Alexa Fluor 568 Donkey Anti-Rabbit IgG			1:500	Invitrogen/Life Technologies
Alexa Fluor 488 Donkey Anti-Mouse IgG			1:500	Invitrogen/Life Technologies
Alexa Fluor 568 Donkey Anti-Mouse IgG			1:500	Invitrogen/Life Technologies
Anti-α-Tubulin−FITC conjugated			1:200	Sigma, F2168

2.2.3 Antibiotics

Ampicillin and kanamycin (Sigma) were made up as stock solutions of 50 mg/ml in sterile, double distilled water, and filtered using a 0.22 μm filter. Stocks were then aliquoted and stored at -20°C. Ampicillin and kanamycin were used at final concentrations of 50 μg/ml. Puromycin (Thermo Fisher Scientific) was used at 3 μg/ml for U2OS cell line selection.

2.2.4 Plasmids

Transient transfection plasmids were constructed using the pcDNA3 or pcDNA3.1(+) vectors from Invitrogen. Flag tagged constructs were cloned using a 3xFLAG-pCMV-7.1 vector derived from D'Angiolella et al. (2012). Myc tagged constructs were generated by introducing the Myc tag sequence to the N or C terminal of the protein using the 5` or 3` primer respectively.

Retroviral constructs for stable cell line production were cloned using the pBabe-puro vector (Addgene, 1764). In all cases, inserts were amplified by polymerase chain reaction (PCR) using Phusion Hot Start II (New England BioLabs). Betaine (Sigma) was added at a final concentration of 1 M for amplification of GC rich sequences. PCR products and vectors were digested using restriction enzymes from New England BioLabs, gel purified using the QIAQuick Gel Extraction Kit (Qiagen), and ligated using T4 DNA Ligase (New England BioLabs) with the insert at a 3 molar excess to the vector. The ligated constructs were transformed into Gold Efficiency α-Select Competent Cells (Bioline), an *E. coli* competent strain DH5α with recA1 and endA1 mutations to prevent recombination and digestion. All constructs were verified by sequencing by Sanger sequencing (Source BioScience).

2.2.5 Primers

The primers used in this study are listed in Table 2.5. Isoform-specific Fbxl13 qPCR primers were designed based on exon-exon spanning sequences or isoform-specific sequences, using the NCBI Primer-BLAST tool. Primers were validated by qPCR, by checking for a single melt-curve, and by running the qPCR product on an agarose gel to check for a single product of 200 bp. The final primer concentration used in qPCR reactions was 50 nM.

Table 2.5 Primers used for quantitative real-time PCR (qPCR)

Primer name	Species	Sequence
Fbxl13-1 Forward	human	5`-GCACTGGCCATTTACTGCATTAACC-3`
Fbxl13-1 Reverse	human	5`-GCTGCCTTCTTGGAAATATTTGTGC-3`
Fbxl13-3 Forward	human	5`-GGAATTCAGATTACTGACTCAGC-3`
Fbxl13-3 Reverse	human	5`-GCTGCCTTCTTGGAAATATTTGTGC-3`
GAPDH Forward	human	5`-ATGCCTCCTGCACCACCAAC-3`
GAPDH Reverse	human	5`-GGGGCCATCCACAGTCTTCT-3`

2.2.6 Software

Table 2.6 Additional software for data analysis

Name	Company, reference, or link
Fiji (Image J ecosystem)	Schindelin et al. (2012)
GelCount™	Oxford Optronix
GraphPad Prism	GraphPad Software Inc.
ModFit LT	Verity Software House
MRI Wound Healing Tool	http://dev.mri.cnrs.fr/projects/imagej-macros/wiki/Wound_Healing_Tool

2.2 Methods

2.2.1 Cell lines

Mammalian cell lines were maintained at 37°C with 5% CO_2 in the following media and supplements:

Table 2.7 Cell line culturing media and supplements

Cell line	Media	Supplements
HEK293T	Dulbecco's Modified Eagle Medium with glucose/L, sodium pyruvate/L and L-glutamine (Corning)	- 100 µg/ml Penicillin-streptomycin (Corning) - 10% (v/v) FBS (PAA)

U2OS	Dulbecco's Modified Eagle Medium with glucose/L, sodium pyruvate/L and L-glutamine (Corning)	- 100 µg/ml Penicillin-streptomycin (Invitrogen/Life Technologies) - 10% (v/v) FBS (PAA)
U2OS pBabe Empty Vector	Dulbecco's Modified Eagle Medium with glucose/L, sodium pyruvate/L and L-glutamine (Corning)	- 100 µg/ml Penicillin-streptomycin (Invitrogen/Life Technologies) - 10% (v/v) FBS (PAA) - 1.5 µg/ml Puromycin
U2OS pBabe Myc-Fbxl13	Dulbecco's Modified Eagle Medium with glucose/L, sodium pyruvate/L and L-glutamine (Sigma)	- 100 µg/ml Penicillin-streptomycin (Invitrogen/Life Technologies) - 10% (v/v) FBS (PAA) - 1.5 µg/ml Puromycin

2.2.2 Cryopreservation of cell lines

Cells at 70% confluency were trypsinised, resuspended in 5 ml of fresh media, and centrifuged at 600 rcf for 3 minutes at room temperature. The pellet was then resuspended in 1 ml of freezing media (10% DMSO in FBS), and transferred to a 2 ml cryovial (Thermo Fisher Scientific). The cryovial was immediately placed on dry ice, and then transferred to liquid nitrogen for long-term storage.

To defrost cells from liquid nitrogen, cryovials were thawed in a 37°C water bath. The thawed cell solution was transferred to 5 ml of pre-warmed fresh media, and centrifuged at 600 rcf for 3 minutes. The pelleted cells were resuspended in fresh media, and plated in a 10 cm dish. The media was changed the following day, and cells were typically ready to be split following 48 hours.

2.2.3 Transient plasmid transfection

HEK293T cells were seeded the previous day prior to transfection using the reagent “PEI Max”, Polyethylenimine HCl Max (Polysciences). This reagent was prepared by dissolving in sterile, double distilled water to a final concentration of 1 mg/ml, and adjusting the pH to 7.5. Importantly, the reagent was filtered through a 0.22 nm filter to ensure sterility, and avoid undissolved crystals that strongly bind DNA but cannot cross the plasma membrane. 7 µl of PEI Max solution was used per 1 µg of DNA, and mixed in autoclaved 150 mM NaCl. The transfection mixture was vortexed and incubated for 10 minutes at room temperature before adding dropwise to cells. Cells were harvested 48 hours post-transfection.

U2OS cells were seeded the day prior to transfection using the reagent X-tremeGENE™ HP DNA Transfection Reagent (Roche) according to the manufacturer’s instructions. In brief, 2 µl of X-tremeGENE reagent and 0.5 - 1 µg of DNA was added to 150 µl of Opti-MEM I Reduced Serum Medium (Thermo Fisher Scientific). The transfection mixture was vortexed and incubated for 5 minutes at room temperature before adding dropwise to cells in a 6-well plate.

2.2.4 Transient siRNA transfection

U2OS cells were seeded at 150,000 cells per 6-well plate 24 hours before transfection. Cells were transfected for 48 hours using HiPerfect Transfection Reagent (Qiagen) in Opti-MEM I Reduced Serum Medium (Thermo Fisher Scientific) according to the manufacturer’s instructions. The siRNAs used in this study, and their working concentrations, are listed in Table 2.8.

Table 2.8 siRNA sequences

Name	siRNA sequence	Working conc.	Reference
siCep152	5`-GCGGATCCAACTGGAAATCTA-3`	50 nM	Graser et al. (2007)
siCep192	5`-AAGGAAGACATTTTCATCTCT-3`	50 nM	Zhu et al. (2008)
siFbxl13 S3	-	60 nM	Dharmacon, 016001-07
siFbxl13 S4	-	60 nM	Dharmacon, 016001-08
siGenome Non-Targeting siRNA Pool 1	5`-UAGCGACUAAACACAUCAA-3` 5`-UAAGGCUAUGAAGAGAUAC-3` 5`-AUGUAUUGGCCUGUAUUAG-3` 5`-AUGAACGUGAAUUGCUCAA-3`	-	Dharmacon, 001206-13
siLacZ	5`-CGTACGCGGAATACTTCGA-3`	-	Elbashir et al. (2001)

For combination siRNA/cDNA transfections, U2OS cells were transfected using Lipofectamine 2000 (Invitrogen/Life Technologies) according to the manufacturer's instructions, and harvested 48 hours post-transfection.

2.2.5 Generation of stable cell lines

For retrovirus production, a pBabe-puro (Addgene, 1764) retroviral vector containing the gene of interest was co-transfected into HEK293T with the pUMVC Gag/Pol vector (Addgene, 8449) packaging vector and pCMV-VSV-G (Addgene, 8454) envelope-encoding vector in a 4:3:3 ratio. The media was changed 24 hours post-transfection. 48 hours later, the media was harvested, and clarified by centrifuging at 800 rcf for 5 minutes, and passing through a 0.45 µm filter. This media contained either retroviral packaged gene of interest (or an empty vector control). The retroviral media was kept at 4°C for 1 week, or -80°C for long-term storage.

Stable shRNA cell lines were generated by Dr Hongbin Yang using a lentiviral system. pGIPZ lentiviral transfer vectors containing a non-targeting shRNA or three shRNAs targeting Fbxl13 were provided by the Target Discovery Institute High Throughput Core (University of Oxford). The shRNA sequences are listed in Table 2.9. Lentivirus were packaged using the pCMV-VSV-G (Addgene, 8454) envelope-encoding vector and the psPAX2 (Addgene, 12260) packaging vector. These were transfected into HEK293T cells in a 4:3:3 ratio, and harvested in the same way as retrovirus particles.

For transduction, U2OS cells were seeded at 30% confluency (as retroviruses only infect S-phase cells). 24 hours later, fresh media was added along with the virus-containing media at a 1:1 ratio, in the presence of 8 μg/ml polybrene to increase infection efficiency. The polybrene-containing media was changed after 16 hours due to toxicity, followed by 3 μg/ml puromycin selection for 72 hours. Expression of the protein of interest was confirmed by Western blot. Stable shRNA incorporation could be confirmed by immunofluorescence using GFP.

Table 2.9 shRNA sequences

Name	shRNA Sequence
shControl (89)	5`-TCTCGCTTGGGCGAGAGTAAG-3`
shFbxl13 (75)	5`-AGGAATTGGATATATTGTA-3`
shFbxl13 (85)	5`-AGCAAGACATAAGAGTAAA-3`
shFbxl13 (87)	5`-CGAGGCACTTCCACAACTT-3`

2.2.6 Protein turnover

Cells were transfected as indicated. Following 48 hours, cells were treated with 50 μg/ml cycloheximide to inhibit further protein synthesis. Samples were collected

at the indicated time points over 12 hours, and protein levels were detected by Western blot using 3 ug of whole-cell lysate.

2.2.7 Hydroxyurea induced centrosome overduplication

U2OS cells were seeded at 150,000 cells per 6-well plate on glass coverslips, and transfected as indicated. The next day, cells were treated with 4 mM hydroxyurea. Hydroxyurea decreases the production of dNTPs by ribonucleotide reductase inhibition. This results in a G1/S phase arrest permissive for centrosome duplication in U2OS cells (Balczon et al., 1995). 72 hours after hydroxyurea treatment, cells were fixed in ice cold methanol for 5 minutes at -20°C. Centrosome overduplication was visualised using immunofluorescence by scoring the percentage of cells with greater than 2 γ-tubulin dots or greater than 4 Centrin-3 dots. Binucleate cells were excluded to control for cytokinesis failure.

2.2.8 Cell-cycle synchronisation

293T and U2OS cells were synchronised using a “16-8-16” double-thymidine block. In brief, cells were seeded at 30% confluency and arrested using 2 mM thymidine for 16 hours. 2 M thymidine was freshly prepared in sterile PBS and filtered using a 0.45 μm filter. Cells were released from the thymidine block by washing twice in PBS, and once in DMEM. Cells were then allowed to grow for 8 hours, and then arrested using 2 mM thymidine again for 16 hours. Upon release, the cells were harvested at the indicated time points over 24 hours. To enrich for mitotic cells, 0.1 mg/ml nocodazole was added 7 hours following the final thymidine washout.

2.2.9 *In vivo* ubiquitylation assay

U2OS cells were plated at 50% confluency and transfected the following day with the indicated plasmids or siRNA for 48 hours. Cells were treated with 10 μM MG132, a 26S proteasome inhibitor, for 5 hours prior to collection. Cells were then lysed in lysis buffer containing 20 mM N-ethylmaleimide (NEM), a broad de-ubiquitinating enzyme (DUB) inhibitor, to prevent deubiquitylation. Ubiquitylated Myc-tagged Cep152 or Myc-tagged Cep192 were immunoprecipitated using anti-Myc antibody coupled to Protein G Sepharose 4 Fast Flow beads (GE Healthcare). Poly-ubiquitylated forms of Cep152 or Cep192 were detected by immunoblot using anti-Myc or anti-HA as indicated.

2.2.10 *In vitro* transcription-translation

The indicated Fbxl13, Cep152, and Cep192 constructs were *in vitro* transcribed and translated using a rabbit reticulocyte system, TNT® Quick Coupled Transcription/Translation System (Promega), according to manufacturer's instructions. The kit consists of cell-free rabbit reticulocyte extracts, which are crude extracts containing the macromolecular components required for transcription and translation of exogenous DNA. Rabbit reticulocytes in particular are commonly used as they are highly specialised to synthesise large amounts of haemoglobin. In brief, 1 μg of plasmid DNA and 1 μl of 1 mM methionine was resuspended in 40 μl of reticulocyte extract, and incubated at 30°C for 1 hour. Reactions were resolved by SDS-PAGE to validate protein expression.

2.2.11 Exposure to γ-irradiation

All irradiations were carried out using a Gamma Service® GSR D1 irradiation containing a Cs^{137} source. The dose rates of the system, as determined by the

supplier, was 1.938 Gy/minute and 1.233 Gy/minute based on the distance from the source. Samples were positioned on shelf 1 and the exposure times were calculated based on these dose rates for each indicated dose.

2.2.12 Clonogenic survival assay

Clonogenic survival assays were established based on a published protocol (Franken et al., 2006). In brief, U2OS cells were transfected with siRNA as indicated. 48 hours following transfection, the treated cells were trypsinised and at a density of 800 cells seeded per 60 mm dish and allowed to adhere overnight. To minimise variation, each cell sample was counted twice using a haemocytometer, and each condition was seeded in triplicate. The following day, the plates were irradiated with 0-3 Gray. The irradiated plates were incubated at 37 °C, 5% CO_2 for 12 days, and the media was changed every 5 days. The media was then removed from the plates, and the colonies fixed by washing once with PBS and incubating with Coomassie blue solution (0.1% Coomassie Brilliant blue, 7% acetic acid, 50% methanol) for 20 minutes. The staining solution was removed, and excess stain was removed by washing in distilled water. The stained and dried plates were then imaged using GelCount™ (Oxford Optronix), and the colonies counted using accompanying GelCount™ software. The surviving fraction was calculated as the number of colonies in the treated plate divided by the number of colonies in the untreated control plate, normalising for plating efficiency (Equation 2.1).

$$\text{Plating efficiency (PE)} = \frac{\text{\# of colonies formed}}{\text{\# of cells seeded}} \times 100\%$$

$$\text{Surviving fraction (SF)} = \frac{\text{\# of colonies formed after IR}}{\text{\# of cells seeded} \times \text{PE}}$$

Equation 2.1 Surviving fraction following irradiation

The surviving fractions were then fitted to a linear quadratic equation first described by Brenner (2008) using GraphPad Prism 6 software (Equation 2.2).

$$Y = e^{-\alpha X + \beta X^2}$$

Equation 2.2 Linear quadratic model for irradiation response

Where Y is surviving fraction (SF), X is the irradiation dose in Gray, and α and β are constants determined in GraphPad Prism 6 that represent two survival response rates to DNA damage. Published in (Brenner, 2008).

2.2.13 Wound healing assay

Following 48 hours of siRNA transfection, U2OS cells were seeded at a density of 400,000 per 6-well plate. When the cells reached 100% confluency 36 hours after seeding, a linear wound was created using a sterilised 10 µl tip. Cell debris around the wound was removed by washing gently with PBS, before replacing with 0.5% FBS supplemented media. Images of the wound were acquired at defined positions at the indicated time-points using the EVOS FL Imaging System (Invitrogen).

The efficiency of wound closure was calculated as the area of the wound closed over time. The area of the wound was determined using the Image J software ecosystem Fiji (Schindelin et al., 2012) and the MRI Wound Healing Tool plugin (http://dev.mri.cnrs.fr/projects/imagej-macros/wiki/Wound_Healing_Tool).

2.3 Protein analysis and biochemistry

2.3.1 Cell lysis

The constitution of the Lysis Buffer is as follows: 50 mM Tris-HCl pH 7.5, 150 mM NaCl, 1mM EDTA, 0.1% NP-40, 10% Glycerol, and 5 mM $MgCl_2$. This was supplemented with the following inhibitors upon each use: 1 mM DTT (reducing agent), 20 mM β-glycerophosphate (serine-threonine phosphatase inhibitor), 0.1 mM PMSF (serine protease inhibitor), 20 nM okadaic acid (type 1 and type 2A protein phosphatases), and a complete protease inhibitor cocktail for mammalian extracts (Sigma) at a 1:500 dilution. The complete protease inhibitor cocktail constituents and their working concentrations used in this study are: 208 nM AEBSF (serine protease inhibitor), 160 nM Aprotinin (serine protease inhibitor), 8 µM Bestatin (aminopeptidase inhibitor), 2.8 µM E-64 (cysteine protease inhibitor), 4 µM Leupeptin (serine and cysteine protease inhibitor), and 3 µM Pepstatin (acid protease inhibitor).

Cell pellets were thoroughly resuspended in 3 volumes of fresh Lysis Buffer, and incubated on ice for 10 minutes with frequent resuspension. Debris was removed by centrifugation at 20,000 rcf for 10 minutes, and the supernatant was transferred to a clean tube for long-term storage at -80 °C.

2.3.2 Protein sample preparation

Cell lysates were quantified using a Lowry-based DC Protein Assay (BioRad). Using a 96-well plate, 2 µl of each protein lysate was mixed with 30 µl of Reagent A (BioRad) and 200 µl of Reagent B (BioRad), and incubated for 15 minutes. The 96-well plate was then read with the SPECTROstar Nano spectrometer (BMG Labtech) at 650-750 nm, using MARS data analysis software (BMG Labtech). Protein concentrations were interpolated from a BSA standard curve.

The appropriate volume of lysate (typically 2 µg for exogenous proteins, or 5-15 µg for endogenous centrosomal proteins) was added to 4 µl of 4 X Laemmli buffer, completed to 1 X final concentration with distilled water, and boiled at 95°C for 5 minutes.

2.3.3 Co-immunoprecipitation

For co-immunoprecipitation, cell lysates were combined with 10 µg of antibody per 1 mg of lysate and incubated for 2 hours at 4°C on a rotator. In the case of low-expression proteins, such as endogenous proteins or low-expression vectors, the incubation was performed overnight at 4°C. The lysate/antibody mix was then incubated with 10 µl washed slurry of Protein G Sepharose Beads (GE Healthcare) for 1.5 hours at 4°C. The samples were then washed 3 times in Lysis Buffer, and resuspended in 12 µl of 2 X Laemmli buffer.

To enrich for F-box binding proteins, cells were incubated with 1 µM MLN4924 (Millenium Pharmaceuticals) for 5 hours prior to harvesting. MLN4924 inhibits cullin-based E3 ubiquitin ligases, blocking substrate ubiquitylation. This treatment enriches substrate-ligase complexes and substrates of ubiquitin mediated proteasome degradation.

2.3.4 SDS-Polyacrylamide Gel Electrophoresis (SDS-PAGE)

Proteins were resolved using Bolt™ 4-12% Bis-Tris Plus gels (Invitrogen/Life Technologies), alongside a PageRuler protein ladder (Thermo Fisher Scientific, 026616) for reference. Gels were electrophoresed using Bolt™ running chambers (Invitrogen/Life Technologies) at 120 V for 90 minutes, using MES-SDS Running Buffer (Invitrogen/Life Technologies).

2.3.5 Western blotting

Following SDS-PAGE, proteins were then transferred to Immobilon-P PVDF membranes (Millipore). As PVDF is highly hydrophobic, membranes were first activated by submerging in methanol for 1 minute. The transfer was performed using the Bolt™ transfer chambers (Invitrogen/Life Technologies) at 23 V for 2.5 hours. The transfer buffer consisted of 25 mM Tris, 190 mM glycine, and 20% methanol.

PVDF membranes were blocked using 5% skim milk for 1 hour, prior to incubation with primary antibodies for 1 hour at room temperature. Low-expression proteins were detected by incubating the primary antibody overnight at 4°C. Primary antibodies were diluted in 5% skim milk as detailed in Table 2.2. Excess primary antibody was removed by washing three times in PBS-0.1% Tween-20, for 10 minutes per wash. Secondary antibodies coupled to HRP were also diluted in 5% skim milk as detailed in Table 2.3, and incubated for 1 hour at room temperature. Excess secondary antibody was also removed by washing three times in PBS-0.1% Tween-20, for 10 minutes per wash. Western blots were developed using SuperSignal West Pico Chemiluminescent Substrate (Thermo Fisher Scientific) using X-ray films (FujiFilm). A more sensitive reagent, SuperSignal West Femto

Maximum Sensitivity Substrate (Thermo Fisher Scientific), was used for low-expression proteins.

2.3.6 Western blot membrane stripping

PVDF membranes were stripped using an SDS-based stripping buffer containing 60 mM Tris-HCl pH 6.8, 2% SDS, and 0.7% β-mercaptoethanol (added fresh). The membrane was stripped at 50°C for 30 minutes, and then re-blocked in 5% skim milk prior to immunoblot.

2.3.7 Immunofluorescence microscopy

Glass coverslips (Thermo Fisher Scientific) were sterilised in 100% ethanol and air-dried in sterile conditions before depositing at the bottom of 6-well plates. Cells were seeded directly onto the coverslips (100,000 cells per 6-well) and transfected or drug-treated the following day. The coverslips were then fixed 48-72 hours after treatment as appropriate.

Coverslips were gently washed three times with PBS prior to fixation, in either methanol or PFA. For microtubule staining, it is important not to wash cells in cold PBS, as cold-treatment is a common method used to depolymerise microtubules.

Methanol fixation was required for all centrosome staining, as centrosomes are proteinaceous, insoluble, and inaccessible without harsh fixation. For methanol fixation, coverslips were submerged in ice-cold 100% methanol for 5 minutes at -20°C. No permeabilisation step was required following methanol fixation, as organic solvents (such as methanol) also remove lipid content and lipid-linked proteins.

For PFA fixation, coverslips were submerged in 4% PFA in PBS for 8 minutes at room temperature. The samples were then permeabilised using 0.2% Triton X-100 in PBS for 5 minutes at room temperature.

Coverslips were blocked using 5% BSA in PBS for 1 hour. Primary antibodies were diluted in the blocking solution as detailed in Table 2.4, and incubated for 1 hour at room temperature in a wet chamber to prevent evaporation. Excess primary antibody was removed by washing three times with 0.1% Triton X-100 in PBS prior to secondary antibody incubation. Secondary antibodies were diluted in blocking solution as detailed in Table 2.4, and incubated for 1 hour at room temperature. Excess secondary antibodies were removed by washing three times with 0.1% Triton X-100 in PBS. Coverslips were then washed once in double distilled water to dissolve salt crystals, and mounted onto glass slides using ProLong Gold Anti-fade Mountant with DAPI (Invitrogen/Life Technologies). The mountant was allowed to cure at room temperature for 24 hours as suggested by the manufacturer. Finally, coverslips were sealed using clear nail polish. Images were acquired on a Zeiss confocal microscope using Zen 2011 software (Carl Zeiss).

2.3.8 Quantification of centrosome intensity

Fluorescence intensity at centrosomes was quantified using the method outlined by Godinho et al. (2014) using Image J (Figure 2.1). In brief, 50x50 and 80x80 pixel regions were centered over each centrosome. The intensity of fluorescence (integrated fluorescence) was measured for each pixel region. The background fluorescence ($F_{background}$) was obtained by subtracting the integrated value of the smaller 50x50 region (F_I) from the larger 80x80 region (F_O), and normalising to the 50x50 area. Centrosome fluorescence intensity ($F_{Centrosome}$) was then obtained by

subtracting the background value ($F_{Background}$) from the total intensity of the 50x50 region (F_I). The advantage of this approach is that the background is derived from the vicinity of the centrosome, which controls for variations in background fluorescence.

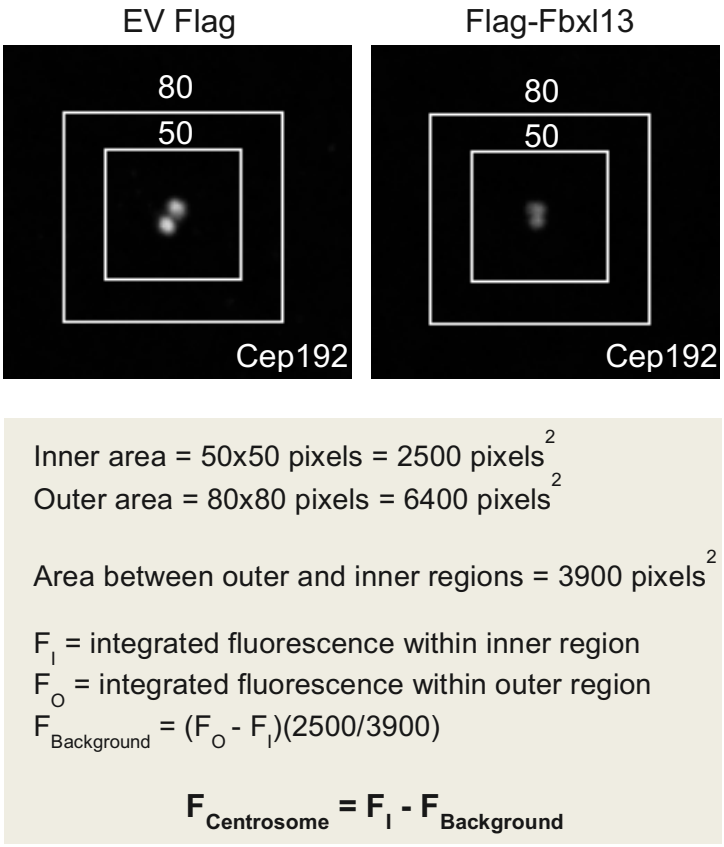

Figure 2.1 Quantification of centrosome intensity

Adapted from *Godinho et al. (2014).*

2.3.9 Flow cytometry

Following 48 hours of transfection, cells were harvested mechanically with scraping and pelleted at 300 rcf for 5 minutes. The cells were then fixed by adding ice cold 70% ethanol to the pellet dropwise, while vortexing. The fixed cells were then pelleted and resuspended in PBS containing PI (10 µg/µl) and RNAse A 100 µg/ml), and incubated at 37°C for 30 minutes. Analysis was carried out for 10,000

cells per sample with the Becton Dickinson FACScan system, using CellQuest Pro and ModFit LT software.

2.4 Molecular biology

2.4.1 Preparation of media and agar plates

Bacterial cultures were grown in LB. This was prepared by dissolving 25 g of LB powder (Sigma) in 1 litre of sterile, double distilled water and autoclaved at 121°C, 15 psi for 30 minutes. LB agar was prepared by dissolving 35 g of LB agar in 1 litre of double distilled water and sterilised by autoclaving. LB agar was then poured by boiling, and allowing to cool to 50°C before supplementing with antibiotics. Approximately 20 ml of liquid LB agar was then poured into sterile 10 cm Petri dishes in a sterile environment, and allowed to set at room temperature prior to storage at 4°C.

2.4.2 Transformation of bacteria

Bacterial transformations for plasmid production were carried out using Gold Efficiency α-Select Competent Cells (Bioline, 85027), an *E. coli* competent strain DH5α with recA1 and endA1 mutations to prevent recombination and digestion. 5 µl of competent cells were thawed on ice prior to addition of 1 µg of DNA, and incubated on ice for 30 minutes. The bacteria were then heat shocked at 42°C for 1 minute, followed by a further 5 minute incubation on ice. 500 µl of LB was then added to the bacteria, and allowed to grow for 30 minutes at 37°C with shaking on an Eppendorf Thermomixer.

2.4.3 Growth of overnight cultures from colonies

A sterile tip was used to pick a single bacterial colony from an LB agar plate. This was placed into 4 ml of LB supplemented with antibiotics in a round-bottomed 14 ml tube, and allowed to grow at 37°C overnight in a shaking incubator.

2.4.4 Agarose gel electrophoresis

DNA analysis was performed using 1% (w/v) agarose gels. Gels were prepared by dissolving 1 g of agarose in 100 ml of 1 X TAE buffer (40 mM Tris, 20 mM acetic acid, 1 mM EDTA). The mixture was heated to boiling point, and then allowed to cool to approximately 50°C prior to the addition of 1 µl ethidium bromide per 25 ml of agarose mixture. DNA samples were diluted with 6 X DNA Gel Loading Dye (Thermo Fisher Scientific) prior to loading, and run alongside a Generuler 1 kb DNA molecular weight marker (Thermo Fisher Scientific). Gel electrophoresis was carried out in 1 X TAE buffer at 8 V/cm, based on the distance between the anode and cathode.

2.4.5 Large-scale preparation (Maxi-preparation) of plasmid DNA

Maxi-preparation of DNA was performed using a Qiagen kit according to the manufacturer's instructions. This method is based on alkaline lysis. In brief, a bacterial cell pellet is lysed in a solution containing sodium hydroxide and SDS. The alkaline sodium hydroxide denatures bacterial DNA – both genomic and plasmid. Upon neutralisation, using a buffer containing acetate, only plasmid DNA can re-anneal due to its much smaller size. Genomic DNA remains precipitated, and can therefore be removed via centrifugation. The plasmid DNA remains in solution, and can be purified using a cation exchange column which binds DNA in low-salt, and is eluted with high salt.

2.4.6 Site-directed mutagenesis

Site directed mutagenesis was carried out using primers designed using the QuikChange® Primer Design Tool (Agilent Technologies) and the high-fidelity polymerase Phusion Hot Start II (New England BioLabs). The PCR mix contained 500 ng of template, 1 M Betaine (Sigma), 125 ng of each forward and reverse primer, 200 µM of each dNTP, 1 U of polymerase, and 1X reaction buffer provided in the kit. The PCR mix was placed into a thermocycler programmed at 98°C for 30 seconds, 55°C for 30 seconds, and 72°C for 1 minute per 2 kb template. The PCR product was then treated with 10 U DpnI (New England BioLabs) and incubated at 37°C for 2 hours to thoroughly digest the parental template. The digest product was then directly transformed into competent DH5α bacteria as outlined in Section 2.4.2, and plated onto LB agar (Sigma) plates containing the appropriate antibiotics. The antibiotic-resistant clones were picked and expanded into 5 ml LB (Sigma) supplemented with antibiotics overnight. The plasmid was extracted using the Qiagen Miniprep kit (Qiagen) and sent for Sanger sequencing (Source BioScience).

2.4.7 Determination of DNA purity and concentration

DNA concentration was determined by measuring the optical density (OD) at A_{260} using the SPECTROstar Nano spectrophotometer (BMG LabTech). Generally, a dsDNA sample of 1 µg/µl has an A_{260} of 50. An A_{260}/A_{280} ratio of ≥1.8 was used to confirm that the DNA was free from protein contamination.

2.4.8 RNA extraction and purification

Total RNA was extracted from cell samples using the RNeasy Mini Kit (Qiagen), in combination with DNase I (Qiagen),

2.4.9 Determination of RNA purity and concentration

RNA concentration was determined by measuring the optical density (OD) at A_{260} using the SpectroStar Nano spectrophotometer (BMG Labtech). Generally, an A_{260} of 1 is equivalent to ~ 40 µg/µl RNA. An A_{260}/A_{280} ratio of ≥2.0 was used to confirm that the RNA was free from protein contamination.

2.5 Quantitative real-time PCR

2.5.1 Reverse transcription

cDNA synthesis was performed with SuperScript III First-Strand Synthesis SuperMix for qRT-PCR (Invitrogen/Life Technologies) following the manufacturer's instructions. The cDNA was then diluted 1:4 for quantitative real-time PCR (qPCR).

2.5.2 qPCR Reaction

Custom Fbxl13 qPCR primers were designed to span 200 bp regions. The Fbxl13 isoform 3 specific primers were designed by using a forward primer that spanned a spliced region specific to this isoform. Specificity was checked using Primer-BLAST, and validated by checking for a single melting curve. Relative quantities of mRNA were normalised using GAPDH as a control.

qPCR was performed using SYBR Select Master Mix (Invitrogen/Life Technologies) the ABI7500 machine (Applied Biosystems), and the 7500 FastReal-Time PCR system (Applied Biosystems) software version v.2.0.3. Software analysis provided the cycle threshold (Ct value). The relative quantities of mRNA (RQ value) between samples was determined using the comparative Ct method, using the following equations:

$$\Delta Ct = Ct_{gene} - Ct_{GAPDH}$$

$$\Delta\Delta Ct = \Delta Ct_{control} - \Delta Ct_{treatment}$$

$$RQ = 2^{\Delta\Delta Ct}$$

Equation 2.3 Comparative Ct method of qPCR analysis

2.6 Liquid chromatography-tandem mass spectrometry

Fbxl13 LC-MS/MS was performed by Dr Vincenzo D'Angiolella using an in-house protocol established for F-box proteins (Raducu et al., 2016). In brief, Flag-Fbxl13 isoforms 1 and 3 were transfected in HEK293T cells for 48 hours. Prior to harvesting, cells were treated with 2 μM of MLN4924 for 5 hours in order to enrich E3 ligase-substrate complexes, and enrich substrates of ubiquitin-proteasome degradation. The HEK293T cells were then lysed, and the Flag-Fbxl13 was purified using Anti-Flag M2 affinity gel beads (Sigma). The co-immunopurified material was then eluted by competition using Flag peptide (Sigma). Supernatant material was processed in collaboration with Professor Benedikt M Kessler (Target Discovery Institute, University of Oxford). There, the eluted material was subject to two rounds of chloroform-methanol precipitation. Samples were then resuspended in 6 M urea, 100 mM ammonium acetate pH ~8 and subjected to in-solution trypsin digestion. The digested peptides were analysed using a Nano-Acquity-UPLC (Waters) coupled to an Orbitrap Velos tandem mass spectrometer (Thermo Scientific) as described (Raducu et al., 2016). The LC-MS/MS data were processed using published guidelines and the spectra compared against the SwissProt database (UniProt_SwissProt, human 20,353 sequences).

The resulting LC-MS/MS data were then processed in-house by subtracting agarose binding proteins downloaded from the Contaminant Respository for Affinity Purification (http://www.crapome.org/), and subtracting interactors identified in other F-box protein LC-MS/MS results (for Fbxl7, Fbxl17, and Fbxo1/Cyclin F) available in our lab.

2.7 Statistical analysis

Quantitative analysis of band intensity was performed using Image J. Data are reported as mean ± SD. Statistical analysis was carried out using GraphPad Prism 6 (GraphPad Software Inc.). Differences between groups were compared using unpaired Student's t-test. Statistically insignificant results are indicated as ns for $P>0.05$. Statistically significant results are indicated as * for $P\leq0.05$, ** for $P\leq0.01$, *** for $P\leq0.001$, and **** for $P\leq0.0001$.

2.8 Custom antibody production

2.8.1 Recombinant protein production

Several constructs were tested for solubility. We first cloned the full-length Fbxl13 protein for both isoforms into a pET His6 GST LIC Cloning Vector (Addgene, Plasmid 29655) using Ligation Independent Cloning (Aslanidis and de Jong, 1990). A small-scale protein induction (see Protein Purification) indicated that the recombinant proteins were highly insoluble (data not shown). Shorter 200-300 amino-acid length fragments of the N and C terminals of both isoforms were then tested, and a 248 amino-acid peptide of the Fbxl13-3 C terminal was most soluble. This construct was carried forward for large scale purification.

2.8.2 Protein purification

Recombinant Fbxl13 constructs were transformed into *E. coli* BL21 (DE3) by heat-shock. Single colonies were picked into 100 ml LB supplemented with 50 µg/µl kanamycin and incubated overnight at 37°C with shaking. This starter culture was then diluted 1:100 into 1 L LB supplemented with kanamycin, and incubated at 37°C with shaking until an OD600 of 0.5 was reached. Protein production was then induced with 10 µM isopropyl β-D-1-thiogalactopyranoside (IPTG). Induced flasks were incubated for 3 hours in a 30°C shaker.

Cells were then pelleted at 6000 rcf for 15 minutes, and resuspended in 20 ml Lysis Buffer per 1 L of culture and lysed for 30 minutes on ice (see Table 2.10). Lysates were sonicated for 5 x 10 seconds with 10 second rests, and then clarified by centrifuging for 10 minutes at 20,000 rcf.

Lysates were then purified using the ÄKTA Start system (GE Healthcare) using a GSTrap HP 1 mL column (GE Healthcare). The column was primed using 5 column volumes (CV) of Binding Buffer (see table of buffers), washed with 20 CV of Binding Buffer, and eluted with 20 CV of Elution Buffer (see Table 2.10). Fractions were analysed by SDS-PAGE, and dialysed overnight using Slide-A-Lyzer 7K Dialysis Cassettes (Thermo Fisher Scientific). Protein concentrations were determined by SpectroStar Nano (BMG Labtech) Uv/Vis absorbance at 650-750 nM using Lowry-based DC Protein Assay (BioRad), or as compared to BSA standards on SDS-PAGE.

Table 2.10 Buffer recipes for protein purification

Lysis Buffer	GSTrap Binding Buffer	GSTrap Elution Buffer
10 % sucrose	50 mM Tris-HCl pH 8.0	50 mM Tris-HCl pH 8.0
50 mM Tris-HCl pH 8.0	300 mM NaCl	200 mM NaCl
150 mM NaCl	0.1% NP-40	25 mM L-Glutathione
0.5 % NP-40	5 mM DTT	
5 mM DTT		
Complete protease inhibitor (Roche)		
150 µg/ml lysozyme		

2.8.3 IgG purification

5 mg of recombinant GST-tagged protein was sent to Cambridge BioChemicals to immunise two rabbits over 77-days. We received two harvest bleeds that we purified using a two-step protocol.

The bleeds were first purified for IgGs. We first centrifuged the bleeds at 20,000 rcf for 10 minutes to remove debris, and diluted them 1:1 with Binding Buffer (100 mM sodium phosphate, 50 mM NaCl pH 7.2). We purified the bleeds using the ÄKTA Start system (GE Healthcare) with a HiTrap Protein A HP 1.0 ml column (GE Healthcare). The column was primed with 5 CV Binding Buffer, washed with 10 CV Binding Buffer, and eluted with 10 CV Elution Buffer (100 mM Glycine pH 3.5) in 1 ml fractions. We added 100 µl of Tris-HCl pH 7.5 to each 1 ml of eluate to neutralise the pH. Fractions containing IgGs were determined using SDS-PAGE and coomassie staining. The IgG containing fractions were then pooled and dialysed overnight in PBS, using Slide-A-Lyzer 7K Dialysis Cassettes (Thermo Fisher Scientific).

2.8.4 GST-antibody subtraction

The second step of rabbit-serum purification was to remove any antibodies recognising the GST-tag. We did this by passing the purified IgGs through homemade GST-bound beads. We first induced *E. coli* BL21 expressing the empty pET HIS6 GST vector to produce GST antigen, which was then enriched using Glutathione Sepharose 4B beads (GE Healthcare). The GST-bound beads were placed in a Poly-Prep Chromatography Column (BioRad), and the antibody was passed through by gravity-flow. All the flow-through was collected, and the new antibody concentration was determined by Lowry-based DC Protein Assay (BioRad). The quality of the purified antibody was determined by immunoblot.

3 Results I

Identification of centrosomal interactors and potential substrates of Fbxl13

3.1 Introduction

In recent years, our lab has focused on investigating F-box proteins involved in tumour progression. F-box proteins are the specificity factors of the SCF (Skp-Cullin-F-box) family of E3 ubiquitin ligases. As F-box proteins are characterised by their high substrate specificity, they have also served as research targets for anti-cancer therapies, such as Compound 25 (for Skp2/Fbxl1) and UB Pharma (for β-TrCP/Fbxw1) (reviewed in Skaar et al. (2014)). The human genome encodes for 69 human F-box proteins, and since their discovery, many have been found to have oncogenic or tumour suppressive properties (Skaar et al., 2009). For example, our lab has recently identified that Fbxl17 (F-box and leucine-rich repeat protein 17) has an oncogenic role in medulloblastoma, by targeting the tumour suppressor Sufu for degradation (Raducu et al., 2016). However, many F-box proteins remain uncharacterised.

In this study, we aim to characterise the orphan F-box protein Fbxl13 (F-box and leucine-rich repeat protein 13). Several genome-wide screens have implicated Fbxl13 in processes such as ionising radiation (IR) sensitivity, genomic instability,

and cell proliferation, although these effects were not validated (Beronja et al., 2013; Cron et al., 2013; Hurov et al., 2010; Paulsen et al., 2009). We therefore wish to investigate whether Fbxl13 does indeed have oncogenic functions. However, the interactors of Fbxl13 are unknown. Thus, the aim of this first chapter is to identify and validate Fbxl13 interactors, in order to facilitate the identification of its substrates and functions.

3.2 Results

3.2.1 Identification of Fbxl13 interactors

To address the function of Fbxl13, we first attempted to identify interactors of Fbxl13 using liquid chromatography tandem mass spectrometry (LC-MS/MS). Mass spectrometry is an analytical technique that can identify the protein composition of a biological sample. The principle of mass spectrometry is that peptides of different amino acid composition have distinct mass/charge ratios when ionised. In this way, proteins can be identified from predicted mass/charge signatures (spectra). These can be so specific that the match of several peptide fragments is sufficient to identify the full protein (reviewed in Alberts et al. (2015)). Following denaturation and trypsinisation steps, peptides are then processed through the mass spectrometer. Here, they undergo ionisation, vaporisation, and acceleration through a vacuum under a varying electric field towards a detector. Separation of a trypsinised sample using liquid chromatography prior to mass spectrometry can lower the complexity of the sample, and yield cleaner spectra. Proteins can then be identified based on known signature spectra from different species databases.

As no commercial antibody was available at the time, the analysis was performed on exogenous 3xFlag-tagged Fbxl13. At the time, only two isoforms of Fbxl13 were

listed on UniProt (Figure 3.1), currently named Fbxl13 isoform 1 (Fbxl13-1) and isoform 3 (Fbxl13-3). These are generated by alternative splicing across exon 16, and results in a 45 amino acid deletion in the leucine-rich C terminal region. As F-box proteins typically target substrates through their variable C terminal regions – for example for Fbxo1/Cyclin F and Fbxl17 (D'Angiolella et al., 2010; Raducu et al., 2016) – we speculate that Fbxl13-1 and Fbxl13-3 may have different substrate pools. For this reason, LC-MS/MS analysis was performed on both Fbxl13 isoforms 1 and 3. At the time of writing, there are two additional isoforms of Fbxl13 listed on UniProt (Figure 3.1), isoforms 2 and 4, which also vary in the C terminal region and arise from alternative splicing. We do not exclude the possibility that Fbxl13-2 and Fbxl13-4 may also have substrate specific functions.

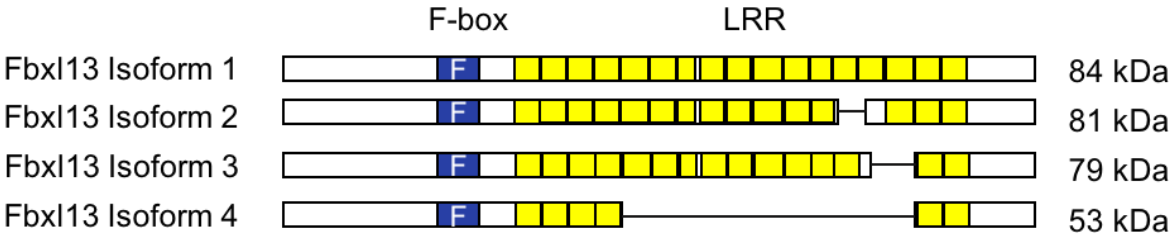

Figure 3.1 The four isoforms of Fbxl13

Scheme representing the four isoforms of Fbxl13 (UniProt Q8NEE6). The isoforms are generated by alternative splicing. The F-box domain is highlighted in blue and leucine rich repeats (LRR) in yellow.

The strategy for Fbxl13 interactor identification is outlined in Figure 3.2, and was performed by Dr Vincenzo D'Angiolella using an in-house protocol briefly described below (Raducu et al., 2016). 3xFlag-tagged Fbxl13-1 or Fbxl13-3 were transiently overexpressed in HEK293T cells for 48 hours. These cells were chosen as they have a high transfection efficiency, and produce large quantities of protein. Prior to harvesting, the cells were additionally treated with 2 μM of MLN4924 for 5 hours. MLN4924 inhibits the NEDD8-activating enzyme (NAE) that modifies and allows the activity of cullin-RING type E3 ubiquitin ligases, such as Skp-Cullin-F-box (SCF) E3 ubiquitin ligases (Soucy et al., 2009). Hence, MLN4924 treatment prevents the potential degradation of any ubiquitylated substrates. This improves our LC-MS/MS strategy in two ways. Firstly, as the ubiquitylation process is blocked, the E3-ligase-substrate complex is enriched. Typically, substrate binding is transient, and released once ubiquitylated (reviewed in Harper and Tan (2012)). By blocking ubiquitin transfer, MLN4924 prevents substrate release and increases the capture rate of transient Fbxl13 interactors. Secondly, any potential Fbxl13 substrates targeted for ubiquitin-proteasome degradation will no longer be degraded. MLN4924 treatment will ensure that any degraded substrates will still be represented in the LC-MS/MS data. This is a preventative measure, as there could be many alternative outcomes of substrate ubiquitylation. We note that the published high-throughput LC-MS/MS screen for all 22 human Fbxl proteins was also conducted in the presence of MLN4924 (Tan et al., 2013).

The exogenous Flag-Fbxl13 was then co-immunopurified from HEK293T whole cell extract using Flag M2 Affinity Agarose Gel, and eluted by competition using Flag peptide. The resulting eluate was processed for LC-MS/MS in collaboration with Professor Benedikt M Kessler at the Target Discovery Institute, University of Oxford.

In brief, proteins were precipitated from the supernatant material using two rounds of chloroform-methanol precipitation. They were then denatured using urea, and digested using trypsin into small peptide fragments. Peptides were desalted using an affinity column based approach. The separation of peptides using nano-liquid chromatography prior to mass spectrometry can result in a lower sample complexity, and higher resolution of peptide spectra. These spectra were then converted into Mascot generic files, which were then searched against the UniProt SwissProt *H. sapiens* database (20,353 sequences). I then processed these LC-MS/MS data using an unbiased two-step strategy (Figure 3.3).

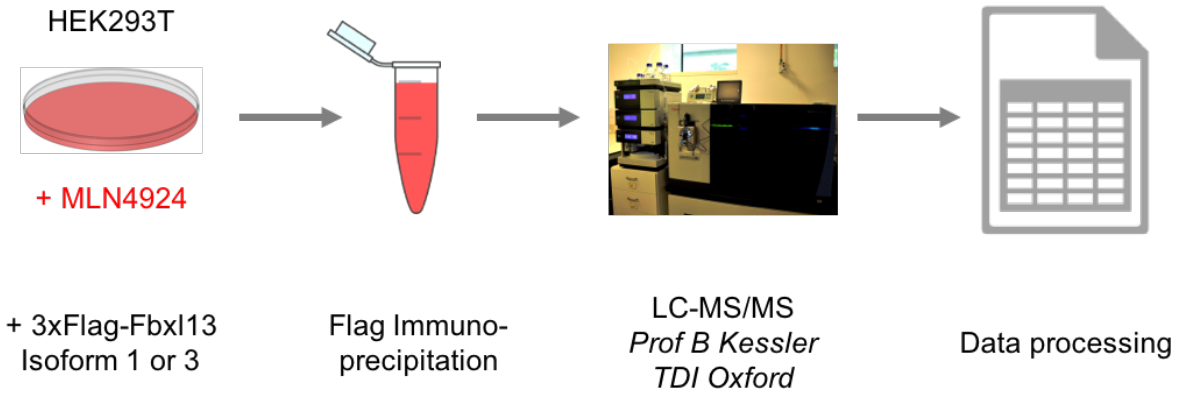

Figure 3.2 Strategy of liquid chromatography tandem mass spectrometry

3xFlag-Fbxl13 isoforms 1 or 3 were transiently overexpressed in HEK293T cells for 48 hours. Samples were treated with MLN4924 (2 μM) for 5 hours prior to collection. Flag-Fbxl13 was then immunopurified from whole cell extract using Flag M2 Affinity Gel, and eluted with Flag peptide. Three biologically independent eluate samples were then processed by Professor Benedikt M Kessler at the Target Discovery Institute, University of Oxford. 3xFlag-Fbxl13 isoforms 1 and 3 were cloned by Dr Nuti Raducu, and three independent purifications were performed by Dr Vincenzo D'Angiolella.

Firstly, agarose-binding proteins were subtracted from our data to remove false-positives. Using the Contaminant Repository for Affinity Purification v1.1 (Mellacheruvu et al., 2013), 30 individual datasets were downloaded for HEK293T whole cell extract affinity purified with Flag M2 agarose beads. These 30 datasets comprised 2,850 unique agarose-binding proteins, which were used as a negative control. The original LC-MS/MS data for Fbxl13-1 totalled 125 interactors. After subtracting agarose-binding proteins, this number was reduced to 43 (Figure 3.3). Similarly, the original LC-MS/MS data for Fbxl13-3 totalled 169 interactors, which was reduced to 48. The large number of proteins subtracted at this stage consisted of mostly heat-shock proteins, ribosomal subunits, and tubulin subunits. We expected the resulting lists to represent only specific immunopurified material. Indeed, prior to subtraction, the two highest scoring protein interactors for both Fbxl13-1 and Fbxl13-3 were heat-shock proteins (HSPA1A and HSPA8). Following subtraction, the top scoring protein was Fbxl13 itself. One drawback of this subtraction step was its stringency. Any proteins present on the list of 2,850 agarose-binding proteins was removed from our LC-MS/MS data regardless of their abundance in our data. This could lead to Type II errors (false negatives). Indeed, the known F-box interactor Skp1 had a score of 526 in the Fbxl13-1 and 440 in the Fbxl13-3 data, however was subtracted as it was present in 1 of the 30 agarose-binding repository datasets. However, due to this level of stringency, we were confident that the Type I error rate (false positives) would be low.

To further enrich our LC-MS/MS data, the data were filtered against three other LC-MS/MS datasets available in our laboratory: Fbxl7 interactors (262 hits, total), Fbxl17 interactors (205 hits, total), and Fbxo1/CCNF interactors (225 hits, total) (Figure 3.3). By subtracting other F-box binding proteins, we reasoned that the

remaining proteins would represent only unique Fbxl13 interactors and substrates. All three datasets were prepared using the same protocol as for Fbxl13, and therefore comparable. This second data processing step narrowed down the list of Fbxl13-1 interactors from 43 to 25 (Table 3.1). For Fbxl13-3, the list of interactors was narrowed down from 48 to 21 (Table 3.2). The common interactors removed at this stage included molecular chaperones (eg. BAG3 and BAG5). The known F-box interacting protein Skp1 would have also been removed at this stage, had it not been subtracted as an agarose-binding protein.

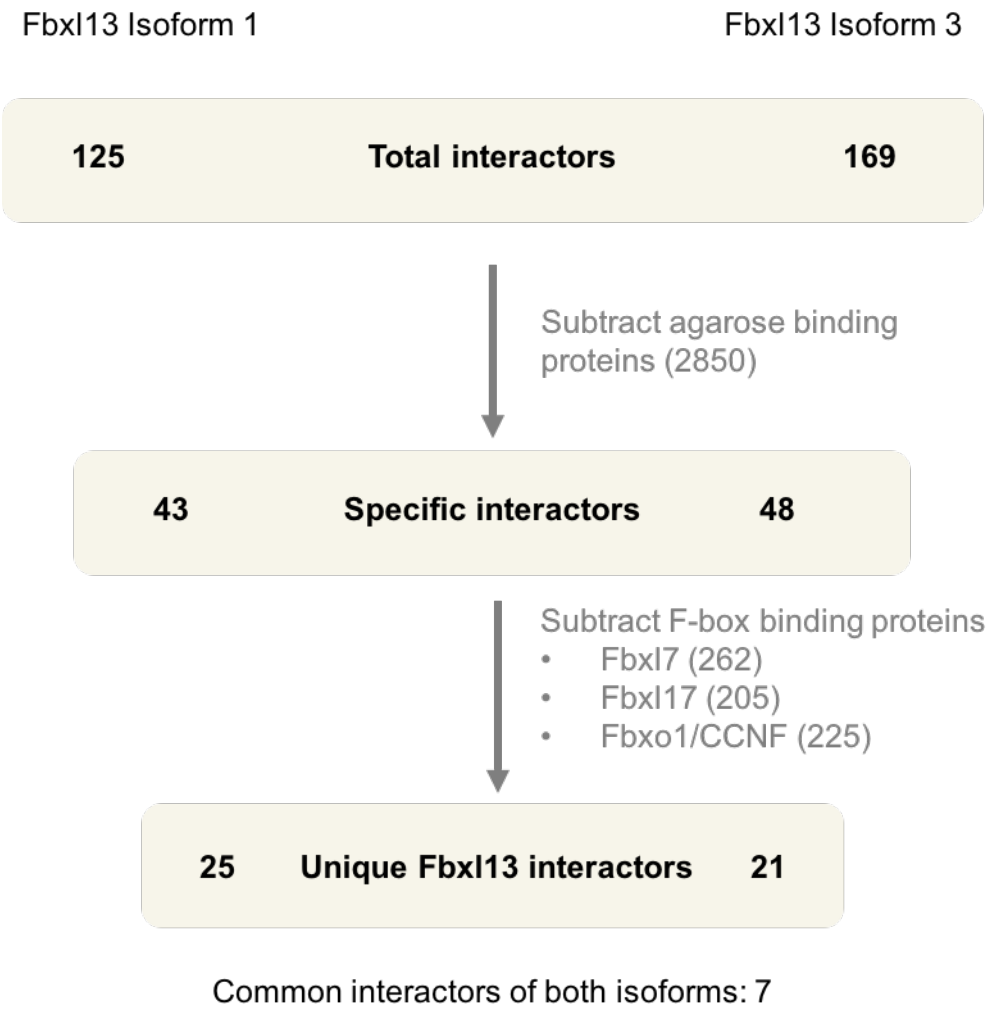

Figure 3.3 Strategy of LC-MS/MS data processing

The total number of interactors by LC-MS/MS is shown at the top, for Fbxl13 isoform 1 on the left, and isoform 3 on the right. Data were first processed by filtering from a repository of agarose binding proteins (2,850) (Mellacheruvu et al., 2013), leaving specific interactors. The data was then subtracted against LC-MS/MS data for three other F-box proteins (Fbxl7, Fbxl17, and Fbxo1/CCNF) available in our laboratory. This left only 25 unique Fbxl13 interactors for isoform 1 (Table 3.1), and 21 for isoform 3 (Table 3.2). The two isoforms had an intersection of 7 common interactors.

Table 3.1 Proteins associated with Fbxl13 isoform 1 identified by LC-MS/MS

Accession	Score	Mass	# matches	# sig. matches	# seq.	# sig. seq.	emPAI	Description
Q8NEE6	7043	85751	501	332	52	47	10.27	F-box/LRR-repeat protein 13
P41208	2182	19726	206	103	11	11	12.81	Centrin-2
O15182	589	19538	51	30	7	5	2.12	Centrin-3
O60749	44	58549	3	1	2	1	0.07	Sorting nexin-2
Q9UPN7	40	97291	3	3	2	2	0.08	Serine/threonine-protein phosphatase 6 regulatory subunit 1
Q9UPW5	38	139786	10	4	3	1	0.03	Cytosolic carboxypeptidase 1
O94986	32	197899	9	3	4	1	0.02	Centrosomal protein of 152 kDa
Q8WZA2	26	116474	4	1	1	1	0.03	Rap guanine nucleotide exchange factor 4
E9PAV3	25	205979	3	1	3	1	0.02	Nascent polypeptide-associated complex subunit alpha, muscle-specific form
P51587	24	388296	11	2	2	1	0.01	Breast cancer type 2 susceptibility protein
Q8N365	23	41702	3	1	3	1	0.09	Circadian-associated transcriptional repressor
Q17RB8	22	88494	4	2	3	1	0.04	LON peptidase N-terminal domain and RING finger protein 1
Q9NZJ4	21	526497	55	1	7	1	0.01	Sacsin
Q6NVU6	21	15335	6	2	1	1	0.27	Inactive Ufm1-specific protease 1
Q14005	20	142976	48	1	2	1	0.03	Pro-interleukin-16
Q9H2P0	19	124854	3	1	3	1	0.03	Activity-dependent neuroprotector homeobox protein
P36888	19	114712	2	1	2	1	0.03	Receptor-type tyrosine-protein kinase FLT3
P20929	18	775393	37	1	10	1	0	Nebulin
Q86SS6	17	56894	8	1	1	1	0.07	Synaptotagmin-9
Q8NGW1	17	37949	101	1	1	1	0.1	Olfactory receptor 6B3
Q8N2E2	16	183221	19	2	2	1	0.02	von Willebrand factor D and EGF domain-containing protein
Q92621	16	230171	3	1	2	1	0.02	Nuclear pore complex protein Nup205
Q9P2M7	16	136532	2	1	2	1	0.03	Cingulin
O43174	14	56961	1	1	1	1	0.07	Cytochrome P450 26A1
Q9HBW1	13	73526	30	1	2	1	0.05	Leucine-rich repeat-containing protein 4

The table represents the Fbxl13 isoform 1 (Fbxl13-1) interactors from three independent 3xFlag-tagged Fbxl13-1 immunoprecipitation experiments followed by liquid chromatography tandem mass spectrometry (LC-MS/MS). The data were processed by subtracting agarose-binding proteins and interactors of 3 unrelated F-box proteins (Fbxl7, Fbxl17, Fbxo1/CCNF). Results were scored according to a probability-based Mowse Score of -10*Log(*P*), where *P* is the probability that the matched peptide is a random event. “Sig.” means significant. Common interactors with Fbxl13-3 are highlighted in grey.

Table 3.2 Proteins associated with Fbxl13 isoform 3 identified by LC-MS/MS

Accession	Score	Mass	# matches	# sig. matches	# seq.	# sig. seq.	emPAI	Description
Q8NEE6	8243	85751	684	423	47	45	10.29	F-box/LRR-repeat protein 13
P41208	1587	19726	137	61	9	8	5.53	Centrin-2
O15182	527	19538	59	29	8	4	1.58	Centrin-3
Q9UPW5	32	139786	10	3	4	1	0.03	Cytosolic carboxypeptidase 1
O94986	31	197899	5	2	2	1	0.02	Centrosomal protein of 152 kDa
Q9NZL4	29	40190	3	1	2	1	0.1	Hsp70-binding protein 1
Q17RB8	29	88494	5	3	2	1	0.04	LON peptidase N-terminal domain and RING finger protein 1
Q9UDR5	26	102808	5	1	2	1	0.04	Alpha-aminoadipic semialdehyde synthase, mitochondrial
P08183	26	141788	1	1	1	1	0.03	Multidrug resistance protein 1
Q9H5Z6	23	51613	2	1	2	1	0.08	Protein FAM124B
Q9NPA8	23	11635	2	1	2	1	0.37	Transcription and mRNA export factor ENY2
Q9H078	23	79193	5	1	5	1	0.05	Caseinolytic peptidase B protein homolog
Q9NZL6	20	87616	5	1	2	1	0.04	Ral guanine nucleotide dissociation stimulator-like 1
P78426	19	37883	6	1	1	1	0.1	Homeobox protein Nkx-6.1
Q6NVV1	18	12184	7	1	2	1	0.35	Putative 60S ribosomal protein L13a protein RPL13AP3
P50616	17	38245	2	1	1	1	0.1	Protein Tob1
P36888	16	114712	1	1	1	1	0.03	Receptor-type tyrosine-protein kinase FLT3
Q5TEZ5	16	38757	3	1	1	1	0.1	Uncharacterized protein C6orf163
Q9NVL8	15	34726	2	1	2	1	0.11	Uncharacterized protein C14orf105
Q7Z3Z3	14	101995	8	1	1	1	0.04	Piwi-like protein 3
P17516	14	37442	1	1	1	1	0.11	Aldo-keto reductase family 1 member C4

The table represents the Fbxl13 isoform 3 (Fbxl13-3) interactors from three independent 3xFlag-tagged Fbxl13-3 immunoprecipitation experiments followed by liquid chromatography tandem mass spectrometry (LC-MS/MS). The data were processed by subtracting agarose-binding proteins and interactors of 3 unrelated F-box proteins (Fbxl7, Fbxl17, Fbxo1/CCNF). Results were scored according to a probability-based Mowse Score of -10*Log(*P*), where *P* is the probability that the matched peptide is a random event. “Sig.” means significant. Common interactors with Fbxl13-1 are highlighted in grey.

The two-step data subtraction resulted in a short list of specific interactors for Fbxl13-1 and Fbxl13-3 (Table 3.1 and Table 3.2). We observed that there was an overlap of 7 proteins between the two Fbxl13 isoforms, highlighted in grey. The substantial number of isoform-specific interactors suggests that Fbxl13-1 and Fbxl13-3 may have specialised roles, for example due to tissue specificity.

Strikingly, the top scoring interactors for both isoforms were Centrin-2 and Centrin-3. Both Centrin-2 and Centrin-3 localise to the lumen of centrioles (Paoletti et al., 1996; Sawant et al., 2015). Whilst Centrin-2 is dispensable for centriole duplication, its depletion attenuated the centriole duplication process as measured by CP110 incorporation in S phase (Yang et al., 2010). In contrast, Centrin-2 overexpression resulted in centriole overduplication. This was dependent on phosphorylation by Mps1 (Yang et al., 2010). In contrast, Centrin-3 was found to inhibit Mps1 and antagonise Centrin-2 activity (Sawant et al., 2015). Centrin-2 also has a role in nucleotide excision repair (Araki et al., 2001). It is important to note that both Centrin-2 and Centrin-3 were also identified, but not validated, as Fbxl13-2 interactors in a high-throughput LC/MS screen of all the Fbxl proteins, supporting the validity of our approach (Tan et al., 2013).

Additionally, we also identified Centrosomal protein of 152 kDa (Cep152) as a potential Fbxl13 interactor. Cep152 is a highly conserved, core component of the centriole duplication pathway (Blachon et al., 2008). Unlike Centrin-2 and Centrin-3, Cep152 is indispensable for centriole duplication, and was not previously identified as a potential Fbxl13 interactor. We also noted that Centrin-2, Centrin-3, and Cep152 are high-scoring, common interactors of both Fbxl13 isoforms, and predict that they may underlie a common function of different Fbxl13 isoforms. We

do not exclude that the other candidate interactors may also represent Fbxl13 regulators and substrates, however due to the high enrichment of centrosomal proteins in our LC-MS/MS data, we considered the centrosomal role of Fbxl13 worth further investigation.

3.2.2 Validation of Fbxl13 centrosomal interactors

In the previous section, our lab identified novel interactors of Fbxl13 using LC-MS/MS. Through data processing, we narrowed down our list of interactors to Fbxl13-specific proteins for both isoforms 1 and 3. Amongst these lists, three centrosomal proteins were highly represented: Centrin-2, Centrin-3, and Cep152. As these proteins were amongst the top scoring in our data, and because Centrin-2 and Centrin-3 were previously independently identified in a high-throughput screen (Tan et al., 2013), we investigated these candidates further. The focus of this next section is therefore to validate the interaction of Fbxl13 isoforms 1 and 3 with these centrosomal proteins using co-immunoprecipitation.

Flag-tagged Fbxl13 isoforms 1 and 3 were immunopurified from HEK293T whole cell extract. The samples were also treated with 2 μM MLN4924 for 5 hours prior to harvesting, to enrich for Fbxl13 interactors. Three other F-box proteins with leucine rich repeats (Fbxl1, Fbxl2, and Fbxl3) were used as negative controls to ensure that our interactors were Fbxl13 specific. The immunopurified material was resolved using SDS-PAGE, and Western blotted for Centrin-2, Centrin-3, Cep152, and Cep192. Cep192 is a known Cep152 cofactor: it recruits Cep152 to the centrosome for centriole duplication in the G1 phase of the cell cycle, where they are both required to fully recruit and organise Plk4 and Sas-6 (Kim et al., 2013; Sonnen et al., 2013).

Endogenous Centrin-2, Centrin-3, and Cep192 were all detected in the immunoprecipitated material of Fbxl13 isoforms 1 and 3 (Figure 3.4). None of these proteins were detected in the immunoprecipitated of Fbxl1, Fbxl2, or Fbxl3, suggesting that their binding is Fbxl13 specific. The binding affinity of the two isoforms of Fbxl13 to these proteins did not appear to differ. These data corroborated our LC-MS/MS results, and are consistent with the published high-throughput screen of Fbxl protein interactors (Tan et al., 2013).

On the other hand, endogenous Cep152 could not be detected by Western blotting (data not shown). To overcome this problem, I attempted to co-immunopurify exogenous Cep152 with Flag-Fbxl13. For this experiment, we kindly received a Myc-tagged Cep152 construct from Professor Erich Nigg. Myc-Cep152 was co-transfected into HEK293T cells with either Fbxl13-1, Fbxl13-3, or an empty vector control. Both isoforms of Flag-Fbxl13 could be detected following Myc-Cep152 pull-down (Figure 3.5). This suggests that Fbxl13 and Cep152 are also valid interactors, as our LC-MS/MS data suggest.

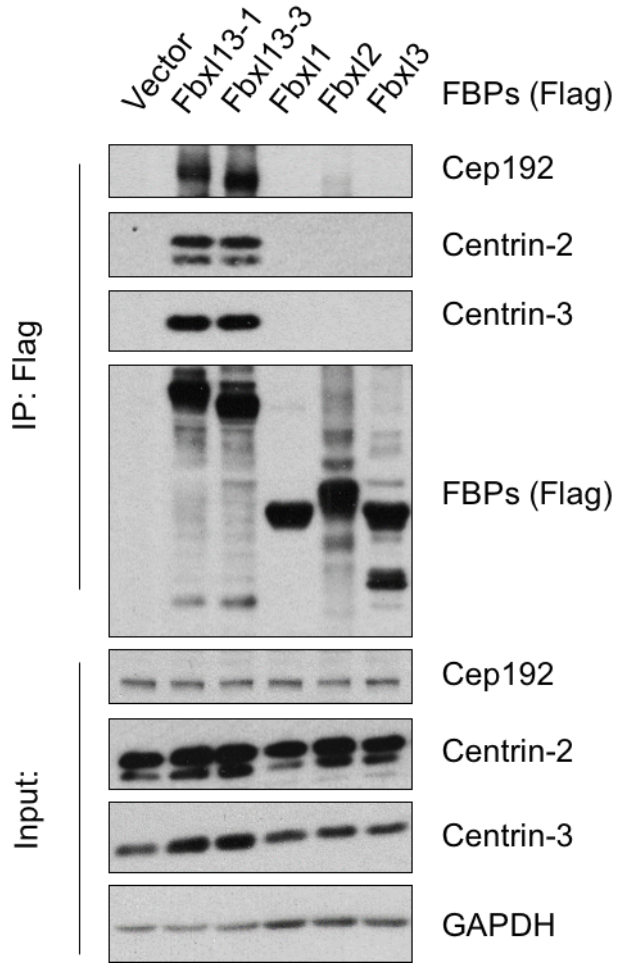

Figure 3.4 Validation of Fbxl13 interactors Cep192, Centrin-2, and Centrin-3

Detection of Cep192, Centrin-2, and Centrin-3 after immunoprecipitation of the indicated Flag-tagged F-box proteins (FBPs) in HEK293T cells. An empty vector (Vector) was used as a negative control. HEK293T cells were treated with MLN4924 (2 μM) for 5 hours prior to collection. N=3 biological replicates.

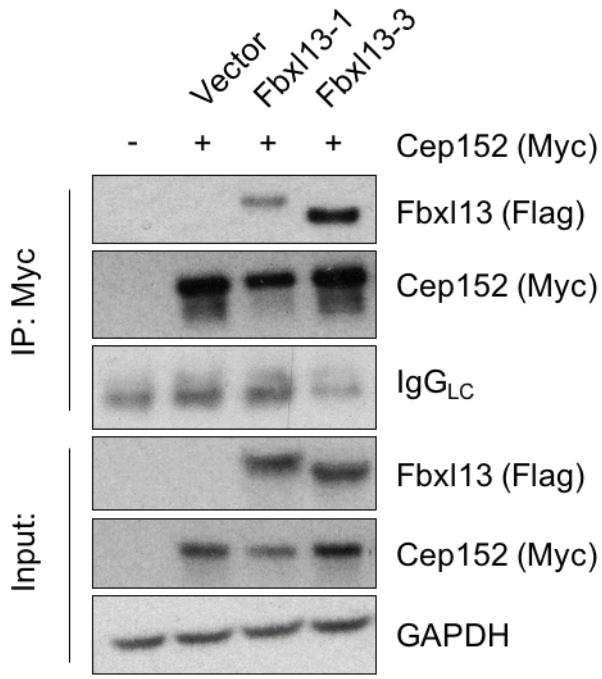

Figure 3.5 Validation of Fbxl13 and Cep152 interaction

Detection of Flag-tagged Fbxl13 after immunoprecipitation of Myc-tagged Cep152 in HEK293T cells. An empty vector (Vector) was used as a negative control. HEK293T cells were treated with MLN4924 (2 μM) for 5 hours prior to collection. N=2 biological replicates.

Taken together, these data support our LC-MS/MS findings, and suggest that Fbxl13 isoforms 1 and 3 indeed interact with Centrin-2, Centrin-3, Cep152. Additionally, we also observed that a fourth centrosomal protein, endogenous Cep192, was also able to specifically interact with Fbxl13. Although Cep192 was not identified in our LC-MS/MS data, we confirmed their interaction *in vivo*. The lack of identification could be due a lack of abundance of Cep192 in the original sample. It is worth noting at this point that from these experiments alone, we cannot exclude that these interactions could be indirect.

We also observed from these experiments that Fbxl13 overexpression upregulated Centrin-2 and Centrin-3 protein levels (Figure 3.4, Inputs), whereas Fbxl13-1 downregulated Myc-Cep152 levels (Figure 3.5, Lane 3 Inputs). However, these samples were treated with MLN4924. As one of the major aims of this study was to identify Fbxl13 ubiquitylation substrates, the next aim was to confirm these effects in the absence of MLN4924, and ask whether this could help us to identify Fbxl13 substrates, and subsequent function.

3.2.3 Identification of potential substrates of Fbxl13

To address how Fbxl13 overexpression would affect the protein levels of our identified interactors, I wished to overexpress Fbxl13 in a cell line which had low levels of Fbxl13. As there was no commercially available Fbxl13 antibody at the time, I tested Fbxl13 expression levels using quantitative real-time PCR (qPCR). This strategy, though informative, is limited to the transcript-level expression of Fbxl13. Whilst this is often a good reflection of protein-level expression, we bear in mind that mRNA-to-protein levels are not always one-to-one.

Isoform-specific qPCR primers against Fbxl13-1 and Fbxl13-3 were designed against exon-exon sequences spanning isoform-specific spliced regions. Using these primers, I tested the Fbxl13 expression level two cell lines: HEK293T, as they were used in our LC-MS/MS screening, and U2OS, a commonly used cell line to study centrosome biology. I found that Fbxl13-1 was much more highly expressed in U2OS cells than in HEK293T cells (Figure 3.6, left panel), as was Fbxl13-3 (data not shown). Therefore, I asked how increased Fbxl13 levels in HEK293T would affect Centrin-2, Centrin-3, Cep152, and Cep192 levels.

Either Fbxl13-1 or Fbxl13-3 were overexpressed in HEK293T cells, lysed into whole cell extract, and resolved by SDS-PAGE. The samples were not treated with MLN4924 to avoid masking any effects of Fbxl13-mediated ubiquitylation. We observed that Fbxl13 overexpression of either isoform downregulated Cep152 and Cep192, and upregulated Centrin-2 and Centrin-3 (Figure 3.6, right panel). The effects of both Fbxl13 isoforms were comparable.

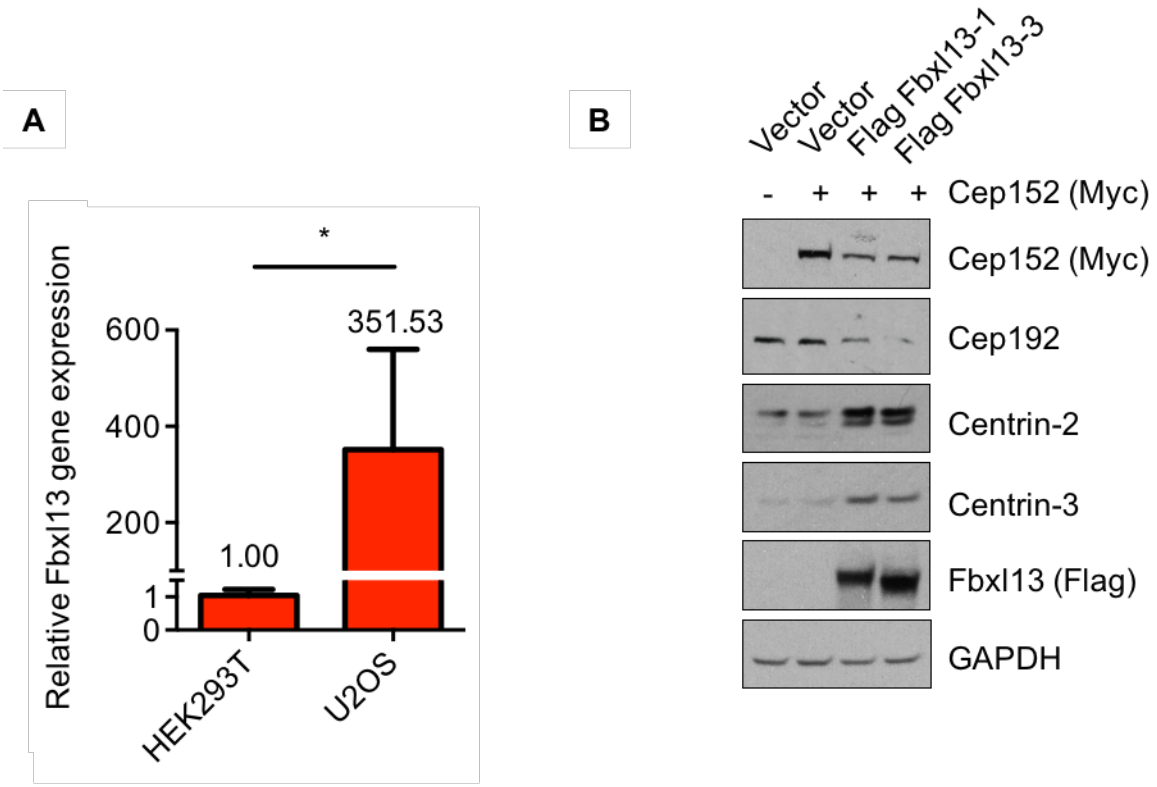

Figure 3.6 Fbxl13 overexpression downregulates Cep152 and Cep192 levels

(A) Fbxl13 mRNA levels in HEK293T and U2OS cells. N=3 biological replicates. Data are shown as mean ± SD. Statistically significant results comparing Fbxl13 gene expression between HEK293T and U2OS cells are indicated as * for P≤0.05, ad analysed by Student's t-test. **(B)** Detection of Myc-tagged Cep152, Cep192, Centrin-2 and Centrin-3 in HEK293T cells transfected with Fbxl13 isoform 1 (Fbxl13-1) or Fbxl13 isoform 3 (Fbxl13-3). An empty vector (Vector) was used as a negative control. N=2 biological replicates.

As centrosomal proteins are often cell-cycle regulated, it is also possible that the effects of Fbxl13 overexpression were due to indirect effects on the cell-cycle. To control for this, I asked whether Fbxl13-1 or Fbxl13-3 overexpression altered the cell cycle profile of HEK293T cells. Using propidium iodide (PI) staining and fluorescence assisted cell sorting (FACS), the cell cycle phase of single cells can be determined from their DNA content. We observed that although Fbxl13 overexpression marginally reduced the G2/M population, the difference was not significant (Figure 3.7). This shows that the effect of Fbxl13 overexpression on centrosomal protein levels was not due to cell cycle effects.

To further control for cell-cycle effects, the cell-cycle profiles of Centrin-2, Centrin-3, Cep152 and Cep192 were determined. Particularly, it was of interest to see if there was a single cell cycle phase that could account for the differences seen in Figure 3.6 following Fbxl13 overexpression, in which Centrin-2 and Centrin-3 were increased, but Cep152 and Cep192 were decreased. Cells can be synchronised using a double-thymidine block, by seeding at a density of 30-40% and treating with thymidine. Thymidine targets the dNTP producing enzyme ribonucleotide reductase (RNR) with its metabolic product (dTTP) through allosteric inhibition, blocking DNA synthesis and arresting cells at the S phase boundary (Bjursell and Reichard, 1973). The thymidine block is reversible and can be removed by wash-out, after which the cells are released into S/G2 phase. Protein levels can be followed over the course of a cell cycle by taking regular time points over approximately 24 hours (Figure 3.8). In doing so, I observed that there was no single cell cycle phase which could explain the combined effect of Fbxl13 overexpression on the protein levels seen in Figure 3.6. Whereas Cep192 was

upregulated in G2/M, Cep152 and Centrin-2 were downregulated. On the other hand, Centrin-3 levels did not change during the cell cycle.

These results suggest that Fbxl13 regulates the levels of Cep152, Cep192, Centrin-2, and Centrin-3 independently of the cell cycle. Particularly striking is the downregulation of Cep152 and Cep192: although ubiquitylation has many outcomes, one of the most common is ubiquitin mediated proteolysis. Furthermore, Cep152 and Cep192 are both known to be ubiquitylated (Elia et al., 2015), however the functions and ligases responsible remain uncharacterised. Therefore, the next aim was to further characterise their Fbxl13-mediated downregulation, and determine whether it could be a result of ubiquitylation. As the behaviour of Fbxl13-1 and Fbxl13-3 were comparable, our studies focused on Fbxl13-1 from this point forwards.

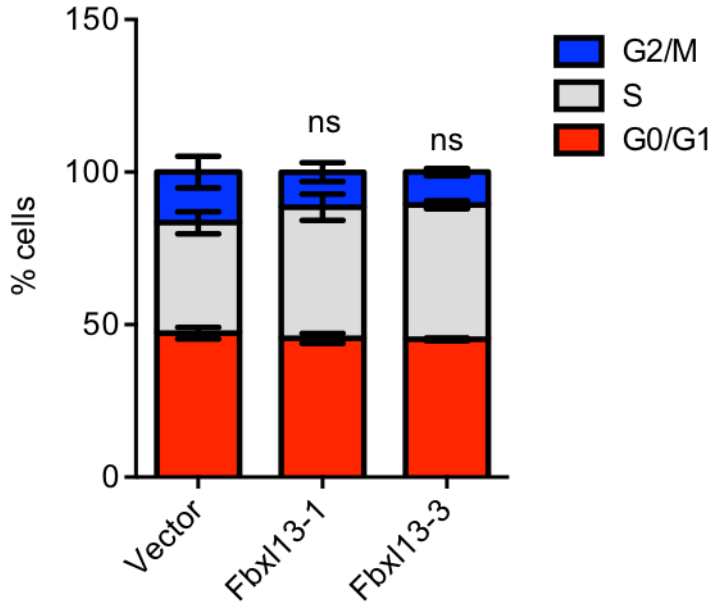

Figure 3.7 Fbxl13 overexpression does not significantly alter cell cycle profile

Quantification of cell cycle profile of HEK293T cells as determined by fluorescence activity sorting assay (FACS). HEK293T cells were transfected with Fbxl13 isoform 1 (Fbxl13-1) or Fbxl13 isoform 3 (Fbxl13-3). An empty vector (Vector) was used as a negative control. N=3 biological replicates. Data are shown as mean ± SD. Statistically insignificant results comparing the G2/M population between control and Fbxl13 overexpressing cells are indicated as ns for P>0.05 as analysed by Student's t-test.

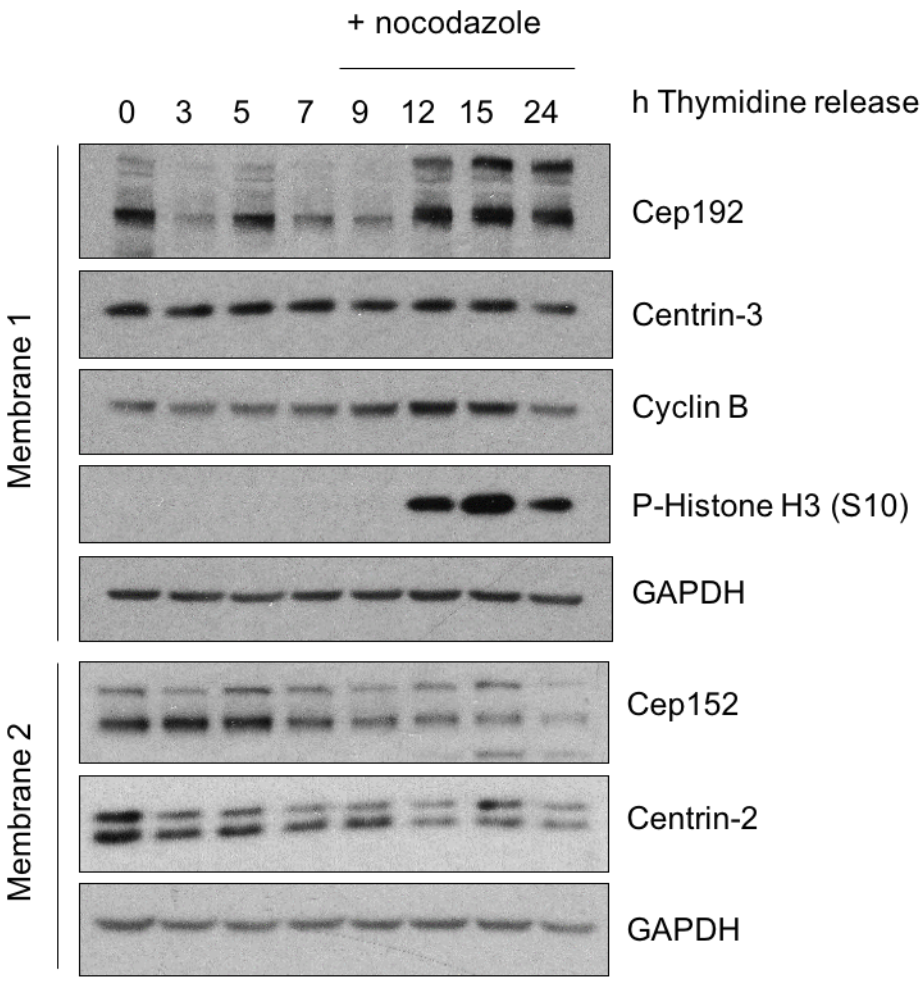

Figure 3.8 Cell cycle profile of Cep152, Cep192, Centrin-2, and Centrin-3

Detection of Cep152, Cep192, Centrin-2 and Centrin-3 protein levels in U2OS cells following double-thymidine release and nocodazole block. U2OS cells were seeded at 30% confluency, and blocked using 2 mM thymidine for 16 hours. Following thymidine washout, the cells were allowed to proceed through the cell cycle for 18 hours. Cells were then blocked a second time with 2 mM thymidine for 16 hours. The thymidine was then washed out, and time points taken as indicated. At 7 hours, cells were treated with 0.1 mg/ml nocodazole to enrich for mitotic cells at the later time points. The vertical lines indicate that the samples were loaded across two gels, and group the western blots to their respective loading controls. N=3 biological replicates.

To get a sense of the time-scale in which this downregulation occurred, I asked how Fbxl13 overexpression affected Cep152 and Cep192 half-life. This can be measured using cycloheximide chase. Cycloheximide treatment inhibits protein translation by targeting translation elongation at the 60S ribosomal subunit. In this way, sampling time points following cycloheximide treatment can reveal how stable a protein pool is under different treatment conditions.

Using this approach, HEK293T cells were transfected with either Fbxl13-1, or an empty vector control. The cells were then treated with cycloheximide for the indicated time points, lysed, and resolved by SDS-PAGE (Figure 3.9). I observed that the half-life of both exogenous Cep152 and Cep192 were very stable, however Fbxl13 overexpression consistently reduced Cep152 and Cep192 levels after 12 hours of cycloheximide treatment. Quantification revealed that Fbxl13 overexpression indeed reduced the half-life of Cep152 and Cep192 to 8-12 hours, compared to over 12 hours in the control. In contrast, we were also able to see that Fbxl13 did not reduce Centrin-2 or Centrin-3 half-life (Figure 3.10). In fact, Fbxl13 seemed to have a stabilising effect on Centrin levels. Interestingly, in all cases, the half-life of Fbxl13 was very short, suggesting that Fbxl13 has a high turnover. It is worth noting that the exposure times of Fbxl13 were very short to avoid saturation, and that Fbxl13 is still present following 12 hours of cycloheximide treatment.

We conclude that Fbxl13 overexpression destabilises Cep152 and Cep192 half-lives to approximately 8-12 hours. This is much longer than expected, as ubiquitin mediated proteolysis is a rapid, post-translational process. One possible explanation for this is that Fbxl13 may regulate specific pools of Cep152 and Cep192, for example at the centrosome, and that this effect is masked when looking

at whole-cell protein levels by Western blot. To validate whether Cep152 and Cep192 could be Fbxl13 substrates, we next asked whether this downregulation could be rescued with MLN4924.

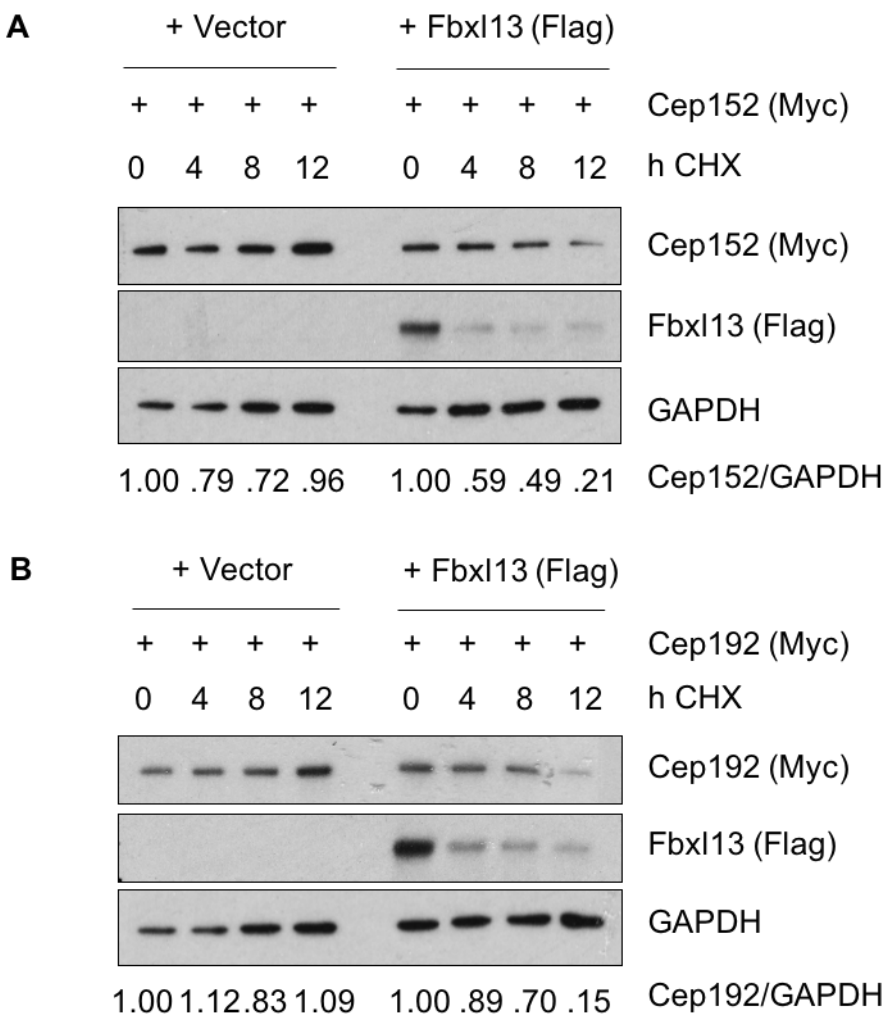

Figure 3.9 Fbxl13 destabilises Cep152 and Cep192 half-life

(A) Exogenous Cep152 protein levels in HEK293T cells following 50 µg/ml cycloheximide (CHX) treatment for the indicated time, with Fbxl13 overexpression. An empty vector (Vector) was used as a negative control. Quantified Cep152 levels (Cep152/GAPDH) are shown normalised to the first time point. **(B)** Exogenous Cep192 protein levels in HEK293T cells following 50 µg/ml cycloheximide (CHX) treatment for the indicated time, with Fbxl13 overexpression. An empty vector (Vector) was used as a negative control. Quantified Cep192 levels (Cep192/GAPDH) are shown normalised to the first time point. N=2 independent experiments.

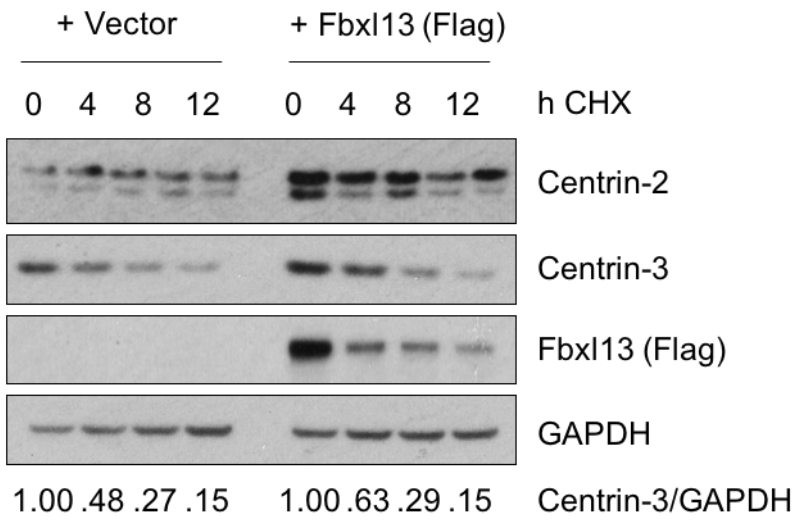

Figure 3.10 Fbxl13 does not destabilise Centrin-2 or Centrin-3 half-life

Detection of Centrin-2 and Centrin-3 protein levels in HEK293T cells following 50 µg/ml cycloheximide (CHX) treatment for the indicated hours, with Fbxl13 overexpression. An empty vector (Vector) was used as a negative control. Quantified Centrin3 levels (Centrin-3/GAPDH) are shown normalised to the first time point. N=2 independent experiments.

As MLN4924 is an inhibitor of cullin-RING E3 ubiquitin ligases, such as SCF^{Fbxl13}, it can also determine whether Fbxl13-mediated Cep152 and Cep192 downregulation is mediated by ubiquitylation. HEK293T cells overexpressing Cep152 or Cep192 were co-transfected with either Fbxl13, or an empty vector control (Figure 3.11). Once again, we saw downregulation of Cep152 and Cep192. The Fbxl13-overexpressing samples were also incubated with 2 μM MLN4924 for the indicated times. We observed that MLN4924 treatment rapidly rescued Cep152 levels back to levels comparable to the control (Figure 3.11, top panel). Over time, it was surprisingly rescued to twice the control levels. One possible reason for this is that Cep152 may be regulated by E3 ubiquitin ligases other than SCF^{Fbxl13}. Although the effect on Cep192 was modest in comparison, quantification revealed that it was also rescued to levels comparable to the empty vector control (Figure 3.11, bottom panel). Together, these data suggest that Fbxl13 indeed downregulates Cep152 and Cep192 levels in a cullin-E3 ubiquitin ligase specific manner. It cannot be concluded from these data alone that these interactors are targeted for SCF^{Fbxl13} mediated ubiquitylation, however they support further investigation.

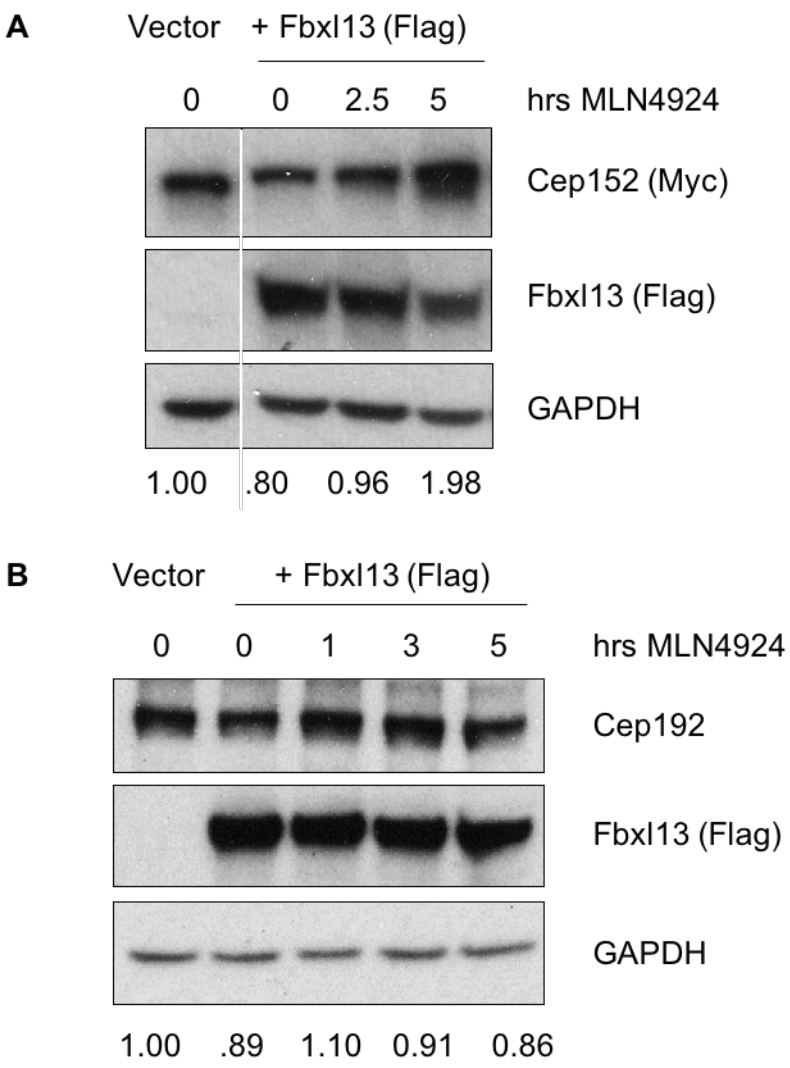

Figure 3.11 MLN4924 rescues Fbxl13-mediated Cep152 and Cep192 downregulation

(A) Exogenous Cep152 protein levels in HEK293T cells following 2 μM MLN4924 treatment for the indicated hours, with Fbxl13 (Isoform 1) overexpression. An empty vector (Vector) was used as a negative control. Quantified Cep152 levels (Cep152/GAPDH) are shown normalised to the Vector control. **(B)** Endogenous Cep192 protein levels in HEK293T cells following 2 μM MLN4924 treatment for the indicated hours, with Fbxl13 overexpression. An empty vector (Vector) was used as a negative control. Quantified Cep192 levels (Cep192/GAPDH) are shown normalised to the Vector control. The white line indicates where two lanes were cropped and placed side by side from the same image. N=2 independent experiments.

3.3 Results summary

The ubiquitin system is one of the major pathways for post-translational modifications in the cell. F-box proteins are a class of specificity factors for the SCF superfamily of E3 ubiquitin ligases, and many have been found to have oncogenic as well as tumour suppressive properties (D'Angiolella et al., 2012; Raducu et al., 2016; Wang et al., 2014). For example, our lab recently identified a tumourigenic role for Fbxl17 in medulloblastoma, where it targets a suppressor of the oncogenic sonic hedgehog pathway for degradation (Raducu et al., 2016). For this reason, our lab wished to further characterise other F-box proteins implicated in tumourigenesis, such as Fbxl13. Not only has Fbxl13 been implicated in resistance to ionising radiation (Hurov et al., 2010), but it is also implicated in genomic instability (Paulsen et al., 2009). Despite these links, Fbxl13 has so far been unstudied, and its substrates and function remain elusive.

To this end, the purpose of this study is to identify interactors and substrates for Fbxl13, in order to uncover its cellular function and potential role in tumourigenesis. Thus far, the data in this chapter offer novel insights into the nature of the orphan protein Fbxl13.

Firstly, using an unbiased proteomics-based approach, we have identified and validated centrosomal interactors for Fbxl13: Centrin-2, Centrin-3, Cep152, and Cep192. It remains to be seen whether all four of the identified interactors can bind Fbxl13 directly. It is possible in our validation approach that some interactors may have co-immunoprecipitated with Fbxl13 in complex with bona fide interactors. In particular, Cep152 and Cep192 are known to interact with each other (Sonnen et al., 2013). Furthermore, it will be interesting to see whether Fbxl13 itself is a

centrosomal protein. All four centrosomal interactors are also found in the cytoplasm, and Centrin-2 is also found in the nucleus (Araki et al., 2001). It is also plausible for Fbxl13 to interact with these proteins outside of the centrosome, for example to downregulate their cytoplasmic pools.

Secondly, the data show that Fbxl13 is able to regulate the protein levels of these interactors in a cell cycle independent manner. Exogenous expression of Fbxl13 upregulates Centrin-2 and Centrin-3, and strikingly, downregulates Cep152 and Cep192. Furthermore, the observed downregulation of Cep152 and Cep192 is rescuable with MLN4924, a cullin-RING E3 ubiquitin ligase inhibitor, whereas the upregulation of Centrin-2 and Centrin-3 is not. This suggests that the protein-level downregulation of Cep152 and Cep192 occurs through SCF^{Fbxl13} mediated activity. Cep152 and Cep192 are therefore strong candidates for Fbxl13 substrates. However, it remains to be seen whether these effects are Fbxl13-specific.

Additionally, we also found that Centrin-2 and Centrin-3 interact with the N terminus of Fbxl13 (Appendix 1) whereas Cep192 interacts with the C terminus of Fbxl13 (Appendix 2), the predicted substrate-targeting region of F-box proteins.

The aim of the next chapter is therefore to further investigate Cep152 and Cep192, determine whether they can bind Fbxl13 directly, and whether Fbxl13 can target them for ubiquitylation.

4 Results II

Fbxl13 targets Cep192 for ubiquitin mediated proteolysis

4.1 Introduction

In the previous chapter, we used liquid chromatography tandem mass spectrometry (LC-MS/MS) to identify interactors for the orphan F-box protein Fbxl13. We found that Fbxl13 interactors were highly enriched in centrosomal proteins, and using co-immunoprecipitation, we were able to validate Fbxl13 binding to Centrin-2, Centrin-3, Cep152, and Cep192. Additionally, Fbxl13 overexpression destabilises both Cep152 and Cep192 in a cullin-RING E3 ubiquitin ligase dependent manner, but not Centrin-2 and Centrin-3 (Figure 3.11). Taken together, Cep152 and Cep192 show promise as candidate Fbxl13 substrates. It remains unclear if Fbxl13 is also able to target these interactors for ubiquitylation.

Both Cep152 and Cep192 are crucial factors involved in centriole duplication and centrosome maturation (Blachon et al., 2008; Hatch et al., 2010; Kim et al., 2013; Sonnen et al., 2013). Together, Cep152 and Cep192 cooperate to recruit Plk4, a polo-like kinase required for centriole formation (Bettencourt-Dias et al., 2005; Habedanck et al., 2005; Kim et al., 2013; Sonnen et al., 2013). The double depletion of both Cep152 and Cep192 completely abolishes Plk4 recruitment and centriole duplication (Sonnen et al., 2013). Additionally, the loss of Cep192 results in

defective centrosome maturation and bipolar spindle formation (Gomez-Ferreria et al., 2007). The fact that Fbxl13 may regulate either of these proteins places it in two highly conserved pathways in centrosome biology.

However, Cep152 and Cep192 interact with one another. At the centriole, Cep152 and Cep192 complex through their centriole binding regions (Sonnen et al., 2013). It is therefore unclear whether Fbxl13 interacts directly with both Cep152 and Cep192. Thus, the first aim of this chapter is to determine whether Fbxl13 binds both of these proteins independently, or in complex.

4.2 Results

4.2.1 Fbxl13 interacts with Cep192 independently of Cep152

To address this question, I generated truncation mutants of Cep152 and Cep192 that lacked the binding region to one another. We reasoned that if these truncation mutants could co-immunoprecipitate Fbxl13, then Cep152 and Cep192 can interact with Fbxl13 independently of one another. Performing the co-immunoprecipitation reaction *in vitro* would allow us to determine whether the interactions occurred directly or not. However, these constructs were highly unstable *in vitro*, and were therefore used for *in vivo* co-immunoprecipitation.

Cep152 was truncated into three constructs as shown in Figure 4.1, to avoid disrupting its major functional domains. The first construct contained the N terminal region, which contains the Plk4 binding region. The second construct contained the centriole targeting region required for Cep192 binding (Sonnen et al., 2013). The third construct contained the C terminal region of Cep152. These constructs were

co-transfected in HEK293T cells with Flag-Fbxl13, and treated with 2 μM MLN4924. The Myc-tagged Cep152 constructs were then immunopurified. Using Western blot, I was able to detect Flag-Fbxl13 pulled down with the centriole targeting region of Cep152 (Cep152 aa221-1319) (Figure 4.2). This region also binds Cep192, suggesting that Cep152 may not bind Fbxl13 independently of Cep192. We also observed that the binding between Fbxl13 and Cep152 aa221-1319 was stronger than to full length Cep152. One possible reason for this could be that Cep152 full length binds Fbxl13 in competition with other proteins, whereas the shorter Cep152 centriole-binding fragment may be targeted by fewer other interactors. Indeed, Cep152 FL contains Plk4 and CPAP binding sites, whereas Cep152 aa221-1319 does not.

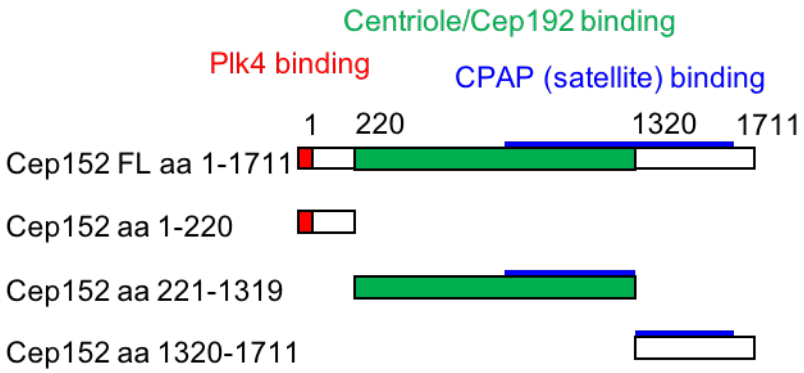

Figure 4.1 Scheme of Cep152 truncation mutants

The Cep152 full length (FL) protein and truncation mutants. The coloured regions show the Plk4 binding region (red), the centriole and Cep192 binding region (green), and the CPAP binding region (blue).

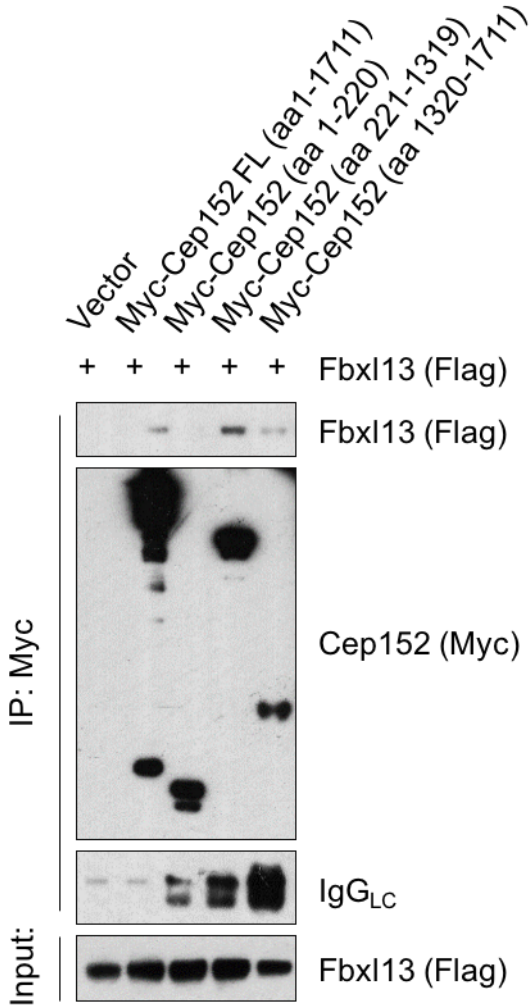

Figure 4.2 Fbxl13 binds the Cep192 binding region of Cep152

Detection of Flag-Fbxl13 after co-immunoprecipitation of Myc-tagged Cep152 constructs. HEK293T cells were co-transfected with Flag-Fbxl13 and Cep152 full length (FL), or three truncation mutants shown in Figure 4.1. Cells were treated with 2 µm MLN4924 5 hours prior to harvesting. Detection of light chains of immunoglobulin (IgG_{LC}) was used to assess the amount of IgG used for each immunoprecipitation reaction. N=3 biological replicates.

Similarly, Cep192 was truncated into two mutants as shown in Figure 4.3. The N terminal construct contained a Plk4 binding region, whereas the C terminal construct contains the Cep152 binding site (Sonnen et al., 2013). Once again, these constructs were co-transfected in HEK293T cells with Flag-Fbxl13, treated with 2 μM MLN4924, and immunoprecipitated.

In this case, we observed a very clear interaction between Fbxl13 and N terminal construct of Cep192 (aa1-630) (Figure 4.4). This mutant lacks the Cep152 binding region, and demonstrates that Cep192 is able to interact with Fbxl13 independently of Cep152. Interestingly, the truncation mutant Cep192 aa1-630 consistently pulled-down Fbxl13 more strongly than wild-type Cep192 (FL), similarly to the binding patterns of Cep152 FL and its truncation mutant. Again, it is possible that Fbxl13 binding to Cep192 (FL) is in competition with other proteins, for example Cep152. Another possible explanation is that the full length protein contains inhibitory regions that prevent Fbxl13 binding.

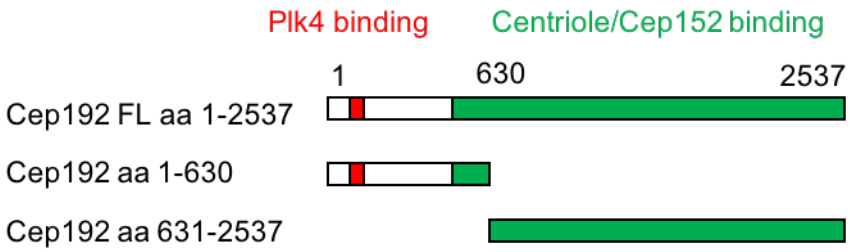

Figure 4.3 Scheme of Cep192 truncation mutants

The Cep192 full length (FL) protein and truncation mutants. The coloured regions show the Plk4 binding region (red), and the centriole and Cep152 binding region (green).

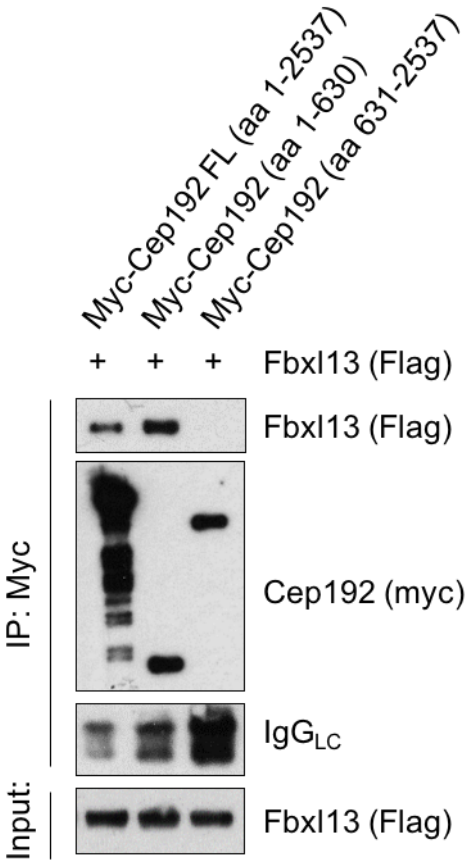

Figure 4.4 Fbxl13 binds the N terminal region of Cep192

Detection of Flag-Fbxl13 after co-immunoprecipitation of Myc-tagged Cep192 constructs. HEK293T cells were co-transfected with Flag-Fbxl13 and Cep192 full length (FL), or two truncation mutants shown in Figure 4.3. Cells were treated with 2 μM MLN4924 5 hours prior to harvesting. Detection of light chains of immunoglobulin (IgG_{LC}) was used to assess the amount of IgG used for each immunoprecipitation reaction. N=3 biological replicates.

Taken together, the results demonstrate that Cep192 is able to bind Fbxl13 independently of Cep152 (Figure 4.4). On the other hand, Cep152 binds Fbxl13 through the same region required for Cep192 binding (Figure 4.2), meaning that this interaction could be mediated through Cep192. If so, it follows that the interaction between Fbxl13 and Cep152 would be abolished following Cep192 depletion.

To test this hypothesis, I asked if the Cep152-Fbxl13 interaction was lost after Cep192 siRNA. Flag-Fbxl13 and Cep152 aa221-1319 were co-transfected in the presence or absence of Cep192 siRNA, and co-immunoprecipitated (Figure 4.5). We observed that binding to Flag-Fbxl13 was strongly reduced following Cep192 depletion. This strongly suggests that the binding between Fbxl13 and Cep152 was mediated through Cep192. There was some residual Fbxl13 in the immunoprecipitate, however this is likely due to the fact that we could only partially deplete Cep192 by siRNA. Although by Western blot, we can confirm that there is a strong Cep192 knockdown (Figure 4.5), this does not exclude that there are residual amounts of Cep192. Indeed, siRNAs do not completely abolish the target protein. This remains to be confirmed using an *in vitro* binding assay, due to the instability of both full length and truncated Cep152 and Cep192 constructs in the *in vitro* rabbit reticulocyte system (data not shown).

The results shown above demonstrate that Fbxl13 binds Cep192 independently of Cep152. For this reason, we decided to investigate the regulation of Cep192 by Fbxl13 moving forward.

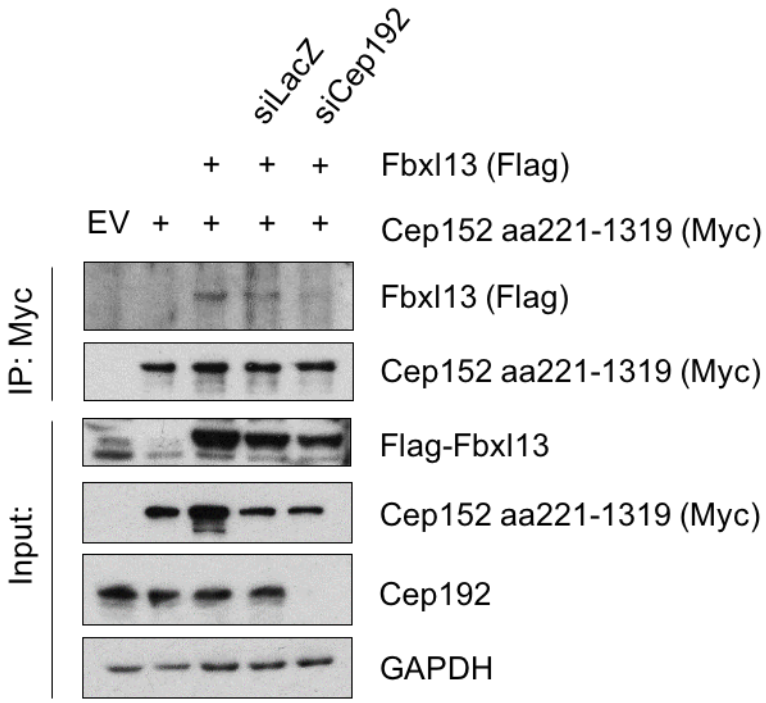

Figure 4.5 Cep152-Fbxl13 binding is reduced following Cep192 siRNA

Detection of Fbxl13 (Flag) following co-immunoprecipitation of Cep152 aa221-1319 (Myc) in the presence of a non-targeting siRNA (siLacZ) or an siRNA against Cep192 (siCep192). U2OS cells were co-transfected with the indicated plasmids and siRNA for 48 hours, and treated with 2 μM MLN4924 for 5 hours prior to harvesting. N=3 biological replicates.

4.2.2 Fbxl13 depletion stabilises the longest isoform of Cep192

In the previous chapter, we observed that Fbxl13 overexpression downregulated Cep192 levels in an MLN4924-rescuable manner, suggesting that Fbxl13 targets Cep192 for ubiquitin mediated degradation. If this were the case, one would expect that Fbxl13 depletion stabilises Cep192 levels.

To address this question, Fbxl13 was silenced in U2OS cells using siRNAs. These siRNA sequences target the 3` untranslated region (UTR), meaning that they silence all Fbxl13 isoforms. U2OS were selected for this assay as they express high levels of Fbxl13 (Figure 3.6). U2OS cells were either mock transfected with the transfection reagent alone (Mock), a control siRNA (siLacZ), or two siRNA oligos targeting Fbxl13 (S3 and S4). Fbxl13 depletion was validated by quantitative real-time PCR (qPCR) and Western blotting (Figure 4.6). Endogenous Fbxl13 was detected in these cells at approximately 100 kDa, which corresponds to the band-height we observe for Fbxl13-1 (83 kDa). It is worth noting that lower molecular weight Fbxl13 isoforms were not detected, suggesting that at least in U2OS, Fbxl13-1 is the predominant isoform. Following Fbxl13 depletion, I observed a marked stabilisation of a high molecular weight band of Cep192 (Figure 4.6, top panel). Surprisingly, lower molecular weight Cep192 bands were not consistently stabilised in the same way. It is possible that Fbxl13 siRNA led to Cep192 accumulation by targeting proteins other than Fbxl13 (a phenomenon known as off-target effect). Thus, we attempted to re-confirm these observations using shRNA.

To do so, we developed cell lines using stably-integrated shRNA targeting Fbxl13 (Figure 4.7, top panel). Four U2OS cell lines were generated containing either a non-targeting shRNA (shControl), or three shRNAs targeting Fbxl13 (75, 85, or 87).

We observed that the higher molecular weight band of Cep192 accumulated in all three Fbxl13 depleted cell lines, whereas the lower molecular weight bands were not. Fbxl13 shRNA silencing was confirmed by qPCR (Figure 4.7, bottom panel). These data corroborate our finding that Fbxl13 downregulates Cep192.

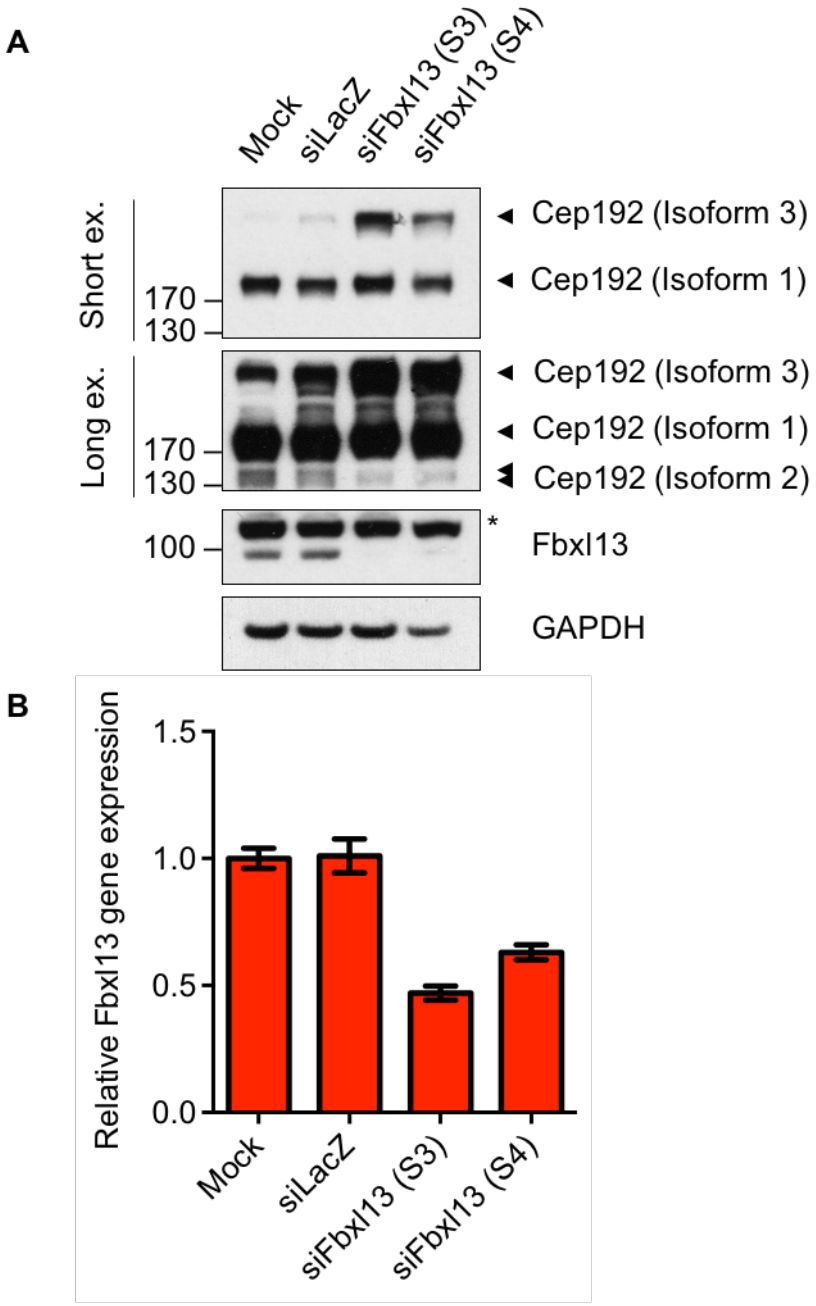

Figure 4.6 Fbxl13 siRNA stabilises a high molecular weight isoform of Cep192

(A) Detection of Cep192 following Fbxl13 siRNA depletion. U2OS were transfected with transfection reagent alone (Mock), a control siRNA (siLacZ), or two siRNAs targeting Fbxl13 (S3 and S4). Two exposures of Cep192 are shown (Short ex. and Long ex.) to show the isoforms of Cep192. N=4 biological replicates, representative image shown. **(B)** Validation of Fbxl13 siRNA using quantitative real-time PCR (qPCR) in the same batch of samples shown in **(A)**. Data are shown as mean ± technical SD between three qPCR triplicates. The anti-Fbxl13 antibody only became available in the late stages of this project.

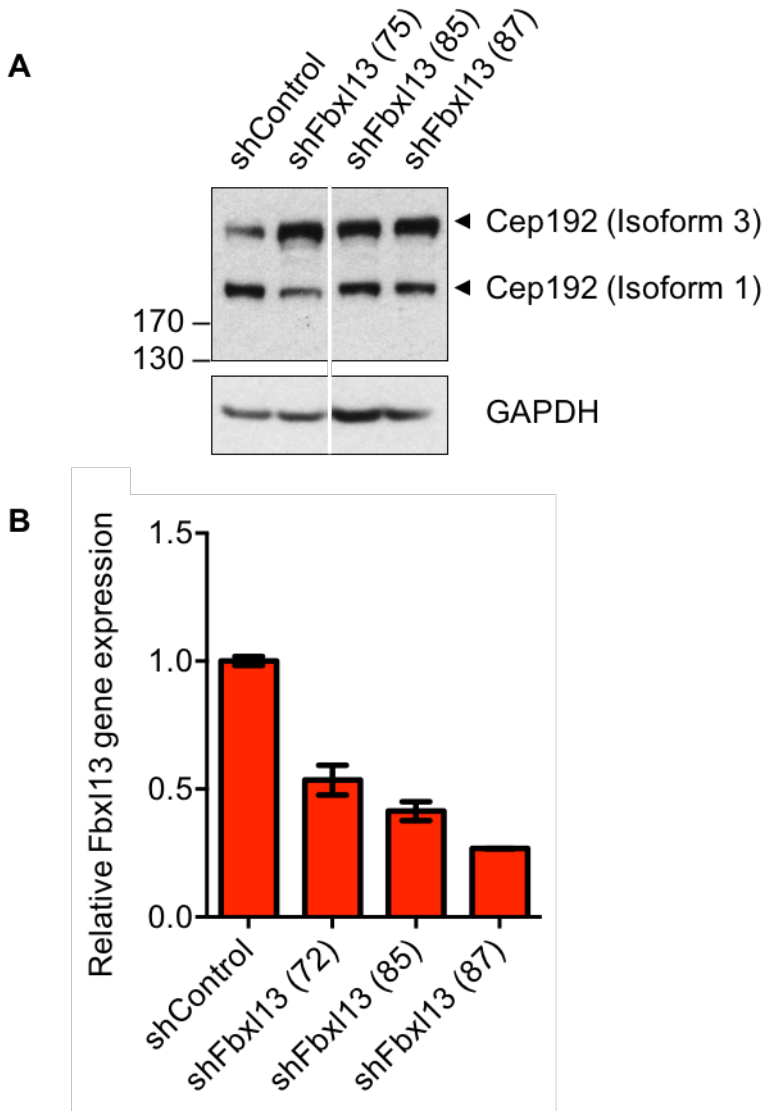

Figure 4.7 Fbxl13 shRNA stabilises a high molecular weight isoform of Cep192

(A) Detection of Cep192 following Fbxl13 shRNA depletion. shRNA control or three shRNAs targeting Fbxl13 were stably integrated into U2OS cells using lentiviral vectors. The white line indicates where two lanes were placed next to one another from the same image. N=2 biological replicates. **(B)** Validation of Fbxl13 siRNA using quantitative real-time PCR (qPCR) in the same batch of samples shown in **(A)**. Data are shown as mean ± technical SD between three qPCR triplicates. shFbxl13 cell lines were established by Dr Hongbin Yang.

It is possible that the Cep192 antibody could recognise non-specific bands. To control for this, the antibody was validated using a published Cep192 siRNA that targets all Cep192 isoforms (Figure 4.9) (Graser et al., 2007). U2OS cells were transfected with an siRNA control (siLacZ) or an siRNA targeting Cep192 (Figure 4.8). We observed that all four bands were depleted following Cep192 siRNA, concluding that they are indeed Cep192 specific. Although there are only three Cep192 isoforms reported on UniProt (Figure 4.9), we hypothesise that the two lower molecular weight bands could represent post-translationally modified Cep192-2 due to their small size difference. Taken together, these data suggest that Fbxl13 specifically downregulates the largest isoform of Cep192 (Cep192-3).

If Fbxl13 does indeed selectively target Cep192-3, one would expect that Fbxl13 binds Cep192-3 on an isoform-specific region. Cep192-3 is characterised by an N terminal extension absent in isoforms 1 and 2 (Figure 4.9). To address this question, I cloned this N terminal extension (aa1-602), and tested its ability to bind Fbxl13 using co-immunoprecipitation (Figure 4.10). We observed that Flag-Fbxl13 was indeed able to interact with this construct. This demonstrates that Fbxl13 specifically targets Cep192-3 by binding its isoform-specific N terminal extension. In sum, we conclude from these data that Fbxl13 specifically regulates Cep192-3, but not isoforms 1 or 2.

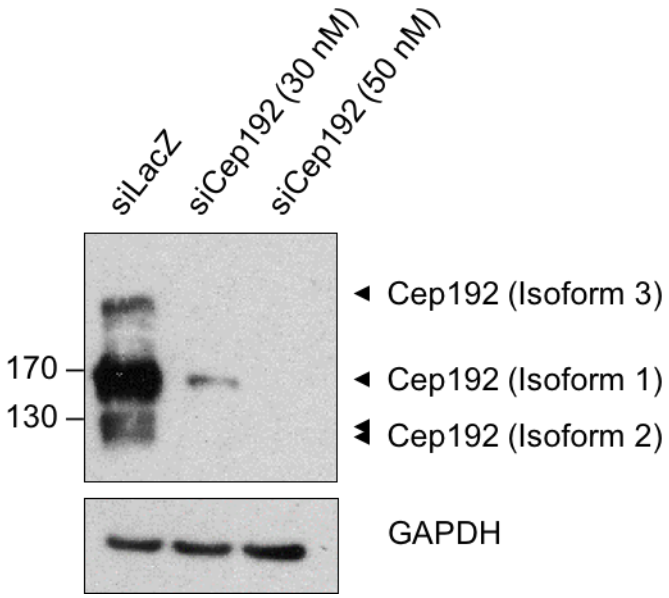

Figure 4.8 Validation of Cep192 antibody

Detection of Cep192 in U2OS following Cep192 siRNA depletion at two different concentrations. The Cep192 antibody was a kind gift from Professor Laurence Pelletier (Gomez-Ferreria et al., 2014). siRNA sequence was published by Graser et al. (2007).

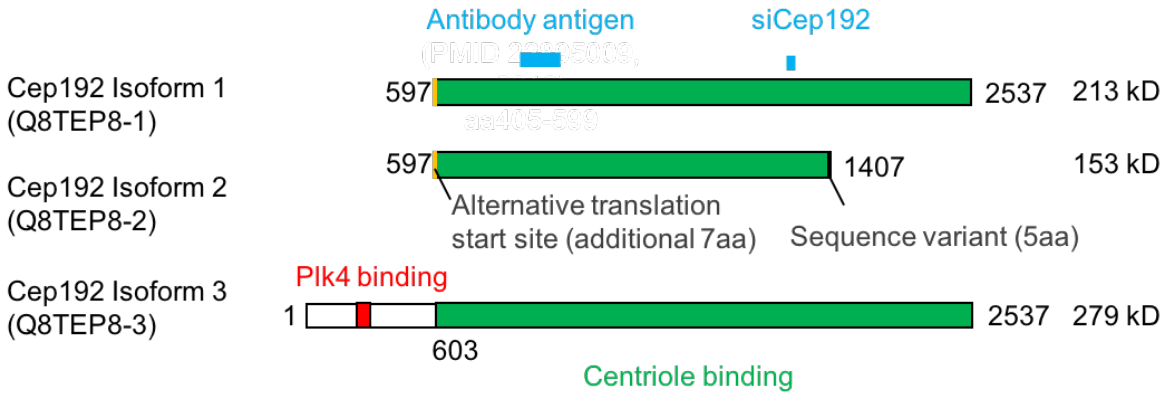

Figure 4.9 Scheme of Cep192 isoforms

Cep192 has three isoforms as reported on UniProt (Q8TEP8). The Plk4 binding region is shown in red, and the centriole binding region in green. The two shorter isoforms (1 and 2) are generated through an alternative translation start site (Sonnen et al., 2013), shown in yellow. Cep192 isoform 2 also contains a sequence variant of 5 amino acids at its C terminal. The antibody used in this study was kindly provided by Professor Laurence Pelletier, raised against the antigen shown in blue (Gomez-Ferreria et al., 2014). The siCep192 sequence (Graser et al., 2007) used in this study targets all three isoforms and is also highlighted in blue.

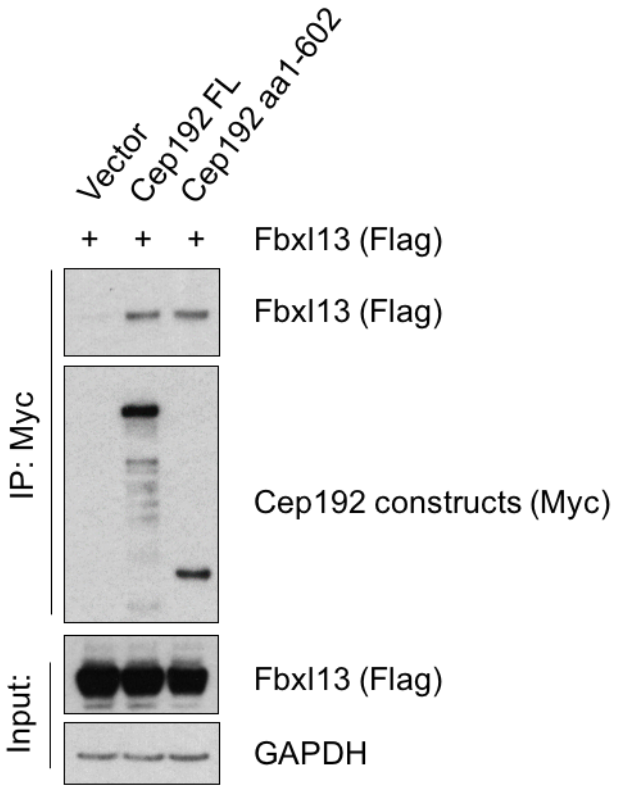

Figure 4.10 Fbxl13 binds to a region specific to Cep192 Isoform 3

Detection of Fbxl13 following co-immunoprecipitation of Myc-tagged full-length Cep192 (FL), or a Cep192 region only present on Cep192 isoform 3 (aa1-602). HEK293T cells were co-transfected with the indicated constructs for 48 hours, and treated with 2 μM of MLN4924 for 5 hours prior to harvesting. N=2 biological replicates.

4.2.3 Fbxl13 ubiquitylates Cep192

As Fbxl13 selectively destabilises Cep192-3, we wished to validate whether this occurs through ubiquitylation. Thus, we asked whether SCF^{Fbxl13} could Cep192-3 for ubiquitylation. As a negative control, I wished to generate an inactive mutant of Fbxl13 unable to ubiquitylate its substrates. This was achieved by deleting the F-box domain, which would result in a Fbxl13 mutant that can still bind substrates, but is defective in Skp1 binding. In this way, the Skp-Cullin-Rbx backbone will not be recruited to form a full SCF^{Fbxl13} E3 ubiquitin ligase complex (Figure 4.11). As the Skp-Cullin-Rbx backbone is responsible for recruiting the E2 ubiquitin conjugating enzyme, its loss means that substrates will not be brought into proximity with activated ubiquitin. Consequently, substrates bound by the Fbxl13 F-box deletion mutant (Fbxl13 ΔF) will not be ubiquitylated (Figure 4.11).

The Fbxl13 ΔF mutant was cloned using the ligation-independent cloning strategy in Figure 4.12 (top panel). Phosphorylated primers were designed to flank the F-box encoding region, and the entire construct was amplified. The methylated parental template was then removed from the PCR product using DpnI restriction enzyme digestion, and the PCR product was directly transformed into competent bacteria. As the primers are phosphorylated, the PCR product was readily re-ligated in the bacteria. The resulting protein would only lack the F-box domain (Figure 4.12, bottom panel). The Fbxl13 ΔF mutant was then validated by Sanger sequencing and co-immunoprecipitation to check for defective Skp1 binding (Figure 4.13). Whereas Skp1 was clearly bound to Fbxl13 WT, no Skp1 was bound to Fbxl13 ΔF, confirming that the ΔF cloning strategy was successful.

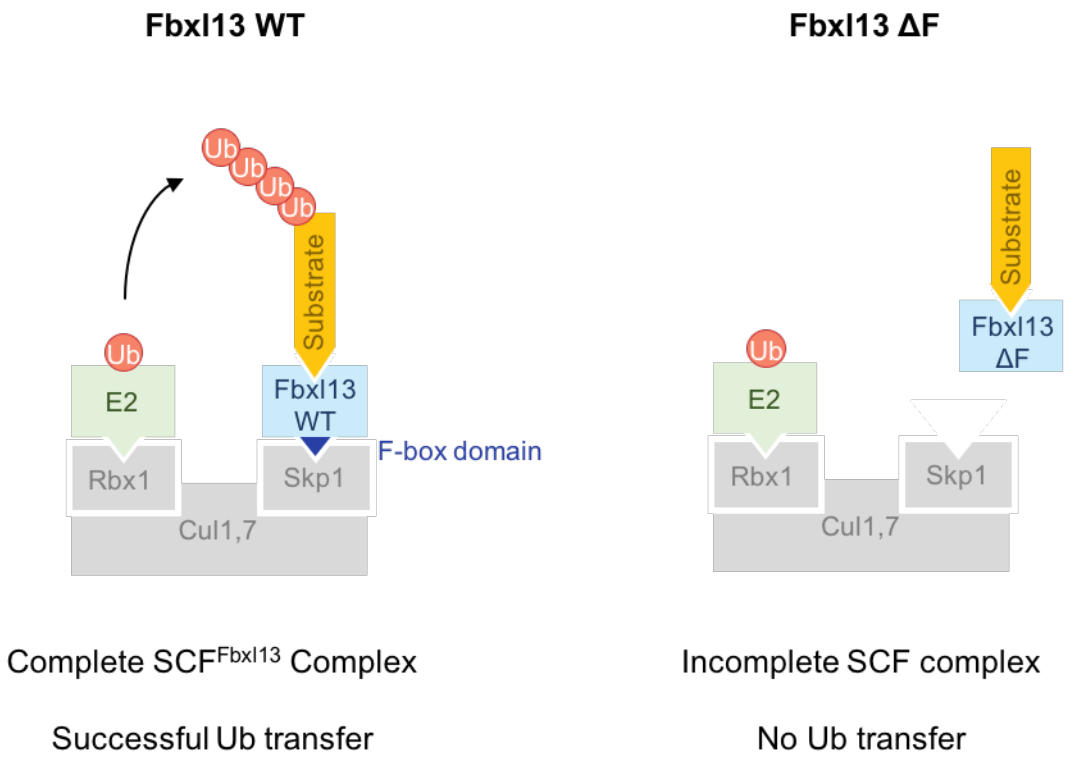

Figure 4.11 F-box deletion mutants cannot form an SCF E3 ubiquitin ligase complex

A full Skp-Cullin-F-box (SCF) E3 ubiquitin ligase complex forms in the presence of Fbxl13 wild type (WT) on the left. On the right, a mutant lacking the F-box (Fbxl13 ΔF) is unable to bind Skp1. In the absence of the F-box (dark blue), the Skp-Cullin-Rbx backbone is no longer recruited. As a result, the substrate (yellow) is not brought into proximity with the activated ubiquitin on the E2 ubiquitin-conjugating enzyme (green). The substrate is not ubiquitylated.

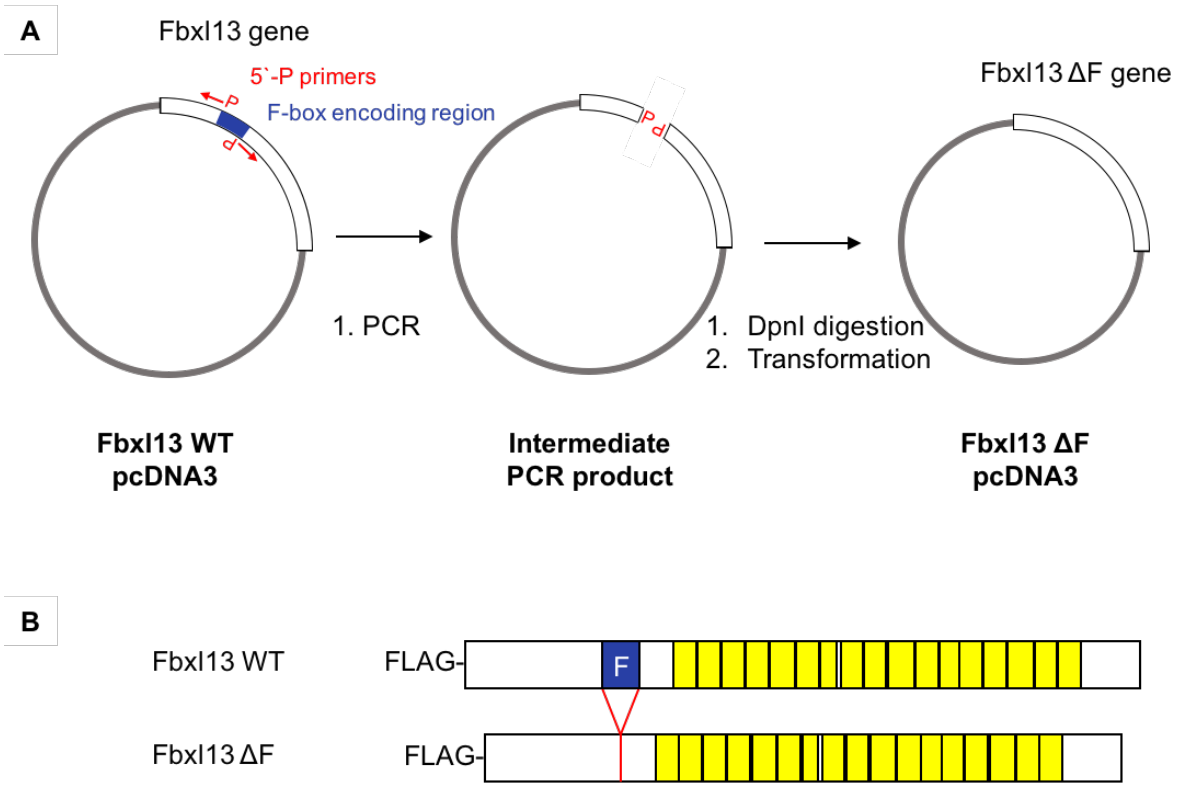

Figure 4.12 Fbxl13 F-box deletion mutant cloning strategy

(A) The cloning strategy to generate a mutant Fbxl13 lacking the F-box (Fbxl13 ΔF). A pcDNA3 vector containing 3xFlag-Fbxl13 was amplified using the primers shown in red, flanking the F-box in blue. The primers were phosphorylated at the 5` end (P). The resulting PCR product lacks the F-box encoding region. Following DpnI digestion, the PCR product was transformed into bacteria resulting in the final product on the right. **(B)** Scheme representing the Fbxl13 wild type (WT) or ΔF proteins. The F-box is highlighted in blue and the leucine-rich repeats (LRR) are highlighted in yellow. The region where the F-box domain was cloned out is shown in red.

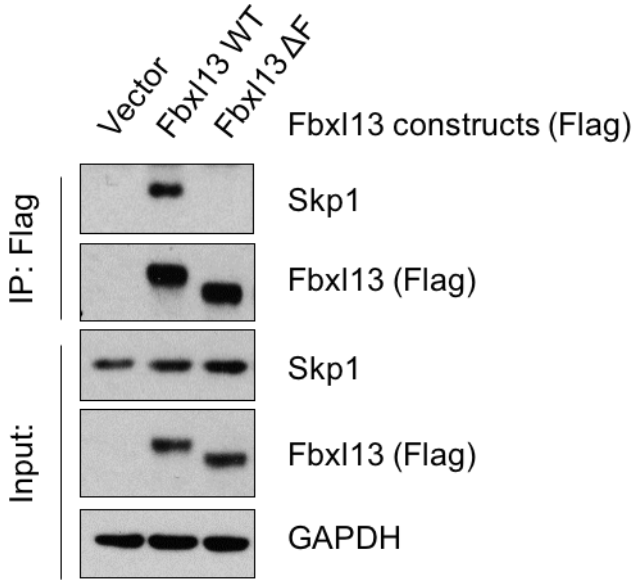

Figure 4.13 Validation of Fbxl13 ΔF loss of Skp1 binding

Detection of Skp1 after immunoprecipitation in HEK293T cells, transfected with either Fbxl13 wild type (Fbxl13 WT) or a mutant lacking the F-box (Fbxl13 ΔF). An empty vector (Vector) was used as a negative control.

Using this inactive Fbxl13 ΔF mutant, we then asked whether Cep192 was an Fbxl13 substrate using an *in vivo* ubiquitylation assay by testing whether Fbxl13 WT overexpression increased Cep192 ubiquitylation relative to Fbxl13 ΔF.

A fragment of Cep192 (aa1-630) was overexpressed in HEK293T cells. A fragment was chosen for this assay as full-length Cep192-3 (279 kDa) ubiquitylation was difficult to resolve. This construct was co-transfected with HA-Ubiquitin and Fbxl13 WT or Fbxl13 ΔF. An empty vector (Vector) was also used as a negative control. To enrich for polyubiquitylated Cep192, the HEK293T cells were treated with 10 μM MG132 for 5 hours prior to harvesting. MG132 is a 26S proteasome inhibitor, and would prevent proteolysis of polyubiquitylated Cep192. The lysis buffer also contained 20 mM N-Ethylmaleimide (NEM), an alkylating agent which inhibits deubiquitinating enzymes (DUBs) by blocking their active cysteine residues. Together, MG132 and NEM treatment would help us enrich polyubiquitylated proteins.

Myc-Cep192 (aa1-630) was then co-immunoprecipitated from the whole cell lysate and resolved using SDS-PAGE (Figure 4.14). Polyubiquitylated Cep192 was detected by Western blot. We observed a strong increase in polyubiquitylation following Fbxl13 WT overexpression, which was reduced following overexpression of the Fbxl13 ΔF negative control. While some ubiquitylation activity was still detectable in the Fbxl13 ΔF control, we still observe that Fbxl13 WT increases Cep192 ubiquitylation relative to Fbxl13 ΔF, and conclude that SCF^{Fbxl13} activity increases Cep192 ubiquitylation. One possible explanation for the residual ubiquitylation activity seen following Fbxl13 ΔF expression is that Cep192 immunoprecipitates contain another ubiquitylated protein.

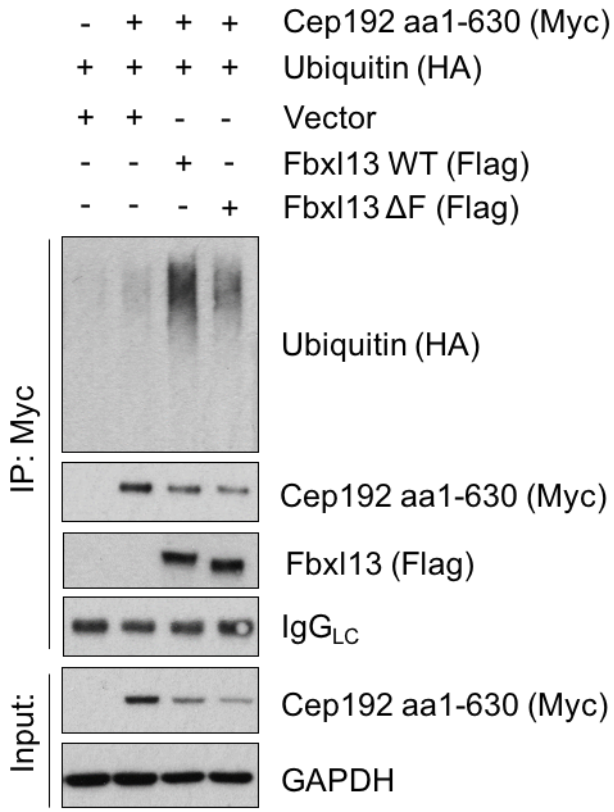

Figure 4.14 FbxI13 increases Cep192 aa1-630 polyubiquitylation

Detection of polyubiquitylated Myc-tagged Cep192 aa1-630 co-immunopurified from HEK293T cells transfected with HA-tagged ubiquitin and either FbxI13 wild type (WT) or FbxI13 lacking the F-box (FbxI13 ΔF). The 26S proteasome inhibitor MG132 (10 μM) was added to all samples 5 hours prior to harvesting, and the lysis buffer contained N-Ethylmaleimide (20 mM), a broad deubiquitinating enzyme inhibitor. Detection of immunoglobulin light chains (IgG_{LC}) was used to assess the amount of IgG used for each immunoprecipitation reaction. N=1 biological replicate.

To validate whether the Cep192 ubiquitylation seen was Fbxl13 specific, we next asked whether it could be downregulated with Fbxl13 depletion. U2OS cells were chosen for this assay as they have amplified levels of Fbxl13, and could address how lowering Fbxl13 in this system would affect Cep192 ubiquitylation. Cep192 aa1-630 was co-transfected in U2OS cells with HA-ubiquitin, and an siRNA control (siRNA LacZ) or two siRNAs targeting Fbxl13 (S3 and S4). The *in vivo* ubiquitylation assay was then performed as described previously, and Fbxl13 siRNA was validated using quantitative real-time PCR (qPCR) (Figure 4.15, right panel).

We observed a striking decrease in Cep192 aa1-630 polyubiquitylation following Fbxl13 depletion with both siRNAs (Figure 4.15, left panel). This shows that the Cep192 ubiquitylation seen is mediated by Fbxl13. Taken together with Figure 4.14, these data show that SCF^{Fbxl13} targets Cep192 for polyubiquitylation.

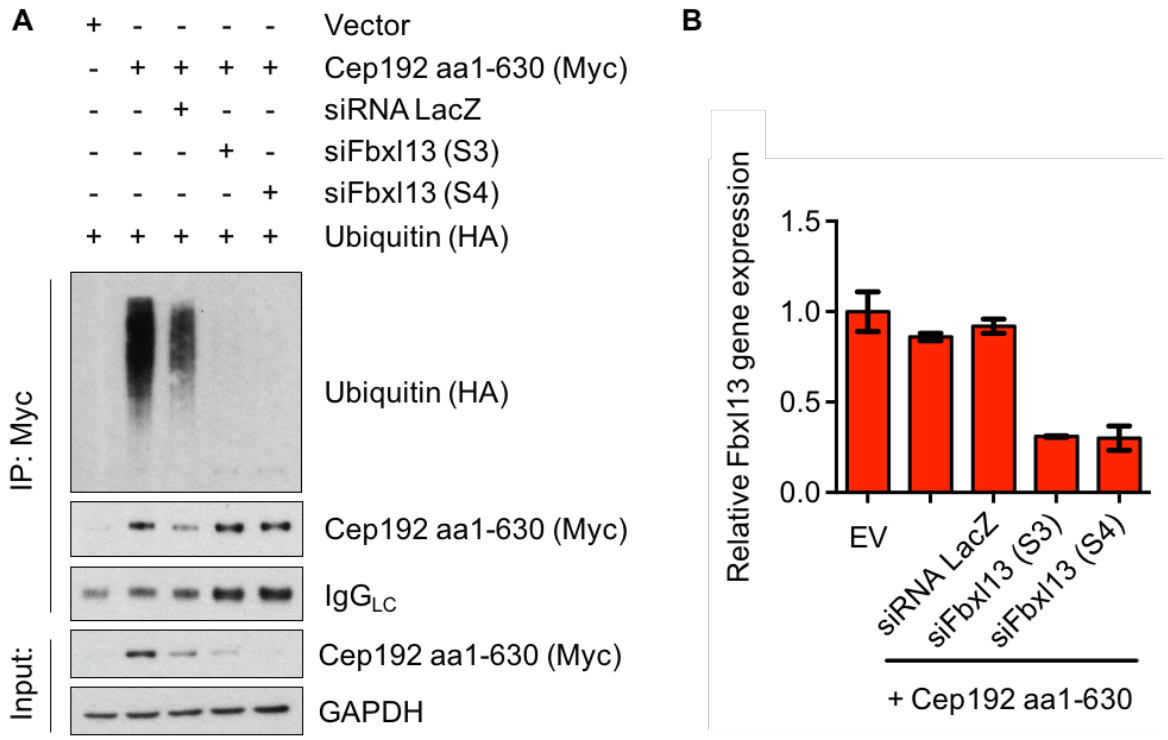

Figure 4.15 Fbxl13 depletion reduces Cep192 aa1-630 ubiquitylation

(A) Detection of polyubiquitylated species of Myc-tagged Cep192 aa1-630 co-immunopurified from U2OS cells co-transfected with HA-tagged ubiquitin (Ub) and either a control siRNA (siRNA LacZ) or two siRNAs against Fbxl13 (S3) and (S4). An empty vector (Vector) was used as a negative control. 10 μM MG132 was added to all samples 5 hours prior to harvesting, and the lysis buffer was supplemented with 20 mM N-Ethylmaleimide. Detection of light chains of immunoglobulin (IgG_{LC}) was used to assess the amount of IgG used for each immunoprecipitation reaction. N=1 biological replicate. **(B)** Fbxl13 mRNA relative levels in U2OS samples collected in **(A)**, following depletion with either a control siRNA (siRNA LacZ) or two siRNAs to Fbxl13 (S3) and (S4). Data are shown as mean ± technical SD between three qPCR triplicates.

4.3 Results summary

Fbxl13 is an orphan E3 ubiquitin ligase specificity factor implicated in tumourigenesis. In the previous chapter, we validated centrosomal interactors of Fbxl13, and found that Fbxl13 downregulated Cep152 and Cep192 in a cullin-RING E3 activity dependent manner. However, it remained unclear whether Fbxl13 interacted with both proteins independently, or in complex. Thus, the purpose of this results chapter was to further investigate the mechanism of interaction between Fbxl13, Cep152, and Cep192, in order to identify direct Fbxl13 interactors and substrates.

Our data demonstrate that Fbxl13 interacts with Cep192 in a Cep152 independent manner (Figure 4.4). In addition, we were also able to detect endogenous Fbxl13 binding to Myc-Cep192 (Appendix 3). On the other hand, our data suggest that Cep152 interacts with Fbxl13 indirectly for two reasons. Firstly, its binding to Fbxl13 is dependent on its Cep192 binding region (Figure 4.2). Secondly, its binding to Fbxl13 was reduced following Cep192 siRNA depletion (Figure 4.5). A formal *in vitro* binding study between Fbxl13 and Cep152 would be required to confirm whether their binding is indirect. Unfortunately in our hands, the expression of these constructs *in vitro* was unstable (data not shown). Moving forwards, we focused on Cep192 for the reasons outlined above.

We demonstrated that Fbxl13 depletion selectively stabilised a high molecular weight isoform of Cep192, which corresponded with Cep192 isoform 3 (Cep192-3). This isoform-specific regulation of Cep192 could be explained by the fact that Fbxl13 bound to a region of Cep192-3 absent in other isoforms. Thus, we concluded that Fbxl13 regulates Cep192-3.

We then provided evidence that this downregulation occurs through ubiquitylation-mediated proteolysis. Firstly, preliminary data showed that Fbxl13 overexpression increased Cep192 ubiquitylation, in a Skp1-Cullin-Rbx1 dependent manner. Furthermore, Fbxl13 siRNA reduced Cep192 ubiquitylation, suggesting that it was Fbxl13-specific (Figure 4.15).

To further investigate this hypothesis, we had also attempted to strengthen our data *in vitro*. We wished to confirm firstly that Fbxl13 and Cep192 interacted directly, and secondly that Fbxl13 ubiquitylated Cep192 directly by reconstituting the ubiquitylation reaction *in vitro*. This would control for any indirect effects in the *in vivo* ubiquitylation assay, and show that SCF^{Fbxl13} is sufficient for Cep192 ubiquitylation. For both these assays, it was necessary to express Fbxl13 and Cep192 *in vitro*.

In vitro protein expression was conducted using a eukaryotic *in vitro* transcription-translation system. This system consists of cell-free rabbit reticulocyte extracts, which are crude extracts containing the macromolecular components required for transcription (RNA polymerase, nucleotides) and translation (70S or 80S ribosomes, tRNAs, aminoacyl-tRNA synthetases, initiation, elongation, and termination factors, ATP, GTP, salts etc.). The *in vitro* expression of proteins in a different eukaryotic background (ie. in a heterologous system) ensures that they are free from any *in vivo* interacting partners. Thus, if two proteins interact *in vitro,* in the absence of other proteins, then their interaction is direct. Unfortunately, full-length Cep192 was highly fragmented when expressed *in vitro* (data not shown). This was likely due to its large size, at 2,537 amino acids. The truncation mutant of Cep192 was successfully expressed, however was highly unstable and could no

longer be detected following immunoprecipitation (data not shown). For future studies, we propose the use of other *in vitro* expression systems, such as wheat-germ extract or baculovirus expression, which may be more stable.

Taken together, we conclude that Fbxl13 downregulates Cep192-3, and propose that this occurs through ubiquitin mediated proteolysis. The aim of the next chapter will therefore be to characterise the function of the Fbxl13-Cep192 axis.

5 Results III

Investigating the cellular function of Fbxl13-dependent Cep192 ubiquitin mediated proteolysis

5.1 Introduction

Fbxl13 is an orphan E3 ubiquitin ligase specificity factor implicated in tumourigenesis (Cron et al., 2013; Hurov et al., 2010; Paulsen et al., 2009). In the previous chapters, we identified novel centrosomal interactors for the Fbxl13, validated their binding *in vivo,* and showed that Fbxl13 downregulates a specific isoform of Cep192, isoform 3 (Cep192-3). Finally, we provided evidence that Cep192-3 is an Fbxl13 substrate. Next, we aimed to investigate the function of Fbxl13-mediated Cep192-3 proteolysis.

Cep192 is a highly conserved protein required for both centriole duplication as well as centrosome maturation (Gomez-Ferreria et al., 2007; Sonnen et al., 2013; Zhu et al., 2008). It is possible that Fbxl13 targets Cep192-3 to regulate these processes. Unfortunately, the isoform-specific function of Cep192-3 is unknown. Interestingly, Cep192-3 contains a Plk4 binding domain absent in Cep192 isoforms 1 and 2 (Sonnen et al., 2013), hinting at possible roles in centriole duplication. Additionally, it is possible that Cep192 has non-canonical functions. In particular, we wish to address whether the Fbxl13-Cep192 axis has a role in in ionising radiation (IR) sensitivity and genome instability, processes in which Fbxl13 has

been implicated (Hurov et al., 2010; Paulsen et al., 2009). The aim of this chapter is therefore to investigate the role of Fbxl13 in these processes.

5.2 Results

5.2.1 Fbxl13 downregulates centrosomal Cep192 levels

To further investigate the role of Fbxl13, we first asked where Fbxl13 localises in the cell, and whether it downregulates centrosomal or cytoplasmic Cep192 pools.

To address this question, U2OS cells were transfected with Flag-tagged Fbxl13 or an empty vector control. Cells were then fixed with methanol and stained for Cep192, Flag, and DNA (Figure 5.1). We observed that the localisation pattern of Flag-Fbxl13 was cytoplasmic with centrosomal enrichment. This corroborates our liquid chromatography tandem mass spectrometry (LC-MS/MS) data, in which centrosomal proteins were highly enriched. The diffuse localisation pattern of Fbxl13 at the centrosome also suggests that Fbxl13 may be part of the pericentriolar matrix (PCM). A formal localisation study looking at endogenous Fbxl13 would allow us to better understand where Fbxl13 is localised within the centrosome.

We next hypothesised that if Fbxl13 is localised at the centrosome, then it may downregulate centrosomal Cep192. To address this question, confocal images of centrosomal Cep192 were acquired at identical, non-saturating conditions.

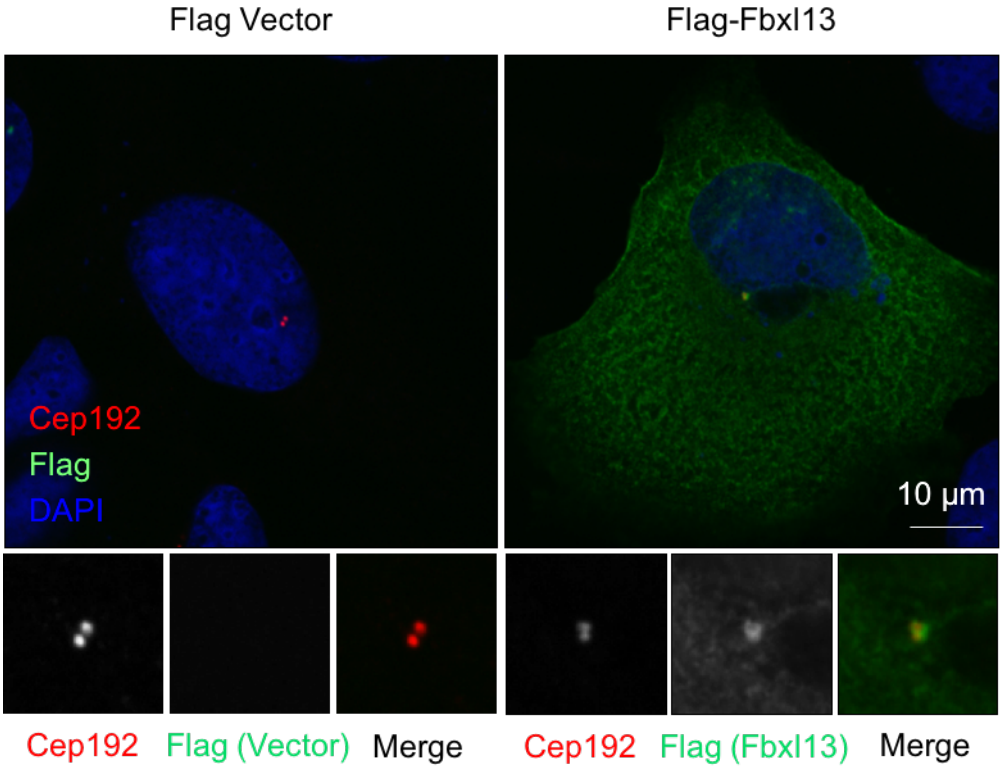

Figure 5.1 Fbxl13 has a cytoplasmic localisation with centrosomal enrichment

Representative images of U2OS cells transfected with Flag-Fbxl13, or an empty vector control (Flag Vector) were fixed with methanol, and stained for Cep192 (red), Fbxl13 (Flag, green), and DNA (DAPI, blue). Images were acquired using confocal microscopy at identical, non-saturating conditions. Scale bar, 10 µM. Anti-Cep192 antibody was a kind gift from Professor Laurence Pelletier (Gomez-Ferreria et al., 2014).

We found that centrosomal Cep192 levels were indeed reduced in cells overexpressing Fbxl13 (Figure 5.1, inset Cep192 images). This reduction could be quantified by measuring Cep192 abundance as fluorescence intensity (Figure 5.2). To control for cell cycle variations in Cep192 levels, only G2 cells were imaged for analysis. G2 cells were chosen as they have higher Cep192 levels than G1 cells, allowing for a better dynamic range in measurements. Additionally, G2 cells can be easily distinguished by nuclei size.

Cep192 fluorescence intensity was quantified using the freeware Image J using a method described by (Godinho et al., 2014). In brief, the fluorescence intensity at the centrosome was measured using a 50x50 pixel region of interest. The average background fluorescence was derived from a larger, 80x80 pixel region around this area using the formulas shown in Figure 5.2, by subtracting the fluorescence of the smaller 50x50 region and normalising by area. The normalised background intensity was then subtracted from the 50x50 region of interest, leaving only the fluorescence signal from the centrosomes. The advantage of this method is that the background is derived from the vicinity of the centrosome, which controls for variations in background fluorescence.

Using this method, the centrosomal Cep192 intensity of the samples in Figure 5.1 were quantified. Our results clearly show that Fbxl13 overexpression significantly downregulated centrosomal Cep192 intensity (Figure 5.2).

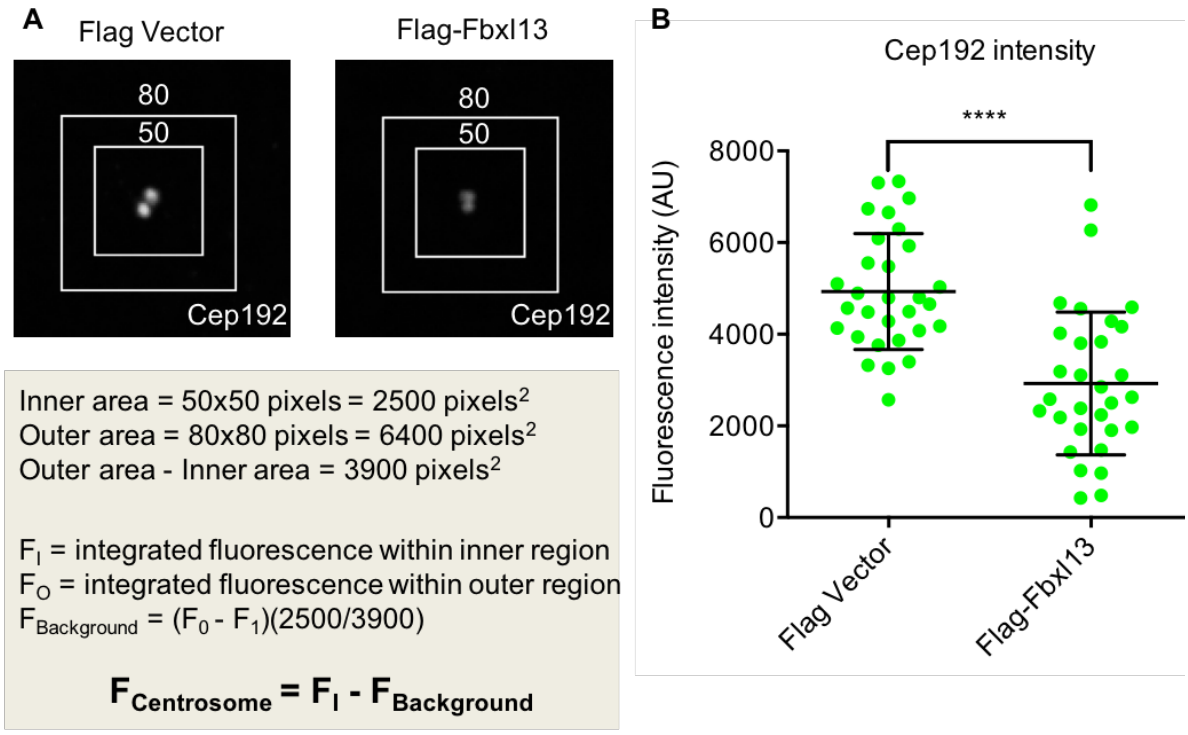

Figure 5.2 Fbxl13 overexpression reduces centrosomal Cep192

(A) Quantification of Cep192 fluorescence intensity associated with the centrosomes was performed as described by Godinho et al. (2014) using Image J. 50x50 and 80x80 pixel regions were centered over each centrosome. The intensity of fluorescence (integrated fluorescence) was measured for each pixel region. The background fluorescence ($F_{background}$) was obtained by subtracting the integrated value of the smaller 50x50 region (F_I) from the larger 80x80 region (F_O), and normalising to the 50x50 area. Centrosome fluorescence intensity ($F_{Centrosome}$) was then obtained by subtracting the background value ($F_{Background}$) from the total intensity of the 50x50 region (F_I). The advantage of this approach is that it controls for non-homogeneity in background fluorescence. Method figure adapted from Godinho et al. (2014). **(B)** Quantified Cep192 fluorescence intensity associated with the centrosomes in U2OS cells following Fbxl13 overexpression. N=2 biological replicates, n>30 cells per condition. Data from only one biological replicate is shown due to variations in baseline fluorescence between biological replicates. Data is shown as mean ± SD. Statistically significant results comparing Cep192 intensity in control and Fbxl13 overexpressing cells are indicated as **** for P≤0.0001, as analysed by Student's t-test.

Taken together, these data show that exogenous Fbxl13 has a cytoplasmic localisation with centrosomal enrichment, and that Fbxl13 overexpression significantly downregulated centrosomal Cep192 levels. This is consistent with our working model that Fbxl13 targets Cep192 for ubiquitin mediated proteolysis (Figure 4.15). It is worth noting that the Cep192 antibody used for immunofluorescence recognises all three isoforms of Cep192, and that we cannot distinguish the relative contributions of each Cep192 isoform to the total fluorescence intensity. The use of an isoform-specific antibody would allow us to determine how Fbxl13 overexpression directly affects Cep192-3 pools at the centrosome.

Due to the centrosomal localisation of Fbxl13, and the clear downregulation of centrosome-associated Cep192 levels, we decided to further investigate the potential role of Fbxl13 in centrosome biology. The remainder of this chapter will therefore focus on how Fbxl13-mediated Cep192-3 downregulation could affect various aspects of centrosome biology in tumourigenesis.

We began by investigating two published functions of Fbxl13 identified in genome-wide screens: ionising radiation (IR) sensitivity, and genomic instability.

5.2.2 Fbxl13 depletion does not sensitise cells to ionising radiation

Fbxl13 was identified in two genome-wide, shRNA screens to sensitise U2OS cells to ionising radiation (IR) (Hurov et al., 2010). It is well established that irradiation induces centrosome overduplication (Bourke et al., 2007; Inanç and Morrison, 2011; Sato et al., 2000a; Sato et al., 2000b), however it is unclear whether this effect is only correlative, or if centrosome overduplication plays an active role in IR response (Mullee and Morrison, 2015; Sato et al., 2000b). To determine whether IR sensitivity could be a phenotype of Fbxl13-mediated Cep192 degradation, we first attempted to validate the findings of the published shRNA screens.

IR sensitivity can be measured using a clonogenic survival assay (Franken et al., 2006). This assay takes advantage of low seeding densities, such that single cells form distinct, visible colonies over time. Cell survival following chemical or physical treatments, such as irradiation, can therefore be calculated from the number of colonies in the treatment plate relative to an untreated control. To address whether Fbxl13 siRNA depletion sensitised cells to IR, U2OS cells were transfected with two siRNAs targeting Fbxl13 (S3 and S4) or an siRNA control (siLacZ) for 48 hours. Cells were then re-seeded at clonal densities (800 cells per 60 mm dish), irradiated the following day with 0, 1, 2, or 3 Gray, and allowed to recover for 12 days. The colonies were then fixed, stained, and counted. Cell survival was then calculated for each IR dose, relative to the untreated control. This was given as the percentage of surviving colonies (surviving fraction). Lastly, the data was fitted to a linear quadratic model (Brenner, 2008). This model most accurately reflects the survival response to IR, as it takes into account two death rates to the DNA damage inflicted by IR: one linear, and one exponential (Figure 5.3).

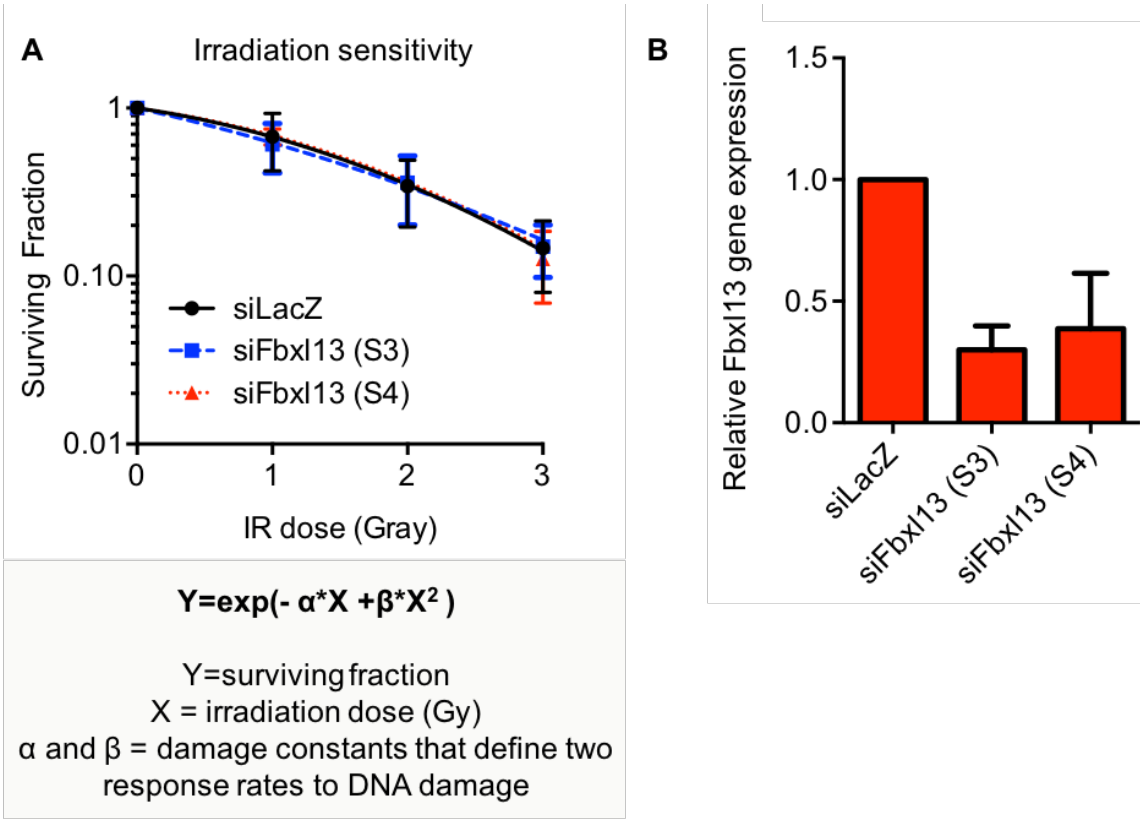

Figure 5.3 Fbxl13 depletion does not sensitise U2OS cells to ionising radiation

(A) Surviving fraction of U2OS cells following irradiation (IR), as measured using a clonogenic survival assay. U2OS cells were transfected with an siRNA control (siLacZ) or two siRNAs targeting Fbxl13 (S3 and S4) for 48 hours. The cells were then re-seeded in triplicate at a clonal density, and irradiated the following day with the indicated doses. 12 days later, the colonies were fixed and stained. The number of colonies formed was used to calculate the surviving fraction for each IR dose using the equations described in Methods 2.2.12. The data were then fitted to a linear quadratic equation using the equation shown (Brenner, 2008). N=3 biological replicates. Data are shown as mean ± SD. **(B)** Validation of Fbxl13 siRNA using quantitative real-time PCR (qPCR) of the samples shown in **(A)** at the time of irradiation. Data are shown as mean ± SD.

We observed that Fbxl13 depletion did not affect IR sensitivity at any of the tested doses, despite Fbxl13 knockdown at the time of irradiation (Figure 5.3). However, although this was observed in two shRNA screens, only one Fbxl13 shRNA in these studies was validated (Hurov et al., 2010). Taken together, we conclude from this data that Fbxl13 does not affect IR sensitivity.

Additionally, Fbxl13 depletion is also implicated in genomic instability. A genome-wide shRNA screen found that Fbxl13 shRNA increase the number of γ-H2AX foci, however this observation was not validated (Paulsen et al., 2009). Genomic instability is a strong indicator of IR sensitivity, as DNA damage resolution is a key factor of IR survival. Due to this link, we wished to confirm whether Fbxl13 could be involved in genomic instability.

Using immunofluorescence, we attempted to reproduce this observation by staining U2OS cells for γ-H2AX following Fbxl13 siRNA (Figure 5.4). Unfortunately, preliminary data suggested that there was no difference in genomic instability in Fbxl13 depleted cells, relative to control. However, we note that this is consistent with the inability of Fbxl13 depletion to sensitise cells to IR in our hands.

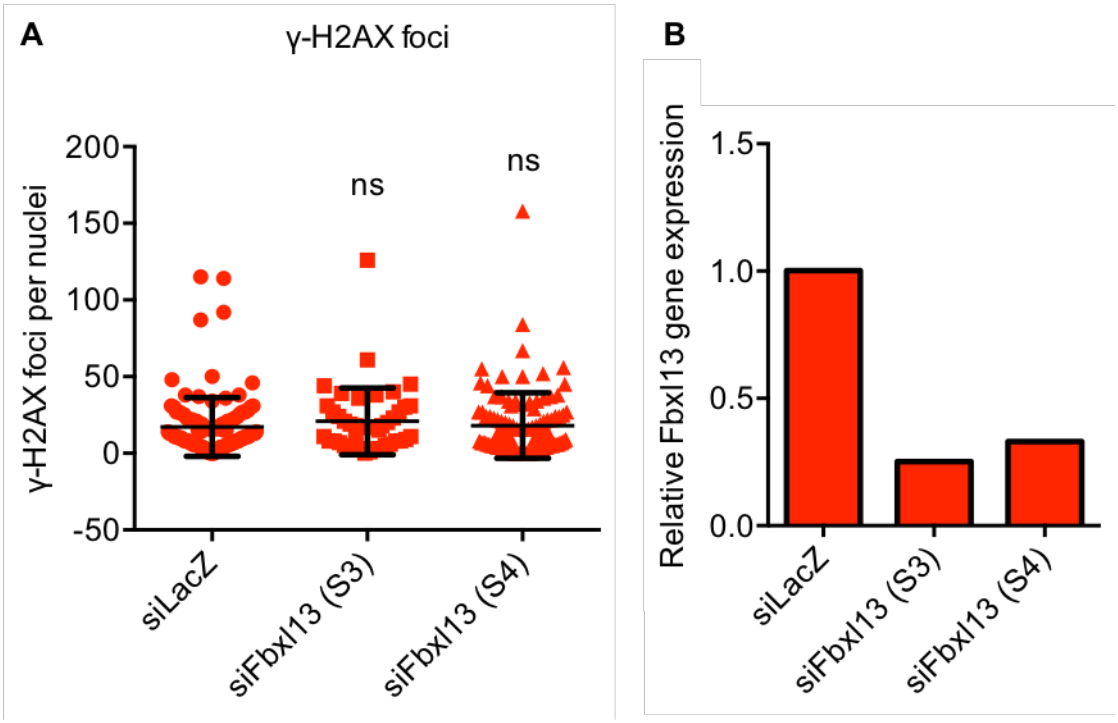

Figure 5.4 Fbxl13 depletion does not increase genomic instability

(A) U2OS cells were transfected with a control siRNA (siLacZ) or two siRNAs targeting Fbxl13 (S3 and S4). Cells were then formalin fixed and stained for γ-H2AX foci. The number of foci per nuclei were scored manually in Image J. Preliminary data, N>100 cells per condition. Data are shown as mean ± SD. Statistically insignificant results comparing γ-H2AX foci numbers in control and siFbxl13 cells are indicated as ns for P>0.05, as analysed by Student's t-test. **(B)** Validation of Fbxl13 siRNA using quantitative real-time PCR (qPCR) in the same batch of samples shown in **(A)**.

As a last indication of whether Fbxl13 could be involved in IR response, we asked whether Fbxl13 expression was altered following irradiation using quantitative real-time PCR (qPCR). Preliminary data showed that Fbxl13 RNA expression did not change following either 4 or 8 Gray of irradiation between 4 to 8 hours (Appendix 4). In contrast, positive controls such as p53 and γ-H2AX are all upregulated at least 2-fold following 4 Gray of irradiation within the first 4 hours of irradiation, at the protein level (Yang HB, unpublished data). We do not exclude the possibility that Fbxl13 could be regulated at the protein level in response to IR, for example through stabilised protein levels or altered localisation. However, taking all these data into consideration, we concluded that IR sensitivity and genomic instability are not regulated by Fbxl13, and are therefore not the functional outputs of Fbxl13-mediated Cep192 proteolysis.

For these reasons, we next turned to one of the major functions of Cep192: centriole duplication (Kim et al., 2013; Sonnen et al., 2013; Zhu et al., 2008).

5.2.3 Fbxl13 does not regulate centrosome duplication

Cep192 is a conserved centrosome duplication factor. Spd-2 (in *C. elegans*) is responsible for recruiting the key kinase ZYG-1 (*C. elegans*) or Plk4 (*H. sapiens*) (Kemp et al., 2004; Kim et al., 2013; Sonnen et al., 2013). In humans, Plk4 is recruited by both Cep192 and Cep152 (Kim et al., 2013; Sonnen et al., 2013). Indeed, Cep152 and Cep192 form two distinct scaffolds which are both responsible for the localisation and activation of Plk4 (Park et al., 2014). However, it has been observed that Cep192 plays a stronger role in Plk4 recruitment: centrosomal Plk4 levels are strongly reduced following Cep192 depletion, but not Cep152 depletion (Sonnen et al., 2013). It has also been predicted that this Cep192 function is specific to isoform 3 (Cep192-3), which uniquely possesses a Plk4 binding domain (Sonnen et al., 2013).

To test whether Fbxl13 regulates centrosome duplication, we asked whether Fbxl13 overexpression and depletion could affect centrosome numbers. We hypothesised that since Fbxl13 downregulates centrosomal Cep192, it could also be a negative regulator of centriole duplication. This working hypothesis is shown in Figure 5.5. Conversely, we also hypothesised that Fbxl13 depletion might induce centrosome overduplication through Cep192-3 accumulation.

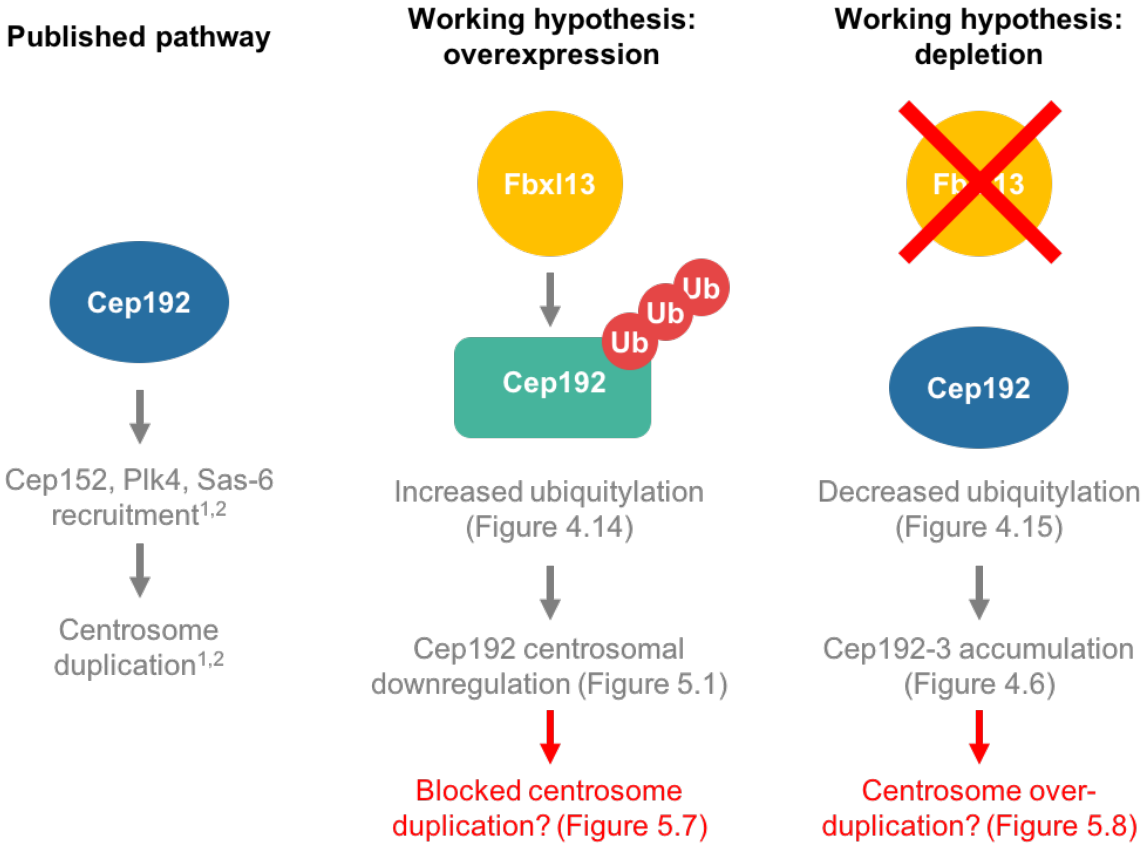

Figure 5.5 Working hypothesis: Fbxl13 and centrosome duplication

Schematic showing a simplified centrosome duplication pathway, and a working hypothesis of Fbxl13 in this process. Cep192 is a crucial centrosome duplication factor, and acts with Cep152 to correctly recruit and activate Plk4 for centrosome duplication (left). We hypothesise that Fbxl13 overexpression downregulates Cep192 and inhibits this pathway, blocking centrosome duplication (middle). Conversely, we hypothesise that Fbxl13 depletion results in Cep192 accumulation, and centrosome over-duplication (right).

[1] Sonnen et al. (2013)

[2] Kim et al. (2013)

To address this question, we stimulated centrosome overduplication and asked if Fbxl13 overexpression could impede this process. The model used for centrosome overduplication was hydroxyurea treatment of U2OS cells.

Hydroxyurea is an inhibitor of ribonucleotide reductase (RNR), and prevents the reduction of NDPs to dNTPs. In this way, hydroxyurea blocks the production of dNTPs for DNA replication, resulting in S-phase arrest. In a subset of cells, such as U2OS cells and Chinese hamster ovary cells, this arrest is permissive for centrosome re-duplication: although the cell cycle is arrested, the centrosome cycle is not (Balczon et al., 1995). This process is dependent on Plk1-mediated centriole disengagement, and results in up to 25% of cells showing an overduplication phenotype after 72 hours of hydroxyurea treatment, as measured by γ-tubulin foci (Figure 5.6)(Loncarek et al., 2010). Thus, this system has been widely used to study the involvement of proteins in centrosome duplication, such as Plk4 (Dzhindzhev et al., 2010). Similarly, we wished to ask if ectopic Fbxl13 could block hydroxyurea-induced centrosome duplication.

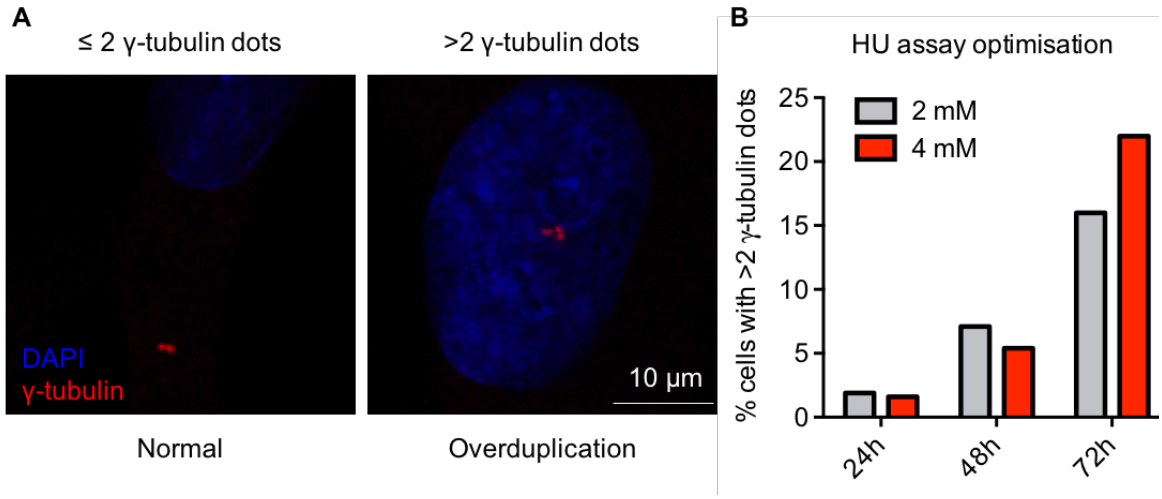

Figure 5.6 Hydroxyurea stimulates centrosome overduplication

(A) U2OS cells were treated with 4mM hydroxyurea (HU) for 72 hours and then methanol fixed. Cells were stained for centrosomes (γ-tubulin, red) and DNA (DAPI, blue). Scale bar, 10 μM. **(B)** Quantification of centrosome overduplication in U2OS cells treated with 2 mM or 4 mM HU for the indicated times. Centrosome overduplication was scored as the percentage of cells containing >2 γ-tubulin dots. N=1 biological replicate, n>200 cells per condition.

To study the effect of Fbxl13 overexpression on centrosome duplication, we established a GFP-Fbxl13 stable cell line using the pBabe retroviral system. We considered this system to be more physiological than transient overexpression, as pBabe is a low-expression vector. The expression of GFP-Fbxl13 was verified by Western blotting (Figure 5.7, inputs). Due to the large size of GFP (27 kDa), it was possible that tag incorporation at the N terminal of Fbxl13 would lead to misfolding, or disruption of function due to steric hindrance. As Centrin-3 binds Fbxl13 through its N terminal (Appendix 1), we reasoned that if the folding of Fbxl13 was intact, then Centrin-3 binding would remain unaffected. Indeed, using co-immunoprecipitation, we observed that GFP-Fbxl13 was still able to bind Centrin-3 (Figure 5.7, left panel).

Using these tools, U2OS cells stably overexpressing either an empty vector control or GFP-Fbxl13 were treated with 4 mM hydroxyurea for 72 hours. The cells were then stained for γ-tubulin and scored for centrosome overduplication (>2 γ-tubulin dots) by immunofluorescence The extra centrosomes scored were not a result of cytokinesis failure, as binucleate cells were not scored. We observed that GFP-Fbxl13 did not significantly alter the percentage of cells with centrosome overduplication (Figure 5.7, right panel). This suggested that although Cep192 is required for centrosome duplication in human cells, Fbxl13-mediated Cep192 downregulation does not regulate centrosome numbers.

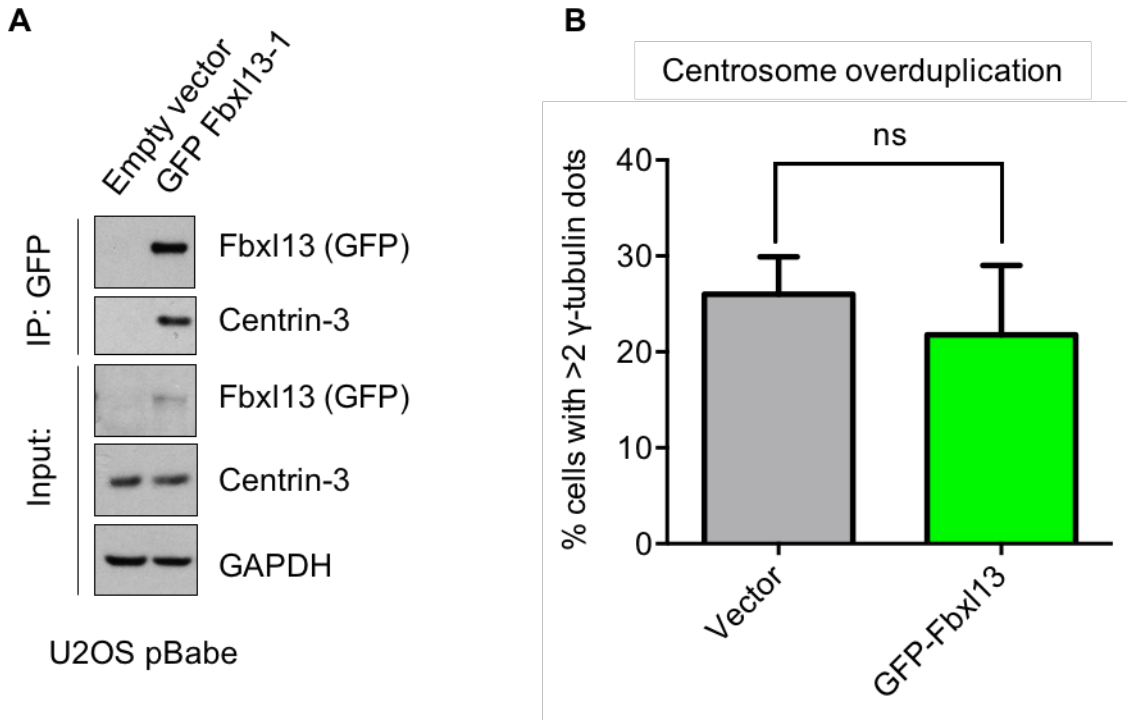

Figure 5.7 Fbxl13 overexpression does not affect HU-induced centrosome duplication

(A) Validation of pBabe GFP-Fbxl13 cell line. Detection of GFP-Fbxl13 in whole cell extract (Input) and following GFP immunoprecipitation. An empty vector stable cell line was used as a negative control. **(B)** Quantification of centrosome overduplication in U2OS cells stably integrated with pBabe GFP-Fbxl13. An empty vector stable cell line was used as a negative control. Cells were treated with 4 mM hydroxyurea (HU) for 72 hours. N=3 biological replicates, n>100 cells per condition. Data are shown as mean ± SD. Statistically insignificant results comparing γ-tubulin foci numbers in control and GFP-Fbxl13 cells are indicated as ns for P>0.05, as analysed by Student's t-test.

Conversely, we also asked whether Fbxl13 depletion could stimulate centrosome duplication in untreated cells. U2OS cells were transfected with an siRNA non-targeting control (siRNA NTC) or two siRNAs targeting Fbxl13 (S3 and S4). Following 72 hours, cells were then fixed and stained for γ-tubulin. We observed that Fbxl13 depletion increased centrosome overduplication from only 2% to 4% (Figure 5.8). Fbxl13 depletion was validated by qPCR (Figure 5.8, right panel). We note that in contrast, positive controls such as Cep152 overexpression resulted in approximately 45% of cells with centrosome overduplication (Dzhindzhev et al., 2010).

One limitation of siRNA is that not 100% of cells are transfected. Furthermore, without an antibody to visualise endogenous Fbxl13 by immunofluorescence, we were unable to distinguish between successfully transfected and untransfected cells. Thus, to confirm this data, we repeated this assay using shRNA depletion.

U2OS cells were stably transfected with an shRNA control, or shRNA oligos targeting Fbxl13 (75, 85, and 87). This had two advantages. Firstly, stable lentiviral integration could be selected using both puromycin and GFP expression, ensuring that 100% of scored cells were shFbxl13 positive. Secondly, the Fbxl13 knockdown efficiency here was higher than with siRNA, with up to 80% knockdown in one of the cell lines. To further improve our previous assay, Centrin-3 foci were scored in lieu of γ-tubulin foci. As Centrin-3 labels individual centrioles, it would be more sensitive to overduplication phenotypes.

Despite these improvements, we observed that shRNA depletion of Fbxl13 resulted in a two-fold increase in cells with centrosome overduplication, from 4% to only 8% (Figure 5.9).

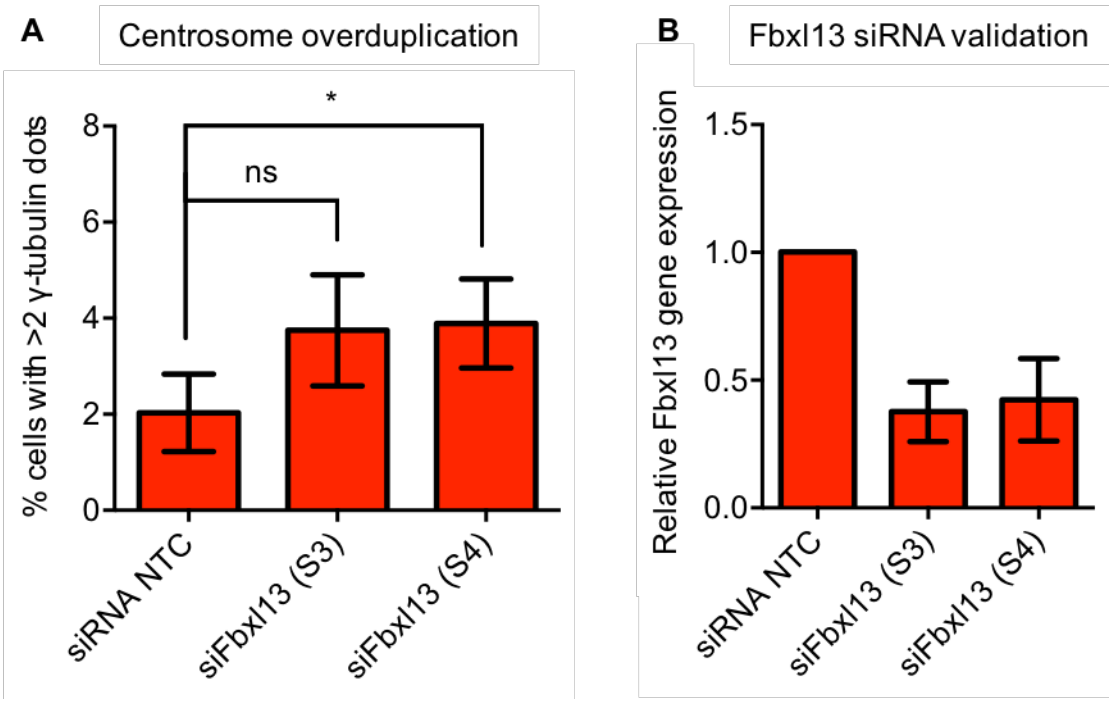

Figure 5.8 Fbxl13 siRNA depletion and centrosome overduplication

(A) Quantification of centrosome overduplication in U2OS cells transfected with a non-targeting siRNA (siRNA NTC), or two siRNA oligos targeting Fbxl13 (S3 and S4). N=3 biological replicates, n>200 cells per condition. Data are shown as mean ± SD. Statistical analyses comparing γ-tubulin foci numbers in control and siFbxl13 cells are indicated as ns for $P>0.05$, and * for $P\leq0.05$, as analysed by Student's t-test. **(B)** Validation of Fbxl13 siRNA using quantitative real-time PCR (qPCR) in the same samples shown in **(A)**. Data are shown as mean ± SD.

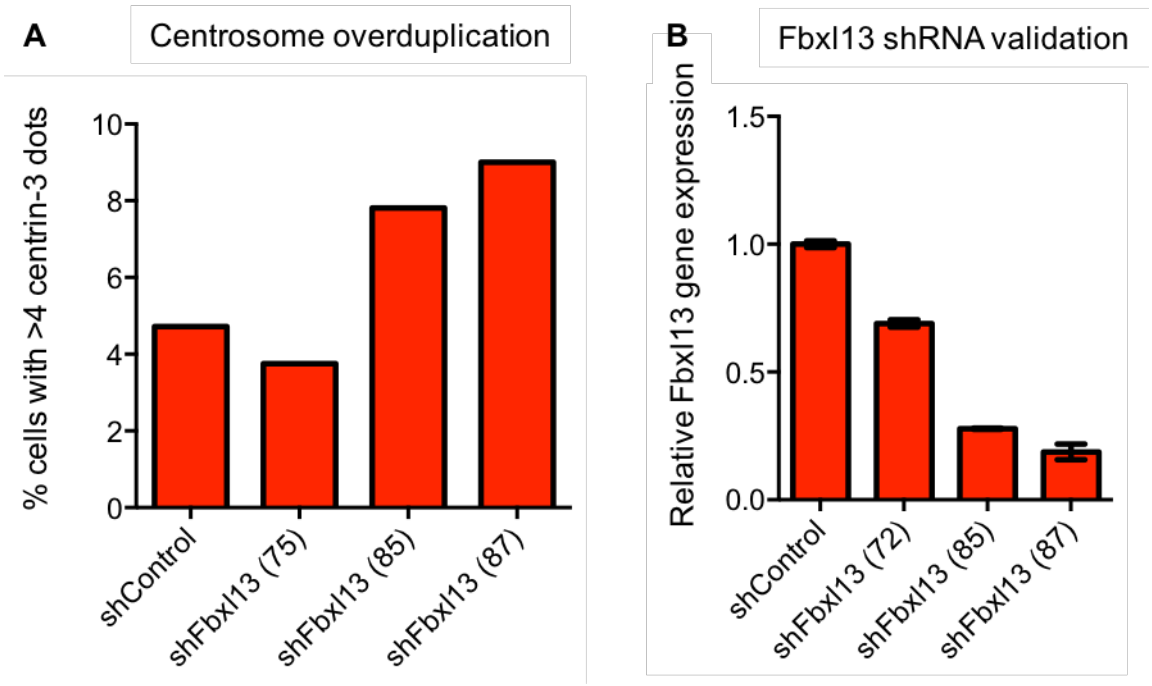

Figure 5.9 Fbxl13 shRNA depletion and centrosome overduplication

(A) Quantification of centrosome overduplication in U2OS cells stably integrated with an shRNA control (shControl) or three shRNA oligos targeting Fbxl13 (75, 85, 87). N=1 biological replicate, n>200 cells per condition. **(B)** Validation of Fbxl13 siRNA using quantitative real-time PCR (qPCR) in the same samples shown in **(A)**. Data are shown as mean ± technical SD between triplicates.

Taken together with the previous data, we conclude that Fbxl13 regulates in part centrosome duplication by controlling Cep192 levels, however this only accounts for a minor role in the centrosome duplication pathway since the effect scored was minor. Although Fbxl13 depletion led to a two-fold change of overduplication from 2 to 4% (siRNA) and 4 to ~8% (shRNA), we considered these differences too small for further investigation.

The next section will therefore focus on a second major Cep192 function, centrosome microtubule organising centre (MTOC) activity, and whether this could be the output of Fbxl13 mediated Cep192 downregulation.

5.2.4 Fbxl13 negatively regulates centrosomal γ-tubulin recruitment

Previously, whilst scoring γ-tubulin foci in preliminary experiments, we had also observed that γ-tubulin intensity at the centrosome was consistently downregulated following Fbxl13 overexpression in interphase cells (Appendix 5). Interestingly, this is consistent with Cep192 function. Cep192 not only plays a major role in centrosome maturation during mitosis, but also maintains centrosomal microtubule nucleation in interphase via γ-tubulin recruitment (O'Rourke et al., 2014). It was reported that Cep192 depletion results in reduced centrosomal γ-tubulin and downregulated centrosomal microtubule arrays in interphase. This led us to hypothesise that Fbxl13 overexpression could have the same effect, as shown in Figure 5.10.

Our first aim was to confirm whether Fbxl13 overexpression indeed downregulated γ-tubulin recruitment to the centrosome. We addressed this question using immunofluorescence. U2OS cells were transfected with either Flag-Fbxl13 or an empty vector control, and stained for γ-tubulin, Flag, and DNA (Figure 5.11). To control for cell-cycle fluctuations in γ-tubulin, only G2 cells were scored. These were differentiated by nuclei size.

Once again, we observed a centrosomal enrichment of Flag-Fbxl13 at the centrosomes. We also observed that γ-tubulin intensity was reduced in cells overexpressing Fbxl13. Quantification revealed that this reduction was significant (Figure 5.11, bottom panel). This confirms our previous observation (Appendix 5), and is consistent with Fbxl13-induced Cep192 downregulation at the centrosome (Figure 5.1-5.2). From these data, we conclude that Fbxl13 overexpression indeed downregulates centrosomal γ-tubulin levels.

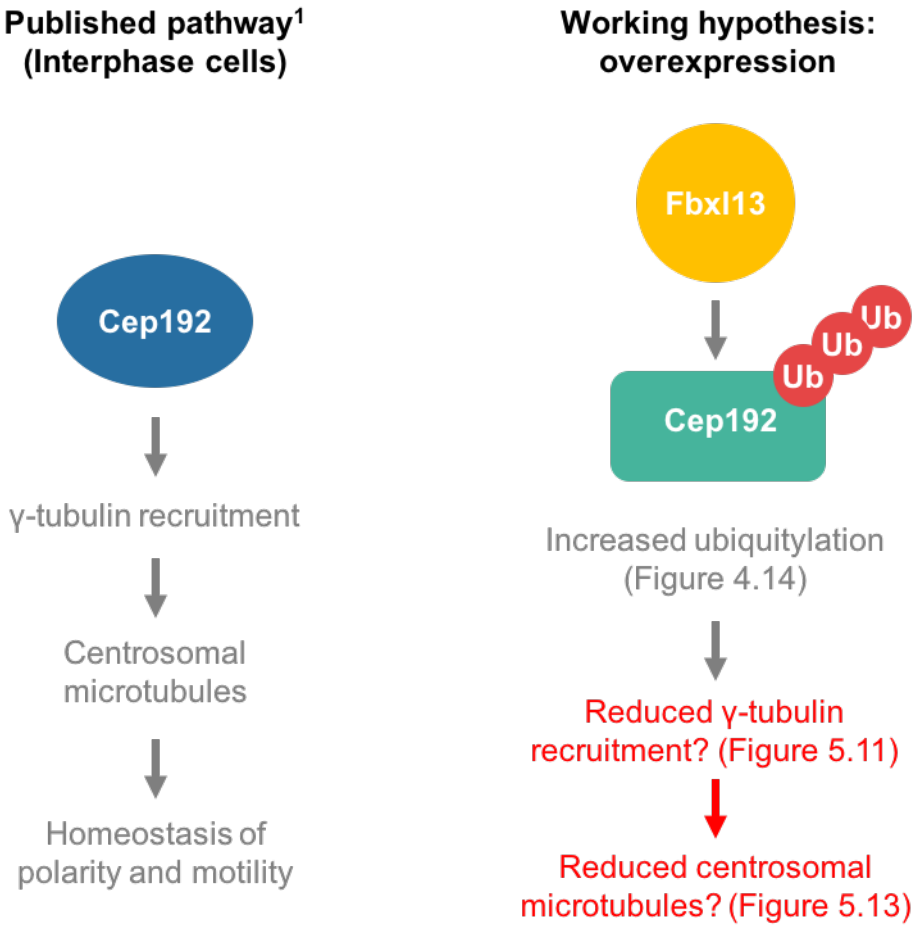

Figure 5.10 Working hypothesis: Fbxl13 and γ-tubulin recruitment

Schematic showing a simplified Cep192 pathway regulating microtubule organising centre (MTOC) activity (left), and a working hypothesis including Fbxl13 in this process (right). Cep192 is required for γ-tubulin recruitment, which forms γ-tubulin ring complexes (γTuRC) to promote microtubule nucleation. This maintains homeostasis of cell polarity and motility (O'Rourke et al., 2014). We hypothesise that Fbxl13 overexpression inhibits this process by downregulating γ-tubulin recruitment and centrosomal microtubule arrays.

[1] O'Rourke et al. (2014)

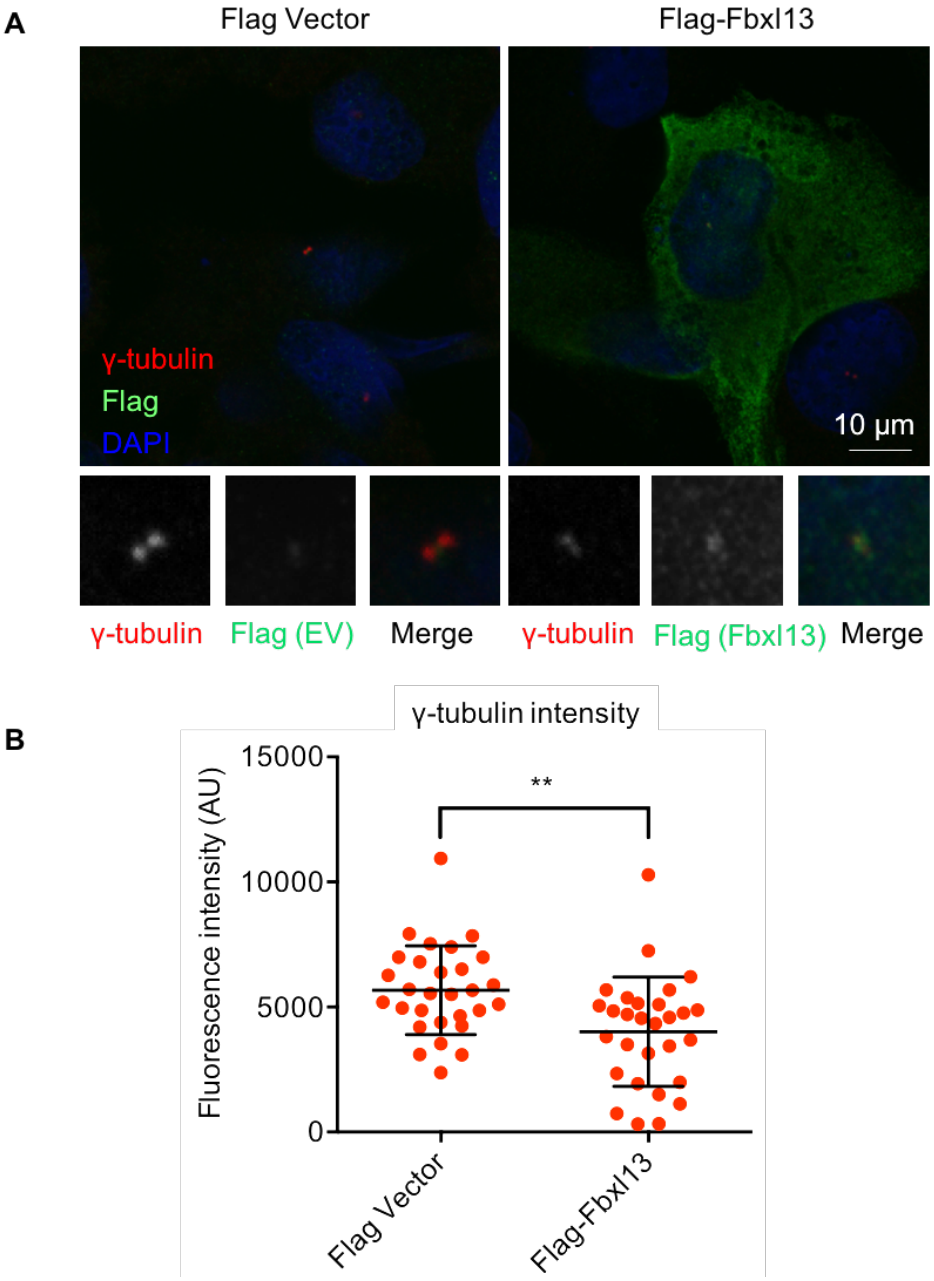

Figure 5.11 Fbxl13 overexpression reduces centrosomal γ-tubulin

(A) Representative images of U2OS cells transfected with Flag-Fbxl13, or an empty vector control were fixed with methanol, and stained for γ-tubulin (red), Fbxl13 (Flag, green), and DNA (DAPI, blue). Images were acquired using confocal microscopy at identical settings. Scale bar, 10 μM. **(B)** Quantified γ-tubulin fluorescence intensity following Fbxl13 overexpression in the samples represented in **(A)**. N=2 biological replicates, n>30 cells per condition. Data from only one biological replicate is shown due to variations in baseline fluorescence between biological replicates. Data is shown as mean ± SD. Statistically significant results comparing γ-tubulin intensity in control and Fbxl13 overexpressing cells are indicated as ** for P≤0.01, as analysed by Student's t-test.

Conversely, according to this hypothesis, one would expect Fbxl13 depletion to result in γ-tubulin accumulation. This was addressed using immunofluorescence in U2OS cell lines stably integrated with Fbxl13 shRNA. We observed that relative to an shRNA control cell line, Fbxl13 shRNA cells contained higher levels of γ-tubulin at the centrosomes (Figure 5.12). Interestingly, across the three shRNA cell lines, γ-tubulin upregulation correlated with Fbxl13 knockdown efficiency as validated by qPCR (Figure 5.12, right panel). From this observation, we hypothesise that Fbxl13 levels are rate-limiting for γ-tubulin recruitment. Relative to control, only one out of three Fbxl13 shRNA cell lines showed significant γ-tubulin upregulation. This cell line also had the highest Fbxl13 knockdown efficiency, at 80%. The fact that a significant phenotype can only be seen following 80% knockdown suggests that residual Fbxl13 could mask phenotypes. This applies particularly for centrosomal proteins, as the centrosome compartment is so minute (1/2000 of the cytoplasm (Lopes et al., 2015)). An antibody recognising endogenous Fbxl13 by immunofluorescence would allow us to confirm effective knockdown of Fbxl13 at the centrosome. Despite these caveats, these data demonstrate that Fbxl13 negatively regulates γ-tubulin recruitment in interphase cells.

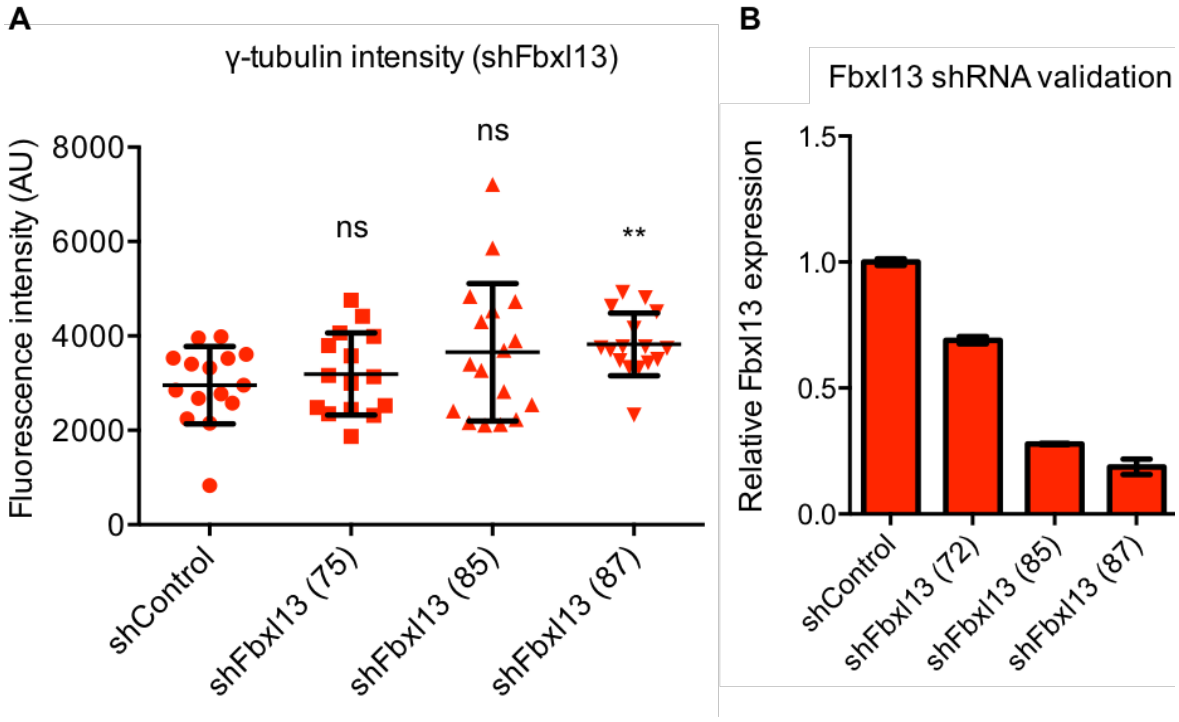

Figure 5.12 shFbxl13 increases γ-tubulin intensity

(A) Quantified γ-tubulin fluorescence intensity in U2OS cells stably integrated with an shRNA control (shControl) or three shRNA oligos targeting Fbxl13 (75, 85, 87). N=2 biological replicates, n>30 cells per condition. Data from only one biological replicate is shown due to variations in baseline fluorescence between biological replicates. Data is shown as mean ± SD. Statistical analyses comparing γ-tubulin intensity in control and shFbxl13 cells are indicated as ns for P>0.05, and ** for P≤0.01, as analysed by Student's t-test. **(B)** Validation of Fbxl13 shRNA using quantitative real-time PCR (qPCR) in the same batch of samples shown in **(A)**. Error bars represent technical SD between three qPCR triplicates.

As γ-tubulin forms the basis of the γ-tubulin ring complex (γTuRC), we next asked whether Fbxl13 mediated γ-tubulin downregulation also inhibits centrosomal microtubule arrays.

U2OS cells were transfected with either Flag-Fbxl13, or an empty vector control. Cells were then methanol fixed and stained for Cep192, α-tubulin, Flag, and DNA (Figure 5.13). Strikingly, we observed that cells overexpressing Flag-Fbxl13 did not have centrosomal microtubule arrays. Preliminary quantification data also revealed that cells overexpressing high levels of Flag-Fbxl13 did not have centrosomal microtubule arrays. Flag-Fbxl13 overexpressing cells also had visibly lower levels of Cep192, consistent with our previous data (Figure 5.1).

Taken together, we demonstrate that Fbxl13 downregulates γ-tubulin recruitment in interphase cells. We suggest that this results in reduced microtubule nucleation capacity of the centrosome. Next, we asked whether Fbxl13-mediated disruption of the microtubule network had further downstream implications.

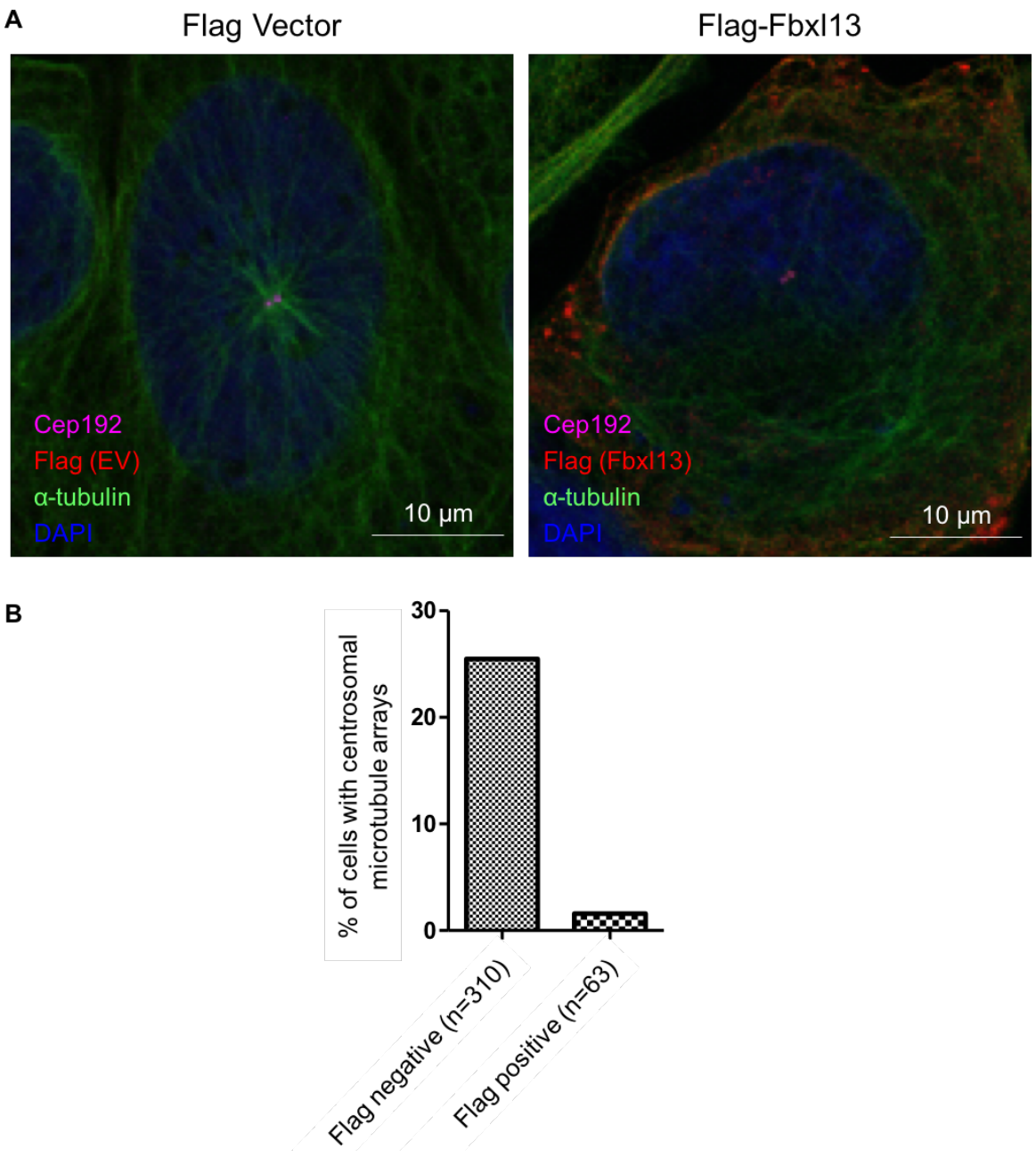

Figure 5.13 Fbxl13 overexpression reduces centrosomal microtubule arrays

(A) Cells were then methanol fixed and stained for Fbxl13 (Flag, red), Cep192 (magenta), microtubules (α-tubulin, green) and DNA (DAPI, blue). Scale bar, 10 μM. N=1 biological replicate. **(B)** Quantification of Flag-Fbxl13 negative and positive cells with centrosomal microtubule arrays, performed by Dr Hongbin Yang. N=1 biological replicate.

5.2.5 Fbxl13 amplification in U2OS cells increases cell motility

Thus far, we have found that Fbxl13 overexpression in interphase cells downregulates centrosomal Cep192, centrosomal γ-tubulin, and centrosomal microtubule arrays. As Cep192 and its role in centrosomal microtubule organisation has been implicated in cell motility and invasiveness (Godinho et al., 2014), we hypothesise that Fbxl13 overexpression may also regulate this pathway. This is especially relevant for tumour progression, as cell motility is indicative of invasiveness and thus poor prognosis. We hypothesise that Fbxl13 overexpression upregulates cell motility, as Cep192 depletion results in hyperpolarisation (O'Rourke et al., 2014) (Figure 5.14). Our next aim was therefore to investigate the role of Fbxl13 in cell motility.

To address how Fbxl13 amplification could impact cell motility in cancer cells, we turned to U2OS cells. As U2OS cells have amplified Fbxl13 levels, we asked whether Fbxl13 depletion could downregulate U2OS cell motility. Our working hypothesis is shown in Figure 5.14.

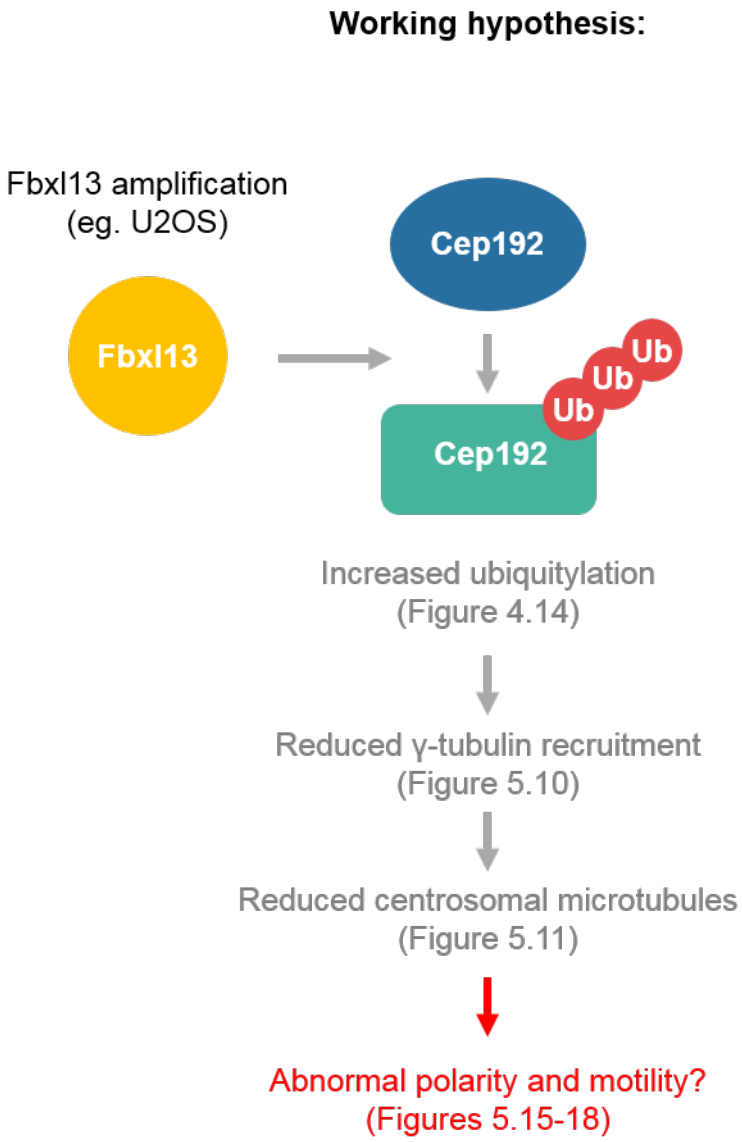

Figure 5.14 Working hypothesis: Fbxl13 and cell motility

A working hypothesis of the Fbxl13-Cep192 pathway identified thus far. Fbxl13 targets Cep192-3 for ubiquitin mediated proteolysis, and results in Cep192 downregulation at the centrosome. Fbxl13 overexpression also results in reduced centrosomal γ-tubulin levels, and reduced centrosomal microtubules. These processes have been implicated in cell polarity and motility in a Cep192 dependent manner (Godinho et al., 2014; O'Rourke et al., 2014). We therefore hypothesise that Fbxl13 also regulates cell polarity and motility.

Cell motility can be measured using a wound healing assay. Wound healing assays are performed on cells that have reached 100% confluency. At this point, a “wound” is introduced using a linear scratch. The cells at the edge of the wound (leading edge) are then able to migrate into the vacant space. Cell motility can then be given as wound closure efficiency, as measured by the wound area closed over time. Here, U2OS cells were transfected with either an siRNA control (siLacZ) or an siRNA oligo targeting Fbxl13 (S4). Following 48 hours, cells were re-seeded at a high density (450,000 cells per 60 mm dish). This re-plating step controls for variations in cell proliferation. The following day, a linear wound was made using a sterile 10 µl tip. To further control for any variations in cell proliferation, the wound healing assay was performed under serum starved conditions (0.5% FBS). Wound healing was observed using microscopy (Figure 5.15). Wound area was measured using an Image J plugin, the MRI Wound Healing Tool (http://dev.mri.cnrs.fr/projects/imagej-macros/wiki/Wound_Healing_Tool).

Using this method, we observed that Fbxl13 depletion reduced wound closure efficiency by 30-40% (Figure 5.16). Fbxl13 depletion was validated by qPCR (Figure 5.16, right panel). We concluded from this data that Fbxl13 depletion downregulates cell motility in U2OS cells. This supports our hypothesis that Fbxl13 amplification in U2OS cells promotes cell motility.

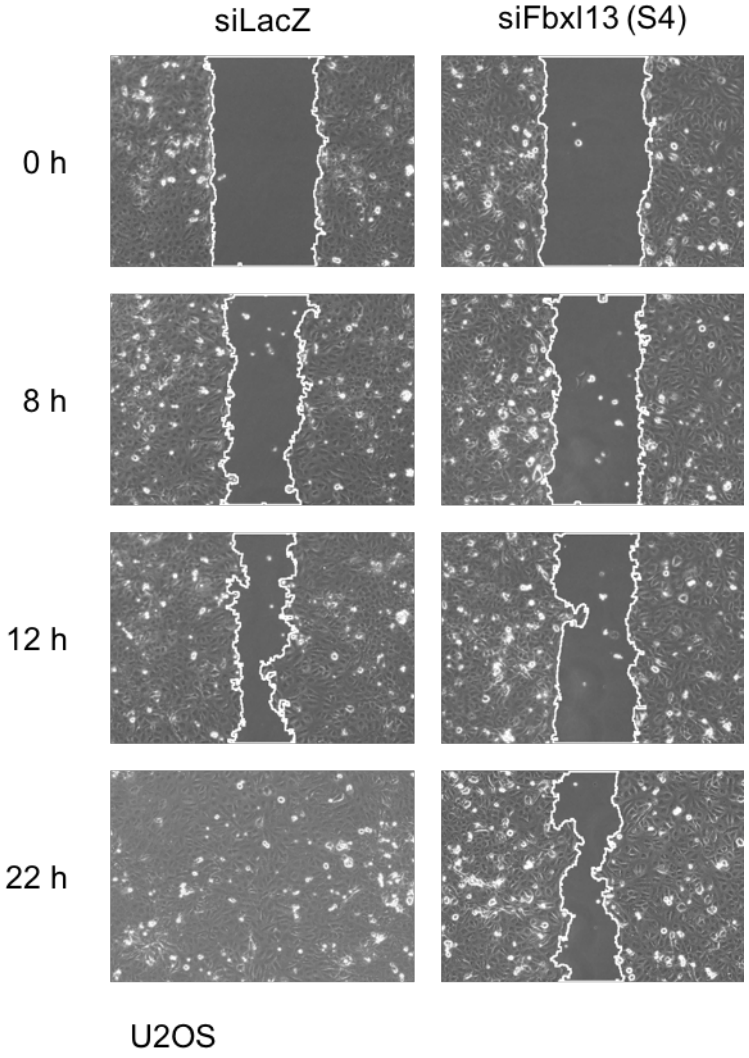

Figure 5.15 Fbxl13 depletion reduces U2OS cell motility

U2OS cells were transfected with a control siRNA (siLacZ) or an siRNA targeting Fbxl13 (S4) for 48 hours. Cells were then re-seeded at 100% density. The following day, a linear wound was made using a sterile 10 µl tip, and the wound was allowed to close in serum-starved conditions (0.5% FBS). Wound margins detected by the MRI Wound Healing Tool in Image J are indicated in white. Images were acquired at identical positions over the indicated time points. Representative images are shown. N=3 biological replicates, n>4 wounds per condition.

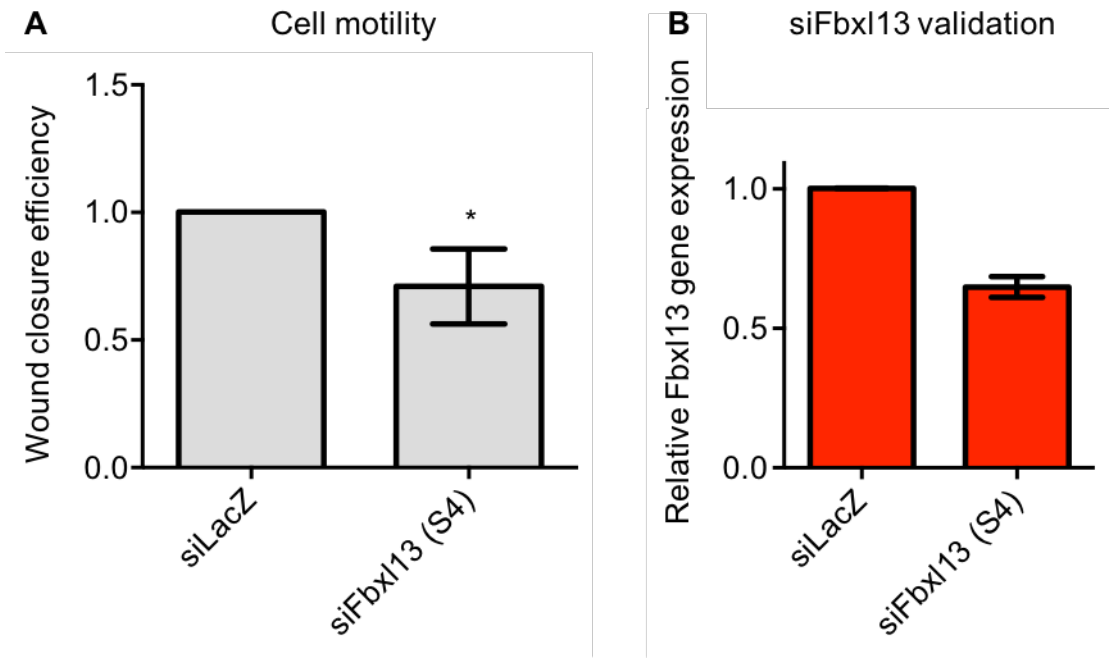

Figure 5.16 Quantification of wound healing following Fbxl13 depletion

(A) Quantification of wound closure efficiency following Fbxl13 depletion by siRNA in Figure 5.15, as measured by wound area. N=3 biological replicates, n=4 wounds per condition. Data are shown as shown as mean ± SD. Statistically significant results comparing wound closure efficiency in control and siFbxl13 cells are indicated as * for P≤0.05 as analysed by Student's t-test. **(B)** Validation of Fbxl13 siRNA using quantitative real-time PCR (qPCR) in the same samples quantified in **(A)**. Error bars represent mean ± SD.

To confirm that this phenotype was Fbxl13 specific, and not an siRNA off-target effect, we next attempted to rescue the phenotype with siRNA resistant Fbxl13. As the siRNA used targets the 3` untranslated region of Fbxl13, an overexpression construct of Fbxl13 would not be degraded. We used a low-level, stable overexpression system as we considered this to be more physiological than transient overexpression.

U2OS cells stably integrated with an empty vector or pBabe-Fbxl13 were transfected with an Fbxl13 siRNA (Figure 5.17, A). A non-targeting siRNA was also used as a control. Fbxl13 depletion and rescue was confirmed using qPCR (Figure 5.17, C). Our data showed once again that Fbxl13 depletion resulted in a reduction in cell motility. Additionally, we observed that the re-expression of Fbxl13 partially rescued this effect (Figure 5.17, B). To improve our assay, this experiment was repeated using a stably integrated Fbxl13 shRNA (Figure 5.18). We observed once again that Fbxl13 depletion reduced cell motility. In this case, the reduction was stronger than with siRNA, likely due to better knockdown (Figure 5.18, C). We also observed a full rescue of the wound healing phenotype. This suggests that the reduced cell motility observed is Fbxl13 specific, and not an off-target effect.

Taken together, these data show that Fbxl13 amplification in U2OS cells promotes cell motility. We also provide evidence that this occurs in an Fbxl13-specific manner.

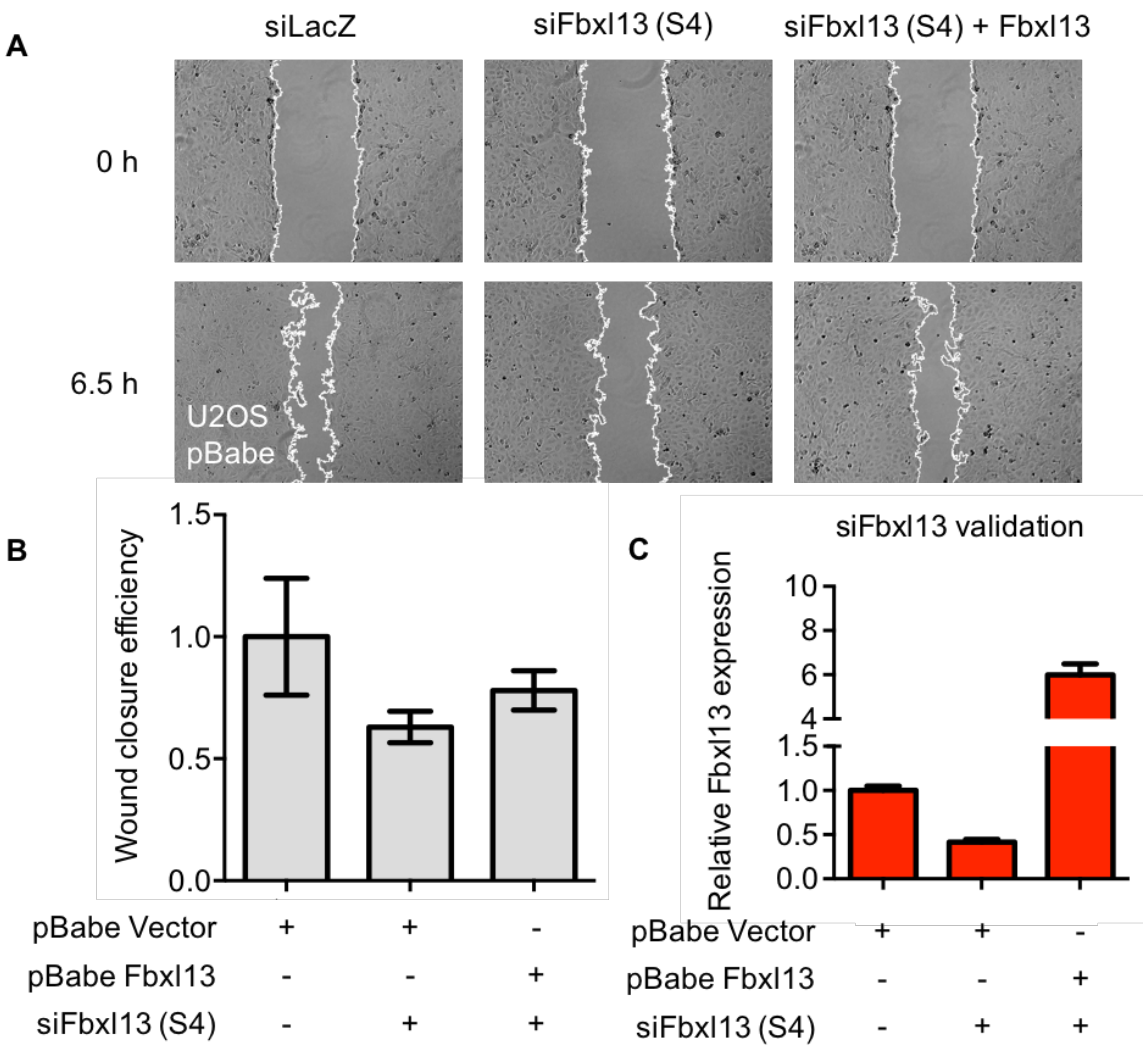

Figure 5.17 siRNA resistant Fbxl13 partially rescues wound healing in U2OS cells

(A) Plain U2OS cells were transfected with a control siRNA (siLacZ) or an siRNA targeting Fbxl13 (S4). U2OS cells stably overexpressing siRNA resistant Fbxl13 were also transfected with siFbxl13 (S4 + Fbxl13). Cells were then re-seeded at 100% density. The following day, a linear wound was made using a sterile 10 µl tip, and the wound was allowed to close in serum-starved conditions (0.5% FBS). Images were acquired at identical positions over the indicated time points. Representative images are shown. Preliminary data, N=1 biological replicate, n>4 wounds per condition. **(B)** Quantification of wound closure efficiency shown in **(A)** as calculated by the percentage of wound area closed. Error bars represent technical SD between four wounds. **(C)** Validation of Fbxl13 siRNA using quantitative real-time PCR (qPCR) in the same batch of samples shown in **(A)**. Error bars represent technical SD between three qPCR triplicates.

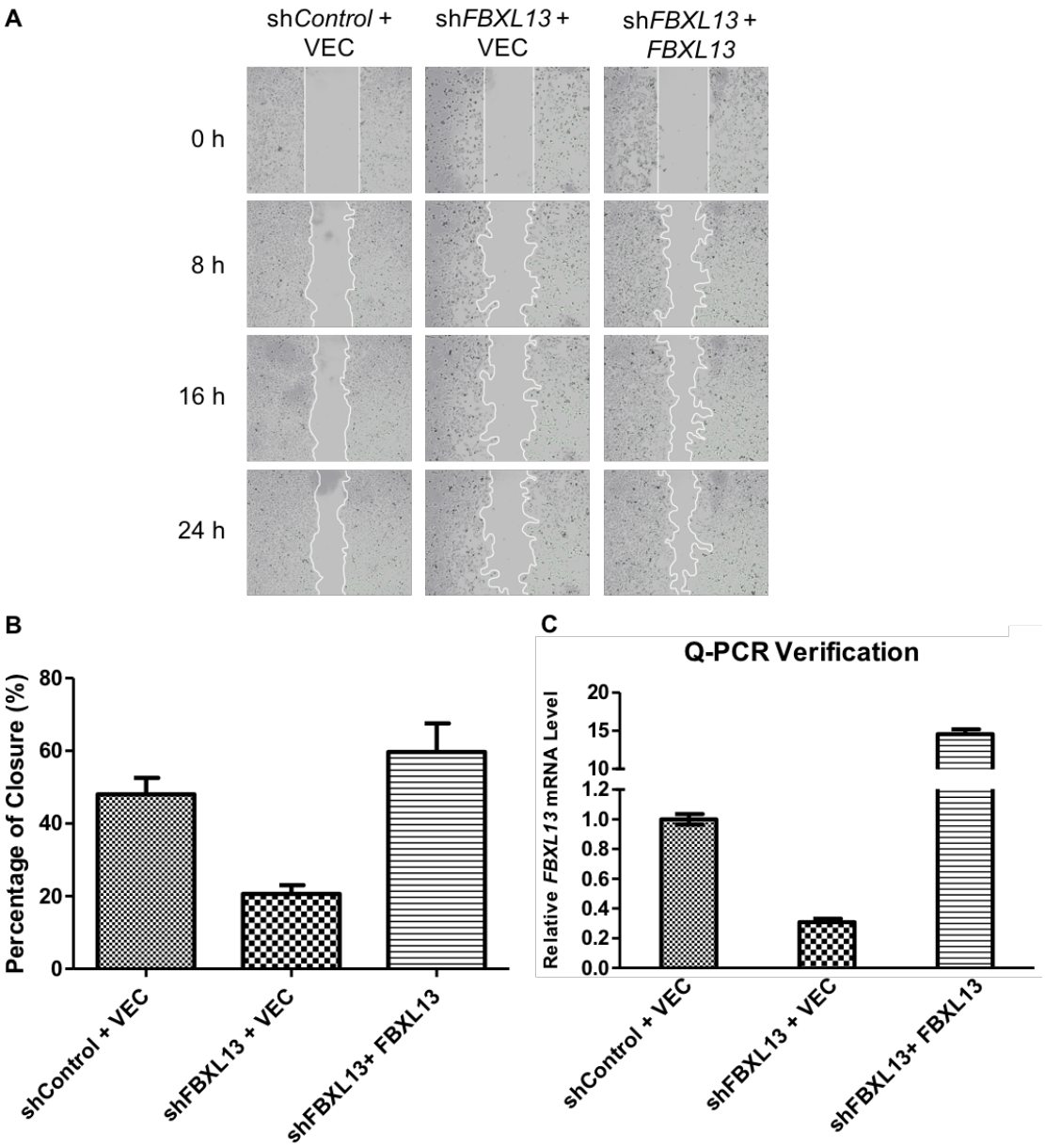

Figure 5.18 shRNA resistant Fbxl13 rescues wound healing in U2OS cells

(A) U2OS cells stably overexpressing pBabe Fbxl13 or an empty vector control (VEC) were transduced with a lentiviral vector containing an shRNA targeting Fbxl13, or an shRNA control. Cells were selected for lentiviral transduction and seeded at 100% density. The following day, a linear wound was made using a sterile 10 µl tip, and allowed to close in serum-starved conditions (0.5% FBS). Images were acquired at identical positions over the indicated time points. Representative images are shown. N=1 biological replicate, n>4 wounds per condition. **(B)** Quantification of wound closure efficiency in **(A)** as the percentage of wound area closed. Error bars represent technical SD between four wounds. **(C)** Validation of Fbxl13 shRNA using quantitative real-time PCR (qPCR) in the same batch of samples shown in **(A)**. Error bars represent technical SD between three qPCR triplicates. Performed by Dr Hongbin Yang.

5.3 Results summary

Fbxl13 has been implicated in tumourigenesis, and is frequently upregulated in solid tumours cohorts originating from tissues such as breast, prostate, head and neck, and oesophageal tissues (cBioPortal). Unfortunately, Fbxl13 remains uncharacterised. The aim of this study was therefore to identify interactors, substrates, and possible functions of Fbxl13.

In the previous chapter, we demonstrated that Fbxl13 downregulates Cep192-3, and provided evidence that this occurs via ubiquitin mediated proteolysis. This chapter aimed to understand the function of the Fbxl13-Cep192-3 axis in normal cells, and how Fbxl13 amplification could contribute to tumourigenesis.

Based on our findings, we propose that in normal cells, Fbxl13 targets centrosomal Cep192-3 for ubiquitin mediated proteolysis to downregulate microtubule nucleation activity. In support of this, we showed that Flag-Fbxl13 was enriched at the centrosome, and that Fbxl13 overexpression significantly reduced centrosomal Cep192 and γ-tubulin levels. Our data also suggest Flag-Fbxl13 overexpression disrupted centrosomal microtubule arrays. These data are consistent with the known role of Cep192 in γ-tubulin recruitment and microtubule nucleation activity (O'Rourke et al., 2014). To confirm our hypothesis, further work is required to show that these effects of Fbxl13 are Cep192 specific.

We also propose that the deregulation of this pathway could contribute to tumourigenesis. Indeed, centrosomal microtubules are important regulators of cell polarity and motility (O'Rourke et al., 2014). Furthermore, recent studies have

shown that perturbed MTOC activity has deleterious effects (Godinho et al., 2014; Schnerch and Nigg, 2016).

Finally, we identify a role for Fbxl13 in tumour-related processes. We observed that U2OS cells, which have amplified Fbxl13 levels, show reduced cell motility following Fbxl13 depletion in a specific, rescuable manner. We propose that when Fbxl13 levels are amplified, the microtubule organising activity of centrosomes is downregulated, increasing in cell motility through hyperpolarisation. To investigate this hypothesis, further work is required to investigate the effect of Fbxl13 on cell polarity, and ask whether Fbxl13 regulates cell motility in other cell lines. For example, another cell line with amplified Fbxl13 levels is the glioblastoma cell line U87. One could ask whether Fbxl13 depletion in U87 reduces cell motility in a rescuable manner.

6 Discussion

6.1 Overview

The ubiquitin system is one of the major pathways for post-translational modifications in the cell. F-box proteins are a class of specificity factors for the SCF superfamily of E3 ubiquitin ligases, many of which have oncogenic as well as tumour suppressive properties (D'Angiolella et al., 2012; Raducu et al., 2016; Wang et al., 2014). Due to their high specificity and implications in tumour biology, F-box proteins are the subject of intense investigation as potential anticancer targets (reviewed in Skaar et al. (2014)). For this reason, our lab wished to characterise novel F-box proteins implicated in tumourigenesis. The topic of this study in particular is Fbxl13.

Fbxl13 was a promising target for investigation due to its identification in several genome-wide screens for IR sensitivity (Hurov et al., 2010) and genomic instability (Paulsen et al., 2009). In addition to this, Fbxl13 was found to be amplified or mutated in many tumour samples (cBioPortal) and cancer cell lines (Barretina et al., 2012). However, Fbxl13 substrates and mechanism of action were completely uncharacterised. Thus, we considered Fbxl13 a promising protein that warranted further investigation. This doctoral thesis aimed to identify Fbxl13 interactors, substrates, and functions, in order to understand its potential role in tumourigenesis.

The results presented in this thesis revealed insights into the mechanism of action of Fbxl13. We identified novel Fbxl13 interactors using liquid chromatography tandem mass spectrometry (LC-MS/MS). Using these data as a starting point, we have demonstrated that Fbxl13 is enriched at the centrosome, where it interacts

with the core centrosome proteins Centrin-2, Centrin-3, Cep152 and Cep192. We show that Fbxl13 destabilises Cep192 isoform 3 (Cep192-3), and provide evidence that Fbxl13 targets Cep192-3 for ubiquitin mediated proteolysis. Functionally, we have shown that Fbxl13 downregulates centrosomal Cep192 and γ-tubulin in U2OS cells. Our data suggest that in this way, Fbxl13 also downregulates the formation of microtubule arrays. Thus, we propose that by regulating Cep192-3 levels, Fbxl13 maintains steady-state microtubule nucleation activity at the centrosome. Finally, we propose that Fbxl13 gain-of-function is oncogenic, as Fbxl13 amplification in U2OS cells is associated with increased cell motility in an Fbxl13-dependent manner.

6.2 Identification of Fbxl13 interactors

Mass spectrometry is one of the most prevalent techniques used to identify novel interactors and substrates of orphan F-box proteins. A recent publication aimed to identify all the interactors of leucine-rich-repeat F-box proteins (Fbxls), including Fbxl13 (Tan et al., 2013). However, substrates for Fbxl13 were not found. Interestingly, Tan et al. also identified Centrin-2 and Centrin-3 as the highest scoring Fbxl13 interactors in their screen, however these interactions were not validated *in vivo*. In the same study, it was reported that Centrin-2 and Centrin-3 did not increase upon MLN4924 or Bortezomib treatment, suggesting that Centrin-2 and Centrin-3 are not Fbxl13 targets for proteolysis. This is consistent with our data, which showed that Fbxl13 overexpression did not downregulate Centrin-2 or Centrin-3 half-life. We also observed that Fbxl13 interacted with Centrin-2 and Centrin-3 through its N terminal domain, and not its leucine-rich repeats (Appendix 1). In contrast, F-box proteins of the Fbxl family typically interact with substrates using their leucine-rich-

repeats (Raducu et al., 2016). These data led us to hypothesise that Centrin-2 and Centrin-3 are not downstream substrates of Fbxl13, but upstream regulators. For example, Centrin-2 or Centrin-3 could be required for Fbxl13 centrosomal localisation. Importantly, while we observe a centrosomal enrichment of Fbxl13, it lacks predicted signals for centriole localisation such as the PACT domain.

Interestingly, our LC-MS/MS data also identified interacting proteins that the study performed by Tan et al. did not. Specifically, only 4/25 Fbxl13-1 interactors were present in their data (Appendix 6). For Fbxl13-3, only 3/21 interactors were present in their data (Appendix 7). This could be due to differences in technical procedure, as well as isoform-specific differences: the isoform used by Tan et al. was Fbxl13 isoform 2 (identified by Jin et al. (2004)), whereas we focused on Fbxl13 isoforms 1 and 3, the isoforms listed on UniProt at the beginning of this study. Nevertheless, several Fbxl13 interacting partners were identified both in our LC-MS/MS analysis as well as by Tan et al. For Fbxl13-1, one such common interactor is NACA (nascent polypeptide-associated complex subunit alpha), a cardiac- and muscle-specific transcription factor. Another is LRRC4 (leucine-rich repeat-containing protein 4), a synaptic adhesion protein that recruits pre- and post-synaptic proteins. For Fbxl13-3, a common interactor also identified by Tan et al. for Fbxl13-2 is CLPB (caseinolytic peptidase B protein homologue), a regulatory ATPase implicated in secretion/protein trafficking. We do not exclude the possibility that any of these other interactors may also be bona fide Fbxl13 substrates. For example, the candidate interactor CLPB was found to be enriched following Bortezomib treatment (Tan et al., 2013), suggesting it could be a proteasome target. Consistent with this, our LC-MS/MS data contain other membrane and trafficking proteins, such as SNX2 (Sorting nexin-2) and SYT9 (Synaptotagmin-9). It is known

that single F-box proteins can target multiple substrates, sometimes with opposing functions. For example, Fbxl1 (Skp2) targets p21/p27 (cell cycle arrest) as well as Cyclin A, Cyclin D1, and Cyclin E (cell cycle progression) (Skaar et al., 2009). This is possible due to spatio-temporal regulation and post-translational modifications (Skaar et al., 2013). In the same way, it is possible that Fbxl13 could target different substrates in different contexts, such as tissue specificity, signalling pathways, localisation, or post-translational modifications.

In the study presented in this thesis, we focused on the centrosomal proteins in our LC-MS/MS data, Centrin-2, Centrin-3, and Cep152, as they were enriched and among the top-scoring interactors. We also note that other LC-MS/MS identified candidates may have centrosome-related functions. For example, Cytosolic carboxypeptidase 1 (AGTPBP1) mediates deglutamylation. Polyglutamylation of α- and β-tubulin is abundant on microtubules of centrioles, basal bodies, and some spindle microtubules, and has a stabilising effect (reviewed in Wloga and Gaertig (2010)) (Eddé et al., 1990). It is possible that Fbxl13 is also able to regulate centrosome activity by modulating tubulin glutamylation. This is an interesting follow-up of other Fbxl13 functions, and could be tested using antibodies that recognise tubulin glutamylation following overexpression and depletion of Fbxl13. It is also worth noting that the centrosome is also a hub for trafficking and signalling (reviewed in Arquint et al. (2014)), which could explain the abundance of trafficking proteins such as Sorting nexin 2 (SNX2) and Synaptotagmin-9 (SYT9) in our LC-MS/MS data. Novel interactors and substrates of Fbxl13 would serve as stepping stones to further understand its function and mechanism of action in tumour progression.

6.3 Cep192 ubiquitylation by Fbxl13

Cep192 belongs to the CEP family of centrosomal proteins, which was first characterised in a mass-spectrometry based study on purified interphase centrosomes (Andersen et al., 2003). Since then, many CEP proteins have been identified as active components of centrosome duplication and function, such as Cep41 (required for tubulin glutamylation in ciliogenesis), Cep152 (centriole duplication), and indeed, Cep192 itself (centriole duplication and centrosome maturation) (reviewed in Kumar et al. (2013)).

It is known that Cep192 levels are highly regulated. For example, Cep192 is enriched at the mitotic centrosome up to 100-fold (Gomez-Ferreria et al., 2007) in a pericentrin and Plk1 dependent manner (Gomez-Ferreria et al., 2007; Haren et al., 2009). However, the mechanism behind Cep192 removal from the mitotic centrosome remains unclear. Cep192 downregulation has also been described as a checkpoint mechanism in several pathways. Under hypoxic conditions, the oxygen-inactivated enzyme PHD1 is able to hydroxylate Cep192, forming a recognition domain for SCF^{Skp2} and targeting Cep192 for ubiquitin-proteasome degradation (Moser et al., 2013). This impedes centriole duplication and centrosome maturation, preventing cell cycle progression in metabolically unfavourable conditions (Moser et al., 2013). Conversely, following ultra-violet (UV) radiation, Cep192 was found to be deubiquitylated in a high-throughput SILAC screen (Elia et al., 2015). However, the players regulating Cep192 in this pathway remain unclear. The investigation of novel Cep192 regulators using mass-spectrometry based techniques has been performed, however additional E3 ubiquitin ligases targeting Cep192 have not been found (Firat-Karalar et al., 2014).

It has also been described that Cep192 levels are highly sensitive to manipulation. For example, Cep192 is a core fitness gene, blocking cell proliferation when knocked out by CRISPR across a panel of 5 cell lines (Hart et al., 2015). This is consistent with Cep192 downregulation as a checkpoint mechanism in hypoxic conditions (Moser et al., 2013). On the other hand, Cep192 overexpression is also unfavourable. Cep192 overexpression has been described to have a dominant negative effect, reducing centrosomal γ-tubulin, most likely through mislocalisation (Moser et al., 2013). Finally, Cep192 was found to be synthetic lethal with MLN4924, suggesting that its regulation by the ubiquitin system is crucial for cell survival (Blank et al., 2013). It follows therefore that physiological Cep192 levels are finely tuned to avoid detriment. However, despite the importance of Cep192 regulation, little is known about how exactly this occurs.

Here, we propose a novel regulatory mechanism for Cep192. Specifically, we demonstrate that Fbxl13 downregulates Cep192 isoform 3 (Cep192-3), and propose that this occurs through ubiquitin mediated proteolysis to regulate microtubule nucleation activity. It is important to note that Cep192-3 was characterised recently (Sonnen et al., 2013), and that previous studies had focused solely on the functions of Cep192 isoforms 1 and 2. As Fbxl13 specifically regulates Cep192-3, it is important to consider what isoform-specific functions Cep192-3 could have.

The major difference between Cep192-1, Cep192-2, and Cep192-3 is that Cep192-3 uniquely contains a Plk4 binding region. Thus, we hypothesised that Fbxl13 may negatively regulate centriole duplication, but found its effect on this process to be minor (Figure 5.8). It is possible that this is due to the redundancy

between Cep152 and Cep192 in centrosome duplication (Sonnen et al., 2013). This could be overcome by depleting Cep152 in future functional studies. We also observed that Cep192-3 levels increased in mitosis, similar to Cep192 isoforms 1 and 2, suggesting it could equally play a role in centrosome maturation and pericentriolar matrix (PCM) expansion (Figure 3.8).

To investigate the isoform-specific function of Cep192-3, we had also attempted to generate a non-degradable Cep192-3 mutant that was unable to bind Fbxl13. This would be re-expressed at low levels in a Cep192 depleted background, to prevent dominant negative effects of transient Cep192 overexpression (Moser et al., 2013). The Cep192-3 region required for Fbxl13 binding was truncated into fragments approximately every 100 base pairs using site-directed mutagenesis, and tested for Fbxl13 binding via co-immunoprecipitation. However, we were unable to identify a linear binding region of Fbxl13 (data not shown). One likely explanation for this is because Fbxl proteins contact substrates through leucine-rich-repeats, which fold into three dimensional, hydrophobic surfaces. The binding region on the substrate is therefore also likely to be a large hydrophobic surface, as opposed to a linear peptide sequence. This is also the case for Fbxl17, for which the binding region on its substrate Sufu could not be identified (Raducu et al., 2016). In contrast, Fbxw and Fbxo families of F-box proteins have consensus linear degrons, for example β-TRCP (Fbxw1) or Cyclin F (Fbxo1) (D'Angiolella et al., 2010; Wu et al., 2003). Due to these structural limitations, we were unable to engineer a non-degradable Cep192-3 mutant. Future investigations could use alternative tools such as isoform-specific antibodies or siRNA sequences to clarify the role of Cep192-3, and further elucidate the role of Fbxl13-mediated Cep192-3 proteolysis.

6.4 Fbxl13 centrosomal localisation

As centrioles are only 250 nm in diameter and 100-150 nm in length, their size is at the resolution limit of conventional light microscopy (0.2 μM). Until recently, structural information was restricted to transmission electron microscopy (TEM), which itself has limitations: density-based visualisation, restricted labelling of individual proteins (gold nanoparticles of differing sizes), delicate sample preparation, and cost. In recent years, multiple super-resolution techniques have been developed that overcome the diffraction limit, such as Structured Illumination Microscopy (SIM, ~100 nm resolution), Stimulated Emission Depletion (STED, ~70 nm resolution), and Stochastic Optical Reconstruction Microscopy/Photo-Activated Localisation Microscopy (STORM/PALM, ~10-55 nm resolution), reviewed in Sydor et al. (2015). These allow the use of conventional sample fixation techniques, conventional “antibody-sandwiches” techniques used in light microscopy, the use of fluorophores, and the possibility of live-cell imaging. Such techniques have given rise to novel insights into centrosome structure. For example, antibodies targeting the N or C terminal of Cep152 revealed distinct scaffolds of two diameters, of 415 nm and 310 nm respectively, demonstrating that Cep152 is positioned radially with its C terminal closest to the centriolar wall (Sonnen et al., 2012). In this way, it has been shown that the pericentriolar matrix (PCM) is a highly ordered scaffold, and not an amorphous structure as previously thought (Lawo et al., 2012; Sonnen et al., 2012). These novel techniques have also provided insights into the regulation of centrosomal proteins in space and time. For example, it was recently shown that Plk4 localisation is altered upon the recruitment of Cep152, from a ~440 nm diameter scaffold (bound to Cep192), to a ~590 nm diameter scaffold (bound to Cep152) (Park et al., 2014). Inhibition of this process resulted in defects in

procentriole formation, suggesting that Plk4 scaffold switching is central to downstream Plk4 activity (Park et al., 2014). The localisation of centrosomal proteins is giving deeper insights to their function and regulation.

Using confocal microscopy, we observed that Flag-Fbxl13 was enriched at the centrosome. The localisation pattern of Flag-Fbxl13 suggested that it was a PCM protein, however a formal study with super-resolution microscopy is required to confirm its localisation. Additionally, cells in all phases of the cell cycle were observed to have centrosomal Flag-Fbxl13 staining, suggesting that its centrosomal localisation is not cell cycle regulated. However, as transient overexpression of Fbxl13 may lead to ectopic localisation patterns, it is also important to confirm these data using tools to visualise endogenous Fbxl13.

One such tool which we had attempted to generate was an antibody against Fbxl13. To do so, a ~200 amino acid peptide of Fbxl13 was cloned into a GST-tagged bacterial expression vector, and purified from BL21 competent *E. coli* cells. The purified peptide was then used for commercial rabbit immunisation. Unfortunately, our antibody was unable to recognise a Fbxl13-specific signal by immunofluorescence, as tested with Fbxl13 siRNA (data not shown). One possible reason for this is that our antibody does not recognise the native form of Fbxl13. Indeed, the entire C terminal region of Fbxl13 consists of consecutive leucine-rich repeats, which are highly hydrophobic and folded. Thus, it is possible that the peptide used to generate the Fbxl13 antibody is not on an accessible surface of the protein. As an alternative approach to visualise low-level expression of Fbxl13, I also generated a stably integrated, tetracycline-inducible, Venus-tagged Fbxl13 U2OS cell line. This was successful, however the clones lost Venus-Fbxl13

expression following several passages (data not shown). One important area for future work will therefore be to establish tools to visualise endogenous Fbxl13. This will allow us to address crucial questions about Fbxl13 such as: its sub-centrosomal localisation, cell-cycle regulation, and variability across a panel of cancer cell lines. Visualisation of endogenous Fbxl13 would also allow us to ask which proteins are required for its recruitment to the centrosomes, such as Centrin-2 or Centrin-3, by siRNA silencing candidate regulators and measuring centrosomal Fbxl13 abundance. It will also allow us to visualise if Fbxl13 localisation is altered in response to stimuli such as chemotaxis of galvanotaxis (wound healing), in order to address the upstream regulation of Fbxl13.

6.5 Fbxl13 in centrosomal microtubule nucleation and cell migration

The microtubule cytoskeleton regulates eukaryotic cell organisation, trafficking, polarity, and motility. The majority of microtubules originate from microtubule organising centres (MTOCs) such as the centrosomes, although acentrosomal MTOC sites such as the Golgi apparatus or chromosomes also exist. Microtubule nucleation at these sites is facilitated by γ-tubulin ring complexes (γ-TuRC), reviewed in Kollman et al. (2011). The regulation of γ-TuRC is therefore central to the dynamic organisation of the microtubule cytoskeleton in response to cell cycle changes and signalling.

Cep192 plays a central role in regulating the microtubule-nucleation capacity of both the mitotic centrosome and the interphase centrosome. In mitosis, Cep192 drives γ-tubulin recruitment and thus γ-TuRC enrichment in a Plk1 and Aurora A dependent manner (Gomez-Ferreria et al., 2007; Joukov et al., 2014; Zhu et al.,

2008). Similarly, Cep192 recruits γ-tubulin at the interphase centrosome, although this pathway is less well defined (O'Rourke et al., 2014). Factors suppressing microtubule nucleation and release have also been described to regulate the interphase centrosome, such as Ninein and Ninein-like protein (Nlp) (Schnerch and Nigg, 2016). It is speculated, but has not been formally shown, that these proteins antagonise Cep192 function to maintain steady-state centrosomal microtubule levels. This has been shown to have important consequences in the tumourigenic process. The deregulation of centrosome microtubule levels has been shown to cause oncogenic aberrations in microtubule-dependent structures and processes (Schnerch and Nigg, 2016). For example, Nlp overexpression in non-transformed mammospheres suppressed microtubule nucleation and severing at the centrosome, resulting in signs of malignant transformation such as a loss of cell-cell adhesion, cell polarisation, and overall mammosphere architecture (Schnerch and Nigg, 2016). Indeed, Nlp is commonly amplified in breast tumours.

In the study presented here, we propose an additional antagonist of Cep192 in the interphase centrosome, namely Fbxl13. We observed that Fbxl13 targets Cep192-3 for ubiquitin mediated proteolysis, and that interphase cells with overexpressed Fbxl13 have reduced Cep192 and γ-tubulin at the centrosomes, and a corresponding reduction of centrosomal microtubule arrays. Further work remains to show whether this pathway is active in other cell lines, and whether this effect is Cep192 dependent, for example by rescuing Fbxl13 depletion with Cep192 depletion. We hypothesise that the physiological function of Fbxl13 is to fine-tune Cep192 levels, and maintain steady-state centrosome microtubule nucleation activity. In support of this, we observed by immunofluorescence that cells overexpressing Fbxl13 frequently exhibited strong morphological phenotypes,

consistent with a disrupted microtubule network (Appendix 8). One open question is whether Fbxl13-mediated Cep192 degradation also regulates the mitotic centrosome. This could be assessed by scoring bipolar spindle abnormalities in cells overexpressing Fbxl13, or by looking at mitotic defect phenotypes such as micronuclei formation or mitotic delay.

We also found that Fbxl13 amplification in U2OS cells was associated with increased cell motility. It will be important to show that this phenotype is Cep192 dependent through rescue experiments, and to demonstrate that this pathway is active in other cell lines. Additionally, it remains to be shown how the perturbation of centrosome microtubule arrays results in decreased cell migration. One possible reason is that these cells are unable to polarise correctly. This could be investigated by immunofluorescence, as correctly polarised migrating cells reorient their microtubules to the wound edge (leading edge) (Schnerch and Nigg, 2016). Lastly, our data suggest that Fbxl13 downregulates centrosomal microtubule arrays through a reduction in microtubule nucleation. However, this could also arise from increased microtubule release from the centrosome. To address how Fbxl13 regulates microtubule dynamics, it will be necessary to perform time-lapse experiments using microtubule regrowth assays. Labelling alpha-tubulin and microtubule plus ends (eg. with the microtubule capping protein EB1-GFP) would reveal dynamic microtubule growth and release patterns from the centrosome over time (Abal et al., 2002).

6.6 Fbxl13 in tumour samples and prognosis

Several lines of evidence suggest that Fbxl13 gain-of-function is oncogenic. An online repository of cancer patient cohorts shows that Fbxl13 is frequently amplified

in solid tumours, such as breast cancer (20%), non-epithelial prostate cancer (20%), head and neck cancer (10%), and oesophageal cancer (10%) (cBioPortal). Furthermore, expression data from the Cancer Cell Line Encyclopedia has revealed Fbxl13 amplification in many cancer cell lines, many of which originate from breast cancers, glioblastomas, and lung cancers (Barretina et al., 2012). Lastly, a recent CRISPR screen has identified that Fbxl13 is a core fitness gene in a patient derived glioblastoma cell line, as its knockout downregulates proliferation (Hart et al., 2015). Thus, not only is Fbxl13 frequently amplified in tumours, but it also serves as a potential drug target for therapy.

We hypothesise that Fbxl13 is frequently upregulated in solid tumours because it favours cell motility. Our working model is that Fbxl13 upregulation reduces centrosomal microtubule nucleation capacity and causes hyperpolarisation, resulting in an increased ability for cells to migrate. We extrapolate that Fbxl13 amplification may also increase cell invasiveness. This is a similar but distinct process from cell migration, as it also involves the degradation of collagen and crossing of the basal membrane. This ability distinguishes benign from malignant tumours, and increased invasiveness would be an important factor in prognosis. Where survival data is available, Fbxl13 amplification appears to correlate with prognosis, however the cohorts are too small to reach statistical significance (Appendix 9) (TCGA Research Network, http://cancergenome.nih.gov/). A formal bioinformatics study of a larger cohort of microarray data would be required to investigate this correlation. Parallel *in vitro* studies could also test the invasive ability of Fbxl13-overexpressing cancer cells by plating cells on matrigel inserts, and measuring their capacity to invade into the matrigel relative to Fbxl13 depleted controls.

As Fbxl13 is a core fitness gene in glioblastoma cells (Hart et al., 2015), it is also possible that Fbxl13 is commonly amplified in cancer cells as it promotes proliferation. This could be tested using cell proliferation assays (eg. MTT assay) following Fbxl13 depletion. However, although Fbxl13 amplification is common in cancer cells, we had also observed by immunofluorescence that very high levels of Fbxl13 overexpression were cytotoxic. This may be due to the loss of Cep192, consistent with Cep192 depletion phenotypes (Gomez-Ferreria et al., 2007; Zhu et al., 2008). This leads us to speculate that Fbxl13 amplification may not exceed a certain threshold, as ectopic Cep192 loss would be cytotoxic, and counter-productive to tumour progression. Correlating Fbxl13 and Cep192 levels across a panel of cancer cell lines or patient samples would provide insights as to how this pathway is deregulated in cancer.

Finally, a database of patient tumours has also revealed that Fbxl13 is frequently mutated in cancer (TCGA Research Network, http://cancergenome.nih.gov/). With few exceptions, these mutations occur along the entire length of Fbxl13 (Appendix 10). For example, the F-box region bears few mutations, which could indicate that the E3 ubiquitin ligase activity of Fbxl13 is essential for survival, or beneficial to tumour progression. There are also several mutation cold-spots in the C terminal region, which could play important roles in substrate binding. Additionally, there are several mutation hot-spots that are frequently mutated in patient samples. It will be important to reproduce these mutations in model systems, and test whether they affect Cep192 binding, Fbxl13 localisation, or Fbxl13 functions. Understanding why these mutations recur could give us a deeper understanding of Fbxl13 function and mechanism of action, and how this is subverted in tumours.

6.7 Future work

Despite being first described over a decade ago, the F-box proteins remain largely uncharacterised. However, due to their roles in tumour progression and characteristic specificity, they represent promising molecular targets for cancer therapy. In this study, we have identified the interactors, a substrate, and potential function of Fbxl13. Our data in U2OS cells are consistent with the hypothesis that Fbxl13 targets Cep192-3 for ubiquitin mediated proteolysis to regulate centrosome microtubules and cell motility. Future investigations should aim to further elucidate the activity of this pathway in other cell lines, the regulation of Cep192 by Fbxl13, and the role of Fbxl13 in cancer.

6.7.1 The regulation of Cep192 by Fbxl13

A key question which remains to be addressed is how the Fbxl13-Cep192 pathway is regulated. One major distinction is whether Fbxl13 constitutively degrades Cep192, or whether this pathway is stimulated. For example, it is possible for Fbxl13 activity to be restricted to interphase, where centrosomal microtubule nucleation activity is lowest. Alternatively, Fbxl13 activity may be induced by external signals, such as chemotaxis or galvanotaxis (including wound healing, development). In either case, such signals could be transduced by post-translational modifications that regulate Fbxl13-Cep192 binding. In the case of RRM2, alanine-scanning mutagenesis revealed that T33 phosphorylation was required for Cyclin F binding (D'Angiolella et al., 2012). The subsequent generation of a phospho-specific antibody to pRRM2 T33 showed that this residue was phosphorylated upon G2 entry, tethering RRM2 degradation to the cell cycle (D'Angiolella et al., 2012). In a

similar way, knowing which residues are important for Fbxl13-Cep192 binding could help us to further elucidate when this interaction takes place.

Mutating crucial binding residues to generate a non-degradable Cep192 mutant would also be useful for functional studies. This was seen in the case of STIL, where mutation of the KEN box prevents APC/C^{Cdh1} binding, and results in STIL stabilisation and centriole amplification (Arquint and Nigg, 2014). Such KEN box mutations are also seen in microcephaly mutants of STIL, suggesting that centriole amplification is the underlying mechanism of microcephaly in these patients (Arquint and Nigg, 2014). Similarly, correlating crucial Fbxl13-Cep192 binding residues with mutations in patient samples could inform us of underlying oncogenic mechanisms. Such knowledge for other E3 ubiquitin ligases has facilitated the generation and implementation of small molecule inhibitors targeting the ligase-substrate interface, such as Compound 25 (for Skp2/Fbxl1) and nutlins (MDM2) (reviewed in Skaar et al. (2014)).

It also remains to be addressed how Fbxl13 itself is regulated. Open questions include: how Fbxl13 is transcriptionally regulated, whether Fbxl13 is cell cycle regulated, whether Fbxl13 activity is post-translationally regulated, and what Fbxl13 regulators are. As Fbxl13 protein levels are so unstable, as revealed by cycloheximide chase experiments, we predict that Fbxl13 is itself targeted for degradation. In the case of the tumour suppressor Fbxw7, identification of upstream regulators has provided opportunities to restore its function in Fbxw7 loss-of-function tumours (reviewed in Wang et al. (2014)). Our mass-spectrometry identified candidate Fbxl13 interactors can be further mined to identify upstream regulators. Two starting points for Fbxl13 regulators are Centrin-2 and Centrin-3, which show

strong Fbxl13 binding. Furthermore, this binding is unchanged in the presence or absence of MLN4924 or Bortezomib (Tan et al., 2013), suggesting that they lie upstream of Fbxl13 function. We do not neglect that the four isoforms of Fbxl13 could be differentially regulated to perform isoform-specific roles.

6.7.2 The role of Fbxl13 in cancer

Translationally, it will be important to investigate the role of Fbxl13 in tumour progression. We have demonstrated that Fbxl13 amplification promotes cell motility in U2OS cells *in vitro*, however these studies must be extended to other systems.

Firstly, it remains to be shown whether this pathway is active in other cell lines and promotes cell invasion, as previously mentioned. In particular, a well-characterised system used to investigate the role of centrosomal proteins in oncogenesis is MCF10A cells. This is a mammary epithelial cell line that forms three dimensional mammospheres in culture. As these cells are non-transformed, this system can be used to determine the contribution of a given protein to the oncogenic process. Changes in cell polarity, migration, cytoskeleton, or cell-cell adhesion are all highly tractable in this system, and result in perturbed mammosphere structure reminiscent of malignant transformation. Indeed, this system has recently been used to show that centrosome amplification results in cell invasion (Godinho et al., 2014), and that structural centrosome aberrations result in depolarisation and overproliferation (Schnerch and Nigg, 2016). This would be an informative model in which to perturb Fbxl13 levels, to further investigate its role in other oncogenic processes.

Secondly, it remains to be shown whether our hypothesis holds *in vivo.* In the case of Fbxl17, its oncogenic role in medulloblastoma was corroborated by an *in*

vivo orthotopic rat model of medulloblastoma. Here, a human medulloblastoma cell line (DAOY) with stable Fbxl17 depletion formed smaller tumours when injected into the cerebellum of rats, compared to control cells (Raducu et al., 2016). Should the *in vitro* studies of Fbxl13 show promise, a similar *in vivo* study would indicate its translational relevance.

Together, a full understanding of Fbxl13 mechanism of action and upstream regulation will allow us to better dissect its contribution to tumourigenesis, and suitability as a future prognostic marker or drug target.

6.8 Conclusive summary

In this doctoral thesis, I present evidence for a novel Cep192 regulatory mechanism through the orphan F-box protein Fbxl13. This occurs through the ubiquitylation of Cep192 isoform 3 (Cep192-3) by SCF^{Fbxl13}, which targets Cep192-3 for proteolysis. This regulation occurs at the centrosome, and results in the downregulation of centrosomal γ-tubulin and centrosomal microtubule arrays. The amplification of Fbxl13 in cancer cell lines has suggested that it plays an oncogenic role, and here I demonstrate that Fbxl13 amplification increases U2OS cell motility in a rescuable manner. I therefore conclude that Fbxl13 plays an important role in the homeostasis of centrosomal Cep192 levels in this cell line, and that deregulation of this pathway leads to tumour-related aberrations in centrosomal microtubule activity and cell motility.

References

Abal, M., M. Piel, V. Bouckson-Castaing, M. Mogensen, J.-B.B. Sibarita, and M. Bornens. 2002. Microtubule release from the centrosome in migrating cells. *The Journal of cell biology*. 159:731-737.

Alberts, B., A. Johnson, J. Lewis, D. Morgan, M. Raff, K. Roberts, and P. Walter. 2015. Molecular Biology of the Cell, Sixth Edition. *Molecular Biology of the Cell, Sixth Edition*:1-1342.

Andersen, J.S., C.J. Wilkinson, T. Mayor, P. Mortensen, E.A. Nigg, and M. Mann. 2003. Proteomic characterization of the human centrosome by protein correlation profiling. *Nature*. 426:570-574.

Araki, M., C. Masutani, M. Takemura, A. Uchida, K. Sugasawa, J. Kondoh, Y. Ohkuma, and F. Hanaoka. 2001. Centrosome protein centrin 2/caltractin 1 is part of the xeroderma pigmentosum group C complex that initiates global genome nucleotide excision repair. *The Journal of biological chemistry*. 276:18665-18672.

Arquint, C., A.-M.M. Gabryjonczyk, and E.A. Nigg. 2014. Centrosomes as signalling centres. *Philosophical transactions of the Royal Society of London. Series B, Biological sciences*. 369.

Arquint, C., and E.A. Nigg. 2014. STIL microcephaly mutations interfere with APC/C-mediated degradation and cause centriole amplification. *Current biology : CB*. 24:351-360.

Aslanidis, C., and P.J. de Jong. 1990. Ligation-independent cloning of PCR products (LIC-PCR). *Nucleic acids research*. 18:6069-6074.

Bahe, S., Y.-D.D. Stierhof, C.J. Wilkinson, F. Leiss, and E.A. Nigg. 2005. Rootletin forms centriole-associated filaments and functions in centrosome cohesion. *The Journal of cell biology*. 171:27-33.

Baker, R.T., and P.G. Board. 1987. The human ubiquitin gene family: structure of a gene and pseudogenes from the Ub B subfamily. *Nucleic acids research*. 15:443-463.

Balczon, R., L. Bao, W.E. Zimmer, K. Brown, R.P. Zinkowski, and B.R. Brinkley. 1995. Dissociation of centrosome replication events from cycles of DNA synthesis and mitotic division in hydroxyurea-arrested Chinese hamster ovary cells. *The Journal of cell biology*. 130:105-115.

Barretina, J., G. Caponigro, N. Stransky, K. Venkatesan, A.A. Margolin, S. Kim, C.J. Wilson, J. Lehár, G.V. Kryukov, D. Sonkin, A. Reddy, M. Liu, L. Murray, M.F. Berger, J.E. Monahan, P. Morais, J. Meltzer, A. Korejwa, J. Jané-Valbuena, F.A. Mapa, J. Thibault, E. Bric-Furlong, P. Raman, A. Shipway, I.H. Engels, J. Cheng, G.K. Yu, J. Yu, P. Aspesi, M. de Silva, K. Jagtap, M.D. Jones, L. Wang, C. Hatton, E. Palescandolo, S. Gupta, S. Mahan, C. Sougnez, R.C. Onofrio, T. Liefeld, L. MacConaill, W. Winckler, M. Reich, N. Li, J.P. Mesirov, S.B. Gabriel, G. Getz, K. Ardlie, V. Chan, V.E. Myer, B.L. Weber, J. Porter, M. Warmuth, P. Finan, J.L. Harris, M. Meyerson, T.R. Golub, M.P. Morrissey, W.R. Sellers, R. Schlegel, and L.A. Garraway. 2012. The Cancer Cell Line Encyclopedia enables predictive modelling of anticancer drug sensitivity. *Nature*. 483:603-607.

Berndsen, C.E., and C. Wolberger. 2014. New insights into ubiquitin E3 ligase mechanism. *Nature structural & molecular biology*. 21.

Beronja, S., P. Janki, E. Heller, W.-H.H. Lien, B.E. Keyes, N. Oshimori, and E. Fuchs. 2013. RNAi screens in mice identify physiological regulators of oncogenic growth. *Nature*. 501:185-190.

Bettencourt-Dias, M., A. Rodrigues-Martins, L. Carpenter, M. Riparbelli, L. Lehmann, M.K. Gatt, N. Carmo, F. Balloux, G. Callaini, and D.M. Glover. 2005. SAK/PLK4 is required for centriole duplication and flagella development. *Current biology : CB*. 15:2199-2207.

Bienko, M., C.M. Green, N. Crosetto, F. Rudolf, G. Zapart, B. Coull, P. Kannouche, G. Wider, M. Peter, A.R. Lehmann, K. Hofmann, and I. Dikic. 2005. Ubiquitin-binding domains in Y-family polymerases regulate translesion synthesis. *Science (New York, N.Y.)*. 310:1821-1824.

Bjursell, G., and P. Reichard. 1973. Effects of thymidine on deoxyribonucleoside triphosphate pools and deoxyribonucleic acid synthesis in Chinese hamster ovary cells. *The Journal of biological chemistry*. 248:3904-3909.

Blachon, S., J. Gopalakrishnan, Y. Omori, A. Polyanovsky, A. Church, D. Nicastro, J. Malicki, and T. Avidor-Reiss. 2008. Drosophila asterless and vertebrate Cep152 Are orthologs essential for centriole duplication. *Genetics*. 180:2081-2094.

Blank, J.L., X.J. Liu, K. Cosmopoulos, D.C. Bouck, K. Garcia, H. Bernard, O. Tayber, G. Hather, R. Liu, U. Narayanan, M.A. Milhollen, and E.S. Lightcap. 2013. Novel DNA damage checkpoints mediating cell death induced by the NEDD8-activating enzyme inhibitor MLN4924. *Cancer research*. 73:225-234.

Bourke, E., H. Dodson, A. Merdes, L. Cuffe, G. Zachos, M. Walker, D. Gillespie, and C.G. Morrison. 2007. DNA damage induces Chk1-dependent centrosome amplification. *EMBO reports*. 8:603-609.

Brenner, D.J. 2008. The linear-quadratic model is an appropriate methodology for determining isoeffective doses at large doses per fraction. *Seminars in radiation oncology*. 18:234-239.

Busino, L., F. Bassermann, A. Maiolica, C. Lee, P.M. Nolan, S.I.H. Godinho, G.F. Draetta, and M. Pagano. 2007. SCFFbxl3 controls the oscillation of the circadian clock by directing the degradation of cryptochrome proteins. *Science*. 316:900-904.

Čajánek, L., T. Glatter, and E.A. Nigg. 2015. The E3 ubiquitin ligase Mib1 regulates Plk4 and centriole biogenesis. *Journal of cell science*. 128:1674-1682.

Cardozo, T., and M. Pagano. 2004. The SCF ubiquitin ligase: insights into a molecular machine. *Nature reviews. Molecular cell biology*. 5:739-751.

Carrano, A.C., E. Eytan, A. Hershko, and M. Pagano. 1999. SKP2 is required for ubiquitin-mediated degradation of the CDK inhibitor p27. *Nature Cell Biology*. 1:193-199.

Carter, S., O. Bischof, A. Dejean, and K.H. Vousden. 2007. C-terminal modifications regulate MDM2 dissociation and nuclear export of p53. *Nature cell biology*. 9:428-435.

Carvalho-Santos, Z., P. Machado, P. Branco, F. Tavares-Cadete, A. Rodrigues-Martins, J.B.B. Pereira-Leal, and M. Bettencourt-Dias. 2010. Stepwise evolution of the centriole-assembly pathway. *Journal of cell science*. 123:1414-1426.

Cenciarelli, C., D.S. Chiaur, D. Guardavaccaro, W. Parks, M. Vidal, and M. Pagano. 1999. Identification of a family of human F-box proteins. *Current biology : CB*. 9:1177-1179.

Chan, T.A., H. Hermeking, C. Lengauer, and K.W. Kinzler. 1999. 14-3-3σ is required to prevent mitotic catastrophe after DNA damage. *Nature*.

Chau, V., J.W. Tobias, A. Bachmair, D. Marriott, D.J. Ecker, D.K. Gonda, and A. Varshavsky. 1989. A multiubiquitin chain is confined to specific lysine in a targeted short-lived protein. *Science (New York, N.Y.)*. 243:1576-1583.

Chen, Z., V.B. Indjeian, M. McManus, L. Wang, and B.D. Dynlacht. 2002. CP110, a cell cycle-dependent CDK substrate, regulates centrosome duplication in human cells. *Developmental cell*. 3:339-350.

Christensen, D.E., P.S. Brzovic, and R.E. Klevit. 2007. E2–BRCA1 RING interactions dictate synthesis of mono- or specific polyubiquitin chain linkages. *Nature Structural & Molecular Biology*. 14:941-948.

Ciechanover, A., S. Elias, H. Heller, S. Ferber, and A. Hershko. 1980. Characterization of the heat-stable polypeptide of the ATP-dependent proteolytic system from reticulocytes. *The Journal of biological chemistry*. 255:7525-7528.

Ciehanover, A., Y. Hod, and A. Hershko. 1978. A heat-stable polypeptide component of an ATP-dependent proteolytic system from reticulocytes. *Biochemical and biophysical research communications*. 81:1100-1105.

Cizmecioglu, O., M. Arnold, R. Bahtz, F. Settele, L. Ehret, U. Haselmann-Weiss, C. Antony, and I. Hoffmann. 2010. Cep152 acts as a scaffold for recruitment of Plk4 and CPAP to the centrosome. *The Journal of cell biology*. 191:731-739.

Clague, M.J., C. Heride, and S. Urbé. 2015. The demographics of the ubiquitin system. *Trends in cell biology*. 25:417-426.

Conduit, P.T., Z. Feng, J.H. Richens, J. Baumbach, A. Wainman, S.D. Bakshi, J. Dobbelaere, S. Johnson, S.M. Lea, and J.W. Raff. 2014a. The centrosome-specific phosphorylation of cnn by polo/plk1 drives cnn scaffold assembly and centrosome maturation. *Developmental cell*. 28:659-669.

Conduit, P.T., J.H. Richens, A. Wainman, J. Holder, C.C. Vicente, M.B. Pratt, C.I. Dix, Z.A. Novak, I.M. Dobbie, L. Schermelleh, and J.W. Raff. 2014b. A molecular mechanism of mitotic centrosome assembly in Drosophila. *eLife*.

Cottee, M.A., N. Muschalik, Y.L. Wong, and C.M. Johnson. 2013. Crystal structures of the CPAP/STIL complex reveal its role in centriole assembly and human microcephaly. *Elife*.

Cron, K.R., K. Zhu, D.S. Kushwaha, G. Hsieh, D. Merzon, J. Rameseder, C.C. Chen, A.D. D'Andrea, and D. Kozono. 2013. Proteasome Inhibitors Block DNA Repair and Radiosensitize Non-Small Cell Lung Cancer. *PLoS ONE*. 8.

Cunha-Ferreira, I., A. Rodrigues-Martins, I. Bento, M. Riparbelli, W. Zhang, E. Laue, G. Callaini, D.M. Glover, and M. Bettencourt-Dias. 2009. The SCF/Slimb ubiquitin ligase limits centrosome amplification through degradation of SAK/PLK4. *Current biology : CB*. 19:43-49.

Curtiss, N.P., J.M. Bonifas, J.O. Lauchle, J.D. Balkman, C.P. Kratz, B.M. Emerling, E.D. Green, M.M. Beau, and K.M. Shannon. 2005. Isolation and analysis of candidate myeloid tumor suppressor genes from a commonly deleted segment of 7q22. *Genomics*. 85:600607.

D'Angiolella, V., V. Donato, F.M. Forrester, Y.T. Jeong, C. Pellacani, Y. Kudo, A. Saraf, L. Florens, M.P. Washburn, and M. Pagano. 2012. Cyclin F-mediated

degradation of ribonucleotide reductase M2 controls genome integrity and DNA repair. *Cell*. 149:1023-1034.

D'Angiolella, V., V. Donato, S. Vijayakumar, A. Saraf, L. Florens, M.P. Washburn, B. Dynlacht, and M. Pagano. 2010. SCF(Cyclin F) controls centrosome homeostasis and mitotic fidelity through CP110 degradation. *Nature*. 466:138-142.

Deshaies, R.J., and C. Joazeiro. 2009. RING Domain E3 Ubiquitin Ligases. *Biochemistry*. 78:399434.

Doil, C., N. Mailand, S. Bekker-Jensen, and P. Menard. 2009. RNF168 binds and amplifies ubiquitin conjugates on damaged chromosomes to allow accumulation of repair proteins. *Cell*.

Doxsey, S., D. McCollum, and W. Theurkauf. 2005. CENTROSOMES IN CELLULAR REGULATION. *Annual Review of Cell and Developmental Biology*. 21:411-434.

Dzhindzhev, N.S., Q.D. Yu, K. Weiskopf, G. Tzolovsky, I. Cunha-Ferreira, M. Riparbelli, A. Rodrigues-Martins, M. Bettencourt-Dias, G. Callaini, and D.M. Glover. 2010. Asterless is a scaffold for the onset of centriole assembly. *Nature*. 467:714-718.

Eddé, B., J. Rossier, J.P. Le Caer, E. Desbruyères, F. Gros, and P. Denoulet. 1990. Posttranslational glutamylation of alpha-tubulin. *Science (New York, N.Y.)*. 247:83-85.

Elbashir, S.M., J. Harborth, W. Lendeckel, A. Yalcin, K. Weber, and T. Tuschl. 2001. Duplexes of 21-nucleotide RNAs mediate RNA interference in cultured mammalian cells. *Nature*. 411:494-498.

Elia, A.E., A.P. Boardman, D.C. Wang, E.L. Huttlin, R.A. Everley, N. Dephoure, C. Zhou, I. Koren, S.P. Gygi, and S.J. Elledge. 2015. Quantitative Proteomic Atlas of Ubiquitination and Acetylation in the DNA Damage Response. *Molecular cell*. 59:867-881.

Finley, D. 2009. Recognition and processing of ubiquitin-protein conjugates by the proteasome. *Annual review of biochemistry*.

Firat-Karalar, E.N., N. Rauniyar, J.R. Yates, and T. Stearns. 2014. Proximity interactions among centrosome components identify regulators of centriole duplication. *Current biology : CB*. 24:664-670.

Fırat-Karalar, E.N., and T. Stearns. 2014. The centriole duplication cycle. *Philosophical transactions of the Royal Society of London. Series B, Biological sciences*. 369.

Franken, N.A.P., H.M. Rodermond, J. Stap, J. Haveman, and C. van Bree. 2006. Clonogenic assay of cells in vitro. *Nature protocols*. 1:2315-2319.

Ganoth, D., G. Bornstein, T.K. Ko, B. Larsen, M. Tyers, M. Pagano, and A. Hershko. 2001. The cell-cycle regulatory protein Cks1 is required for SCFSkp2-mediated ubiquitinylation of p27. *Nature cell biology*. 3:321-324.

Godinho, S.A., and D. Pellman. 2014. Causes and consequences of centrosome abnormalities in cancer. *Philosophical transactions of the Royal Society of London. Series B, Biological sciences*. 369.

Godinho, S.A., R. Picone, M. Burute, R. Dagher, Y. Su, C.T. Leung, K. Polyak, J.S. Brugge, M. Théry, and D. Pellman. 2014. Oncogene-like induction of cellular invasion from centrosome amplification. *Nature*.

Godinho, S.I.H., E.S. Maywood, L. Shaw, V. Tucci, A.R. Barnard, L. Busino, M. Pagano, R. Kendall, M.M. Quwailid, M.R. Romero, J. O'Neill, J.E. Chesham, D. Brooker, Z. Lalanne, M.H. Hastings, and P.M. Nolan. 2007. The after-

hours mutant reveals a role for Fbxl3 in determining mammalian circadian period. *Science*. 316:897-900.
Gomez-Ferreria, M., M. Bashkurov, M. Mullin, A.-C. Gingras, and L. Pelletier. 2014. CEP192 interacts physically and functionally with the K63-deubiquitinase CYLD to promote mitotic spindle assembly. *Cell Cycle*. 11:3555-3558.
Gomez-Ferreria, M., U. Rath, D.W. Buster, S.K. Chanda, J.S. Caldwell, D.R. Rines, and D.J. Sharp. 2007. Human Cep192 Is Required for Mitotic Centrosome and Spindle Assembly. *Current Biology*. 17:1960-1966.
Gomez-Ferreria, M.A., M. Bashkurov, A.O. Helbig, B. Larsen, T. Pawson, A.-C.C. Gingras, and L. Pelletier. 2012. Novel NEDD1 phosphorylation sites regulate γ-tubulin binding and mitotic spindle assembly. *Journal of cell science*. 125:3745-3751.
Graser, S., Y.-D.D. Stierhof, S.B.B. Lavoie, O.S. Gassner, S. Lamla, M. Le Clech, and E.A. Nigg. 2007. Cep164, a novel centriole appendage protein required for primary cilium formation. *The Journal of cell biology*. 179:321-330.
Gregory, M.A., and S.R. Hann. 2000. c-Myc proteolysis by the ubiquitin-proteasome pathway: stabilization of c-Myc in Burkitt's lymphoma cells. *Molecular and cellular biology*. 20:2423-2435.
Guichard, P., D. Chrétien, S. Marco, and A.-M.M. Tassin. 2010. Procentriole assembly revealed by cryo-electron tomography. *The EMBO journal*. 29:1565-1572.
Habedanck, R., Y.-D.D. Stierhof, C.J. Wilkinson, and E.A. Nigg. 2005. The Polo kinase Plk4 functions in centriole duplication. *Nature cell biology*. 7:1140-1146.
Haren, L., T. Stearns, and J. Lüders. 2009. Plk1-dependent recruitment of gamma-tubulin complexes to mitotic centrosomes involves multiple PCM components. *PloS one*. 4.
Harper, W.J., and M.-K. Tan. 2012. Understanding cullin-RING E3 biology through proteomics-based substrate identification. *Molecular & Cellular Proteomics*. 11:1541-1550.
Hart, M., J.P. Concordet, I. Lassot, I. Albert, R. del los Santos, H. Durand, C. Perret, B. Rubinfeld, F. Margottin, R. Benarous, and P. Polakis. 1999. The F-box protein beta-TrCP associates with phosphorylated beta-catenin and regulates its activity in the cell. *Current biology : CB*. 9:207-210.
Hart, M.J., R. de los Santos, I.N. Albert, B. Rubinfeld, and P. Polakis. 1998. Downregulation of beta-catenin by human Axin and its association with the APC tumor suppressor, beta-catenin and GSK3 beta. *Current biology : CB*. 8:573-581.
Hart, T., M. Chandrashekhar, M. Aregger, Z. Steinhart, K.R. Brown, G. MacLeod, M. Mis, M. Zimmermann, A. Fradet-Turcotte, S. Sun, P. Mero, P. Dirks, S. Sidhu, F.P. Roth, O.S. Rissland, D. Durocher, S. Angers, and J. Moffat. 2015. High-Resolution CRISPR Screens Reveal Fitness Genes and Genotype-Specific Cancer Liabilities. *Cell*. 163:1515-1526.
Hatch, E.M., A. Kulukian, A.J. Holland, D.W. Cleveland, and T. Stearns. 2010. Cep152 interacts with Plk4 and is required for centriole duplication. *The Journal of cell biology*. 191:721-729.
Hermeking, H., C. Lengauer, K. Polyak, T.C. He, and L. Zhang. 1997. 14-3-3σIs a p53-Regulated Inhibitor of G2/M Progression. *Molecular cell*.
Hilbert, M., A. Noga, D. Frey, V. Hamel, P. Guichard, S.H. Kraatz, M. Pfreundschuh, S. Hosner, I. Flückiger, R. Jaussi, M.M. Wieser, K.M. Thieltges, X. Deupi,

D.J. Müller, R.A. Kammerer, P. Gönczy, M. Hirono, and M.O. Steinmetz. 2016. SAS-6 engineering reveals interdependence between cartwheel and microtubules in determining centriole architecture. *Nature cell biology*. 18:393-403.

Hoeller, D., and I. Dikic. 2009. Targeting the ubiquitin system in cancer therapy. *Nature*. 458:438-444.

Holland, A.J., W. Lan, S. Niessen, H. Hoover, and D.W. Cleveland. 2010. Polo-like kinase 4 kinase activity limits centrosome overduplication by autoregulating its own stability. *The Journal of cell biology*. 188:191-198.

Huang, F., D. Kirkpatrick, X. Jiang, S. Gygi, and A. Sorkin. 2006a. Differential regulation of EGF receptor internalization and degradation by multiubiquitination within the kinase domain. *Molecular cell*. 21:737-748.

Huang, T.T., S.M. Nijman, K.D. Mirchandani, P.J. Galardy, M.A. Cohn, W. Haas, S.P. Gygi, H.L. Ploegh, R. Bernards, and A.D. D'Andrea. 2006b. Regulation of monoubiquitinated PCNA by DUB autocleavage. *Nature cell biology*. 8:339-347.

Huen, M.S.Y., R. Grant, I. Manke, K. Minn, X. Yu, and M.B. Yaffe. 2007. RNF8 transduces the DNA-damage signal via histone ubiquitylation and checkpoint protein assembly. *Cell*.

Hurov, K.E., C. Cotta-Ramusino, and S.J. Elledge. 2010. A genetic screen identifies the Triple T complex required for DNA damage signaling and ATM and ATR stability. *Genes & development*. 24:1939-1950.

Inanç, B., and C.G. Morrison. 2011. Getting permission: how DNA damage causes centrosome amplification. *Cell cycle (Georgetown, Tex.)*. 10:1890-1891.

Jin, J., T. Cardozo, R.C. Lovering, S.J. Elledge, M. Pagano, and J.W. Harper. 2004. Systematic analysis and nomenclature of mammalian F-box proteins. *Genes & development*. 18:2573-2580.

Jin, J., X. Li, S.P. Gygi, and J.W. Harper. 2007. Dual E1 activation systems for ubiquitin differentially regulate E2 enzyme charging. *Nature*. 447:1135-1138.

Joukov, V., J.C. Walter, and A. Nicolo. 2014. The cep192-organized aurora a-plk1 cascade is essential for centrosome cycle and bipolar spindle assembly. *Molecular cell*. 55:578-591.

Kemp, C.A., K.R. Kopish, P. Zipperlen, and J. Ahringer. 2004. Centrosome maturation and duplication in C. elegans require the coiled-coil protein SPD-2. *Developmental cell*.

Kerscher, O., R. Felberbaum, and M. Hochstrasser. 2006. Modification of proteins by ubiquitin and ubiquitin-like proteins. *Annual review of cell and developmental biology*. 22:159-180.

Khodjakov, A., and C.L. Rieder. 1999. The Sudden Recruitment of γ-Tubulin to the Centrosome at the Onset of Mitosis and Its Dynamic Exchange Throughout the Cell Cycle, Do Not Require Microtubules. *The Journal of Cell Biology*. 146:585-596.

Kim, T.-S.S., J.-E.E. Park, A. Shukla, S. Choi, R.N. Murugan, J.H. Lee, M. Ahn, K. Rhee, J.K. Bang, B.Y. Kim, J. Loncarek, R.L. Erikson, and K.S. Lee. 2013. Hierarchical recruitment of Plk4 and regulation of centriole biogenesis by two centrosomal scaffolds, Cep192 and Cep152. *Proceedings of the National Academy of Sciences of the United States of America*. 110:57.

Kitagawa, D., I. Vakonakis, N. Olieric, M. Hilbert, D. Keller, V. Olieric, M. Bortfeld, M.C.C. Erat, I. Flückiger, P. Gönczy, and M.O. Steinmetz. 2011. Structural basis of the 9-fold symmetry of centrioles. *Cell*. 144:364-375.

Kleylein-Sohn, J., J. Westendorf, M. Clech, R. Habedanck, Y.-D. Stierhof, and E.A. Nigg. 2007. Plk4-Induced Centriole Biogenesis in Human Cells. *Developmental Cell*.

Koepp, D.M., L.K. Schaefer, X. Ye, K. Keyomarsi, C. Chu, J.W. Harper, and S.J. Elledge. 2001. Phosphorylation-dependent ubiquitination of cyclin E by the SCFFbw7 ubiquitin ligase. *Science*. 294:173-177.

Kollman, J.M., A. Merdes, L. Mourey, and D.A. Agard. 2011. Microtubule nucleation by γ-tubulin complexes. *Nature reviews. Molecular cell biology*. 12:709-721.

Komander, D., and M. Rape. 2012. The Ubiquitin Code. *Annual Review of Biochemistry*. 81:203229.

Kravtsova-Ivantsiv, Y., and A. Ciechanover. 2015. The ubiquitin-proteasome system and activation of NF-κB: involvement of the ubiquitin ligase KPC1 in p105 processing and tumor suppression. *Molecular & cellular oncology*. 2.

Kulak, N.A., G. Pichler, I. Paron, N. Nagaraj, and M. Mann. 2014. Minimal, encapsulated proteomic-sample processing applied to copy-number estimation in eukaryotic cells. *Nat. Methods*.

Kumar, A., V. Rajendran, R. Sethumadhavan, and R. Purohit. 2013. CEP proteins: the knights of centrosome dynasty. *Protoplasma*. 250:965-983.

Lawo, S., M. Hasegan, G.D. Gupta, and L. Pelletier. 2012. Subdiffraction imaging of centrosomes reveals higher-order organizational features of pericentriolar material. *Nature Cell Biology*. 14:1148-1158.

Lee, I., and H. Schindelin. 2008. Structural insights into E1-catalyzed ubiquitin activation and transfer to conjugating enzymes. *Cell*. 134:268-278.

Lee, K., and K. Rhee. 2012. Separase-dependent cleavage of pericentrin B is necessary and sufficient for centriole disengagement during mitosis. *Cell cycle (Georgetown, Tex.)*. 11:2476-2485.

Li, J., V. D'Angiolella, E.S. Seeley, S. Kim, T. Kobayashi, W. Fu, E.I. Campos, M. Pagano, and B.D. Dynlacht. 2013. USP33 regulates centrosome biogenesis via deubiquitination of the centriolar protein CP110. *Nature*. 495:255-259.

Li, M., C.L. Brooks, F. Wu-Baer, D. Chen, R. Baer, and W. Gu. 2003. Mono- versus polyubiquitination: differential control of p53 fate by Mdm2. *Science (New York, N.Y.)*. 302:1972-1975.

Li, S., J.-J.J. Fernandez, W.F. Marshall, and D.A. Agard. 2012. Three-dimensional structure of basal body triplet revealed by electron cryo-tomography. *The EMBO journal*. 31:552-562.

Lin, Y.-C.C., C.-W.W. Chang, W.-B.B. Hsu, C.-J.C.J. Tang, Y.-N.N. Lin, E.-J.J. Chou, C.-T.T. Wu, and T.K. Tang. 2013. Human microcephaly protein CEP135 binds to hSAS-6 and CPAP, and is required for centriole assembly. *The EMBO journal*. 32:1141-1154.

Liu, C., Y. Li, M. Semenov, C. Han, G.H. Baeg, Y. Tan, Z. Zhang, X. Lin, and X. He. 2002. Control of beta-catenin phosphorylation/degradation by a dual-kinase mechanism. *Cell*. 108:837-847.

Loncarek, J., P. Hergert, and A. Khodjakov. 2010. Centriole reduplication during prolonged interphase requires procentriole maturation governed by Plk1. *Current biology : CB*. 20:1277-1282.

Lopes, C.A., S.C. Jana, I. Cunha-Ferreira, S. Zitouni, I. Bento, P. Duarte, S. Gilberto, F. Freixo, A. Guerrero, M. Francia, M. Lince-Faria, J. Carneiro, and M. Bettencourt-Dias. 2015. PLK4 trans-Autoactivation Controls Centriole Biogenesis in Space. *Developmental cell*. 35:222-235.

Lüders, J. 2012. The amorphous pericentriolar cloud takes shape. *Nature cell biology*.

Lüders, J., U.K. Patel, and T. Stearns. 2006. GCP-WD is a gamma-tubulin targeting factor required for centrosomal and chromatin-mediated microtubule nucleation. *Nature cell biology*. 8:137-147.

Mailand, N., S. Bekker-Jensen, H. Faustrup, and F. Melander. 2007. RNF8 ubiquitylates histones at DNA double-strand breaks and promotes assembly of repair proteins. *Cell*.

Matsumoto, M.L., K.E. Wickliffe, K.C. Dong, C. Yu, I. Bosanac, D. Bustos, L. Phu, D.S. Kirkpatrick, S.G. Hymowitz, M. Rape, R.F. Kelley, and V.M. Dixit. 2010. K11-linked polyubiquitination in cell cycle control revealed by a K11 linkage-specific antibody. *Molecular cell*. 39:477-484.

Mellacheruvu, D., Z. Wright, A.L. Couzens, J.-P.P. Lambert, N.A. St-Denis, T. Li, Y.V. Miteva, S. Hauri, M.E. Sardiu, T.Y. Low, V.A. Halim, R.D. Bagshaw, N.C. Hubner, A. Al-Hakim, A. Bouchard, D. Faubert, D. Fermin, W.H. Dunham, M. Goudreault, Z.-Y.Y. Lin, B.G. Badillo, T. Pawson, D. Durocher, B. Coulombe, R. Aebersold, G. Superti-Furga, J. Colinge, A.J. Heck, H. Choi, M. Gstaiger, S. Mohammed, I.M. Cristea, K.L. Bennett, M.P. Washburn, B. Raught, R.M. Ewing, A.-C.C. Gingras, and A.I. Nesvizhskii. 2013. The CRAPome: a contaminant repository for affinity purification-mass spectrometry data. *Nature methods*. 10:730-736.

Meng, L., J.-E. Park, T.-S. Kim, E. Lee, S.-Y. Park, M. Zhou, J.K. Bang, and K.S. Lee. 2015. Bimodal Interaction of Mammalian Polo-Like Kinase 1 and a Centrosomal Scaffold, Cep192, in the Regulation of Bipolar Spindle Formation. *Molecular and cellular biology*. 35:2626-2640.

Mizuno, E., T. Iura, A. Mukai, T. Yoshimori, N. Kitamura, and M. Komada. 2005. Regulation of epidermal growth factor receptor down-regulation by UBPY-mediated deubiquitination at endosomes. *Molecular biology of the cell*. 16:5163-5174.

Moritz, M., M.B. Braunfeld, J.W. Sedat, B. Alberts, and D.A. Agard. 1995. Microtubule nucleation by gamma-tubulin-containing rings in the centrosome. *Nature*. 378:638-640.

Moser, S.C., D. Bensaddek, B. Ortmann, J.-F.F. Maure, S. Mudie, J.J. Blow, A.I. Lamond, J.R. Swedlow, and S. Rocha. 2013. PHD1 links cell-cycle progression to oxygen sensing through hydroxylation of the centrosomal protein Cep192. *Developmental cell*. 26:381-392.

Mukhopadhyay, D., and H. Riezman. 2007. Proteasome-independent functions of ubiquitin in endocytosis and signaling. *Science (New York, N.Y.)*. 315:201-205.

Mullee, L.I., and C.G. Morrison. 2015. Centrosomes in the DNA damage response-the hub outside the centre. *Chromosome research : an international journal on the molecular, supramolecular and evolutionary aspects of chromosome biology*.

Nakazawa, Y., M. Hiraki, R. Kamiya, and M. Hirono. 2007. SAS-6 is a cartwheel protein that establishes the 9-fold symmetry of the centriole. *Current biology : CB*. 17:2169-2174.

Nalepa, G., and W.J. Harper. 2003. Therapeutic anti-cancer targets upstream of the proteasome. *Cancer treatment reviews*. 29 Suppl 1:49-57.

Nicassio, F., N. Corrado, J.H. Vissers, L.B. Areces, S. Bergink, J.A. Marteijn, B. Geverts, A.B. Houtsmuller, W. Vermeulen, P.P. Di Fiore, and E. Citterio.

2007. Human USP3 is a chromatin modifier required for S phase progression and genome stability. *Current biology : CB*. 17:1972-1977.

O'Rourke, B.P., M.A. Gomez-Ferreria, R.H. Berk, A.M. Hackl, M.P. Nicholas, S.C. O'Rourke, L. Pelletier, and D.J. Sharp. 2014. Cep192 controls the balance of centrosome and non-centrosomal microtubules during interphase. *PloS one*. 9.

Ohta, M., T. Ashikawa, Y. Nozaki, H. Kozuka-Hata, H. Goto, M. Inagaki, M. Oyama, and D. Kitagawa. 2014. Direct interaction of Plk4 with STIL ensures formation of a single procentriole per parental centriole. *Nature communications*. 5:5267.

Paintrand, M., M. Moudjou, H. Delacroix, and M. Bornens. 1992. Centrosome organization and centriole architecture: their sensitivity to divalent cations. *Journal of structural biology*. 108:107-128.

Paoletti, A., M. Moudjou, M. Paintrand, J.L. Salisbury, and M. Bornens. 1996. Most of centrin in animal cells is not centrosome-associated and centrosomal centrin is confined to the distal lumen of centrioles. *Journal of cell science*. 109 (Pt 13):3089-3102.

Park, S.-Y., J.-E. Park, T.-S. Kim, J. Kim, M.-J. Kwak, B. Ku, L. Tian, R.N. Murugan, M. Ahn, S. Komiya, H. Hojo, N.-H. Kim, B. Kim, J.K. Bang, R.L. Erikson, K. Lee, S. Kim, B.-H. Oh, W. Yang, and K.S. Lee. 2014. Molecular basis for unidirectional scaffold switching of human Plk4 in centriole biogenesis. *Nature Structural & Molecular Biology*. 21:696-703.

Paulsen, R.D., D.V. Soni, R. Wollman, A.T. Hahn, M.-C. Yee, A. Guan, J.A. Hesley, S.C. Miller, E.F. Cromwell, D.E. Solow-Cordero, T. Meyer, and K.A. Cimprich. 2009. A Genome-wide siRNA Screen Reveals Diverse Cellular Processes and Pathways that Mediate Genome Stability. *Molecular Cell*. 35:228-239.

Pickart, C.M., and M.J. Eddins. 2004. Ubiquitin: structures, functions, mechanisms. *Biochimica Et Biophysica Acta-Molecular Cell Research*. 1695:55-72.

Pihan, G.A. 2013. Centrosome dysfunction contributes to chromosome instability, chromoanagenesis, and genome reprograming in cancer. *Frontiers in oncology*. 3:277.

Puklowski, Homsi, Keller, May, Chauhan, Kossatz, Grünwald, Kubicka, Pich, Manns, Hoffmann, Gönczy, and Malek. 2011. The SCF-FBXW5 E3-ubiquitin ligase is regulated by PLK4 and targets HsSAS-6 to control centrosome duplication. *Nature cell biology*.

Raducu, M., E. Fung, S. Serres, P. Infante, A. Barberis, R. Fischer, C. Bristow, M.-L.L. Thézénas, C. Finta, J.C. Christianson, F.M. Buffa, B.M. Kessler, N.R. Sibson, L. Marcotullio, R. Toftgård, and V. D'Angiolella. 2016. SCF (Fbxl17) ubiquitylation of Sufu regulates Hedgehog signaling and medulloblastoma development. *The EMBO journal*. 35:1400-1416.

Reyes-Turcu, F.E., K.H. Ventii, and K.D. Wilkinson. 2009. Regulation and cellular roles of ubiquitin-specific deubiquitinating enzymes. *Annual review of biochemistry*. 78:363-397.

Rodrigo-Brenni, M.C., and D.O. Morgan. 2007. Sequential E2s drive polyubiquitin chain assembly on APC targets. *Cell*. 130:127-139.

Rogers, G.C., N.M. Rusan, D.M. Roberts, M. Peifer, and S.L. Rogers. 2009. The SCFSlimb ubiquitin ligase regulates Plk4/Sak levels to block centriole reduplication. *Journal of Cell Biology*. 184:225-239.

Rossi, M., S. Duan, Y.-T.T. Jeong, M. Horn, A. Saraf, L. Florens, M.P. Washburn, A. Antebi, and M. Pagano. 2013. Regulation of the CRL4(Cdt2) ubiquitin ligase and cell-cycle exit by the SCF(Fbxo11) ubiquitin ligase. *Molecular cell*. 49:1159-1166.

Sato, N., K. Mizumoto, M. Nakamura, and M. Tanaka. 2000a. Radiation-induced centrosome overduplication and multiple mitotic spindles in human tumor cells. *Experimental cell research*. 255:321-326.

Sato, N., K. Mizumoto, M. Nakamura, H. Ueno, Y.A. Minamishima, J.L. Farber, and M. Tanaka. 2000b. A possible role for centrosome overduplication in radiation-induced cell death. *Oncogene*. 19:5281-5290.

Sawant, D.B., S. Majumder, J.L. Perkins, C.-H.H. Yang, P.A. Eyers, and H.A. Fisk. 2015. Centrin 3 is an inhibitor of centrosomal Mps1 and antagonizes centrin 2 function. *Molecular biology of the cell*. 26:3741-3753.

Schindelin, J., I. Arganda-Carreras, E. Frise, V. Kaynig, M. Longair, T. Pietzsch, S. Preibisch, C. Rueden, S. Saalfeld, B. Schmid, J.-Y.Y. Tinevez, D.J. White, V. Hartenstein, K. Eliceiri, P. Tomancak, and A. Cardona. 2012. Fiji: an open-source platform for biological-image analysis. *Nature methods*. 9:676-682.

Schnerch, D., and E.A. Nigg. 2016. Structural centrosome aberrations favor proliferation by abrogating microtubule-dependent tissue integrity of breast epithelial mammospheres. *Oncogene*. 35:2711-2722.

Sims, J.J., and R.E. Cohen. 2009. Linkage-specific avidity defines the lysine 63-linked polyubiquitin-binding preference of rap80. *Molecular cell*. 33:775-783.

Sivakumar, S., and G.J. Gorbsky. 2015. Spatiotemporal regulation of the anaphase-promoting complex in mitosis. *Nature reviews. Molecular cell biology*. 16:82-94.

Skaar, J.R., V. D'Angiolella, J.K. Pagan, and M. Pagano. 2009. SnapShot: F Box Proteins II. *Cell*. 137.

Skaar, J.R., J.K. Pagan, and M. Pagano. 2013. Mechanisms and function of substrate recruitment by F-box proteins. *Nature reviews. Molecular cell biology*. 14:369-381.

Skaar, J.R., J.K. Pagan, and M. Pagano. 2014. SCF ubiquitin ligase-targeted therapies. *Nature reviews. Drug discovery*. 13:889-903.

Sonnen, K.F., A.-M.M. Gabryjonczyk, E. Anselm, Y.-D.D. Stierhof, and E.A. Nigg. 2013. Human Cep192 and Cep152 cooperate in Plk4 recruitment and centriole duplication. *Journal of cell science*. 126:3223-3233.

Sonnen, K.F., L. Schermelleh, H. Leonhardt, and E.A. Nigg. 2012. 3D-structured illumination microscopy provides novel insight into architecture of human centrosomes. *Biology open*. 1:965-976.

Soucy, T.A., P.G. Smith, M.A. Milhollen, A.J. Berger, J.M. Gavin, S. Adhikari, J.E. Brownell, K.E. Burke, D.P. Cardin, S. Critchley, C.A. Cullis, A. Doucette, J.J. Garnsey, J.L. Gaulin, R.E. Gershman, A.R. Lublinsky, A. McDonald, H. Mizutani, U. Narayanan, E.J. Olhava, S. Peluso, M. Rezaei, M.D. Sintchak, T. Talreja, M.P. Thomas, T. Traore, S. Vyskocil, G.S. Weatherhead, J. Yu, J. Zhang, L.R. Dick, C.F. Claiborne, M. Rolfe, J.B. Bolen, and S.P. Langston. 2009. An inhibitor of NEDD8-activating enzyme as a new approach to treat cancer. *Nature*. 458:732-736.

Spruck, C., H. Strohmaier, M. Watson, A.P.L. Smith, A. Ryan, W. Krek, and S.I. Reed. 2001. A CDK-independent function of mammalian Cks1: Targeting of SCFSkp2 to the CDK inhibitor p27(Kip1). *Molecular Cell*. 7:639-650.

Strnad, P., S. Leidel, T. Vinogradova, U. Euteneuer, A. Khodjakov, and P. Gönczy. 2007. Regulated HsSAS-6 levels ensure formation of a single procentriole per centriole during the centrosome duplication cycle. *Developmental cell*. 13:203-213.

Strohmaier, H., C.H. Spruck, P. Kaiser, K.A. Won, O. Sangfelt, and S.I. Reed. 2001. Human F-box protein hCdc4 targets cyclin E for proteolysis and is mutated in a breast cancer cell line. *Nature*. 413:316-322.

Sydor, A.M., K.J. Czymmek, E.M. Puchner, and V. Mennella. 2015. Super-Resolution Microscopy: From Single Molecules to Supramolecular Assemblies. *Trends in cell biology*. 25:730-748.

Tan, M.-K.K., H.-J.J. Lim, E.J. Bennett, Y. Shi, and J.W. Harper. 2013. Parallel SCF adaptor capture proteomics reveals a role for SCFFBXL17 in NRF2 activation via BACH1 repressor turnover. *Molecular cell*. 52:9-24.

Tang, C.-J.C.J., R.-H.H. Fu, K.-S.S. Wu, W.-B.B. Hsu, and T.K. Tang. 2009. CPAP is a cell-cycle regulated protein that controls centriole length. *Nature cell biology*. 11:825-831.

Tang, C.-J.C.J., S.-Y.Y. Lin, W.-B.B. Hsu, Y.-N.N. Lin, C.-T.T. Wu, Y.-C.C. Lin, C.-W.W. Chang, K.-S.S. Wu, and T.K. Tang. 2011. The human microcephaly protein STIL interacts with CPAP and is required for procentriole formation. *The EMBO journal*. 30:4790-4804.

Tenno, T., K. Fujiwara, H. Tochio, K. Iwai, E.H. Morita, H. Hayashi, S. Murata, H. Hiroaki, M. Sato, K. Tanaka, and M. Shirakawa. 2004. Structural basis for distinct roles of Lys63- and Lys48-linked polyubiquitin chains. *Genes to cells : devoted to molecular & cellular mechanisms*. 9:865-875.

Tsou, and Stearns. 2006. Mechanism limiting centrosome duplication to once per cell cycle. *Nature*.

Tsou, M.-F.B.F., W.-J.J. Wang, K.A. George, K. Uryu, T. Stearns, and P.V. Jallepalli. 2009. Polo kinase and separase regulate the mitotic licensing of centriole duplication in human cells. *Developmental cell*. 17:344-354.

Urano, T., T. Saito, T. Tsukui, M. Fujita, T. Hosoi, M. Muramatsu, Y. Ouchi, and S. Inoue. 2002. Efp targets 14-3-3 for proteolysis and promotes breast tumour growth. *Nature*. 417:871-875.

van Breugel, M., M. Hirono, A. Andreeva, H.-a.A. Yanagisawa, S. Yamaguchi, Y. Nakazawa, N. Morgner, M. Petrovich, I.-O.O. Ebong, C.V. Robinson, C.M. Johnson, D. Veprintsev, and B. Zuber. 2011. Structures of SAS-6 suggest its organization in centrioles. *Science (New York, N.Y.)*. 331:1196-1199.

Vulprecht, J., A. David, A. Tibelius, A. Castiel, G. Konotop, F. Liu, F. Bestvater, M.S. Raab, H. Zentgraf, S. Izraeli, and A. Krämer. 2012. STIL is required for centriole duplication in human cells. *Journal of cell science*. 125:1353-1362.

Wang, L., X. Ye, Y. Liu, W. Wei, and Z. Wang. 2014. Aberrant regulation of FBW7 in cancer. *Oncotarget*. 5:2000-2015.

Welcker, M., and B.E. Clurman. 2008. FBW7 ubiquitin ligase: a tumour suppressor at the crossroads of cell division, growth and differentiation. *Nature reviews. Cancer*. 8:83-93.

Wiborg, O., M.S. Pedersen, A. Wind, L.E. Berglund, K.A. Marcker, and J. Vuust. 1985. The human ubiquitin multigene family: some genes contain multiple directly repeated ubiquitin coding sequences. *The EMBO journal*. 4:755-759.

Wilkinson, K.D., M.K. Urban, and A.L. Haas. 1980. Ubiquitin is the ATP-dependent proteolysis factor I of rabbit reticulocytes. *The Journal of biological chemistry*. 255:7529-7532.

Winey, M., and E. O'Toole. 2014. Centriole structure. *Philosophical transactions of the Royal Society of London. Series B, Biological sciences*. 369.

Winston, J.T., D.M. Koepp, C. Zhu, S.J. Elledge, and J.W. Harper. 1999. A family of mammalian F-box proteins. *Current biology : CB*. 9:1180-1182.

Wloga, D., and J. Gaertig. 2010. Post-translational modifications of microtubules. *Journal of cell science*. 123:3447-3455.

Wong, Y.L., J.V. Anzola, R.L. Davis, M. Yoon, A. Motamedi, A. Kroll, C.P. Seo, J.E. Hsia, S.K. Kim, J.W. Mitchell, B.J. Mitchell, A. Desai, T.C. Gahman, A.K. Shiau, and K. Oegema. 2015. Cell biology. Reversible centriole depletion with an inhibitor of Polo-like kinase 4. *Science (New York, N.Y.)*. 348:1155-1160.

Wu, G., G. Xu, B.A. Schulman, P.D. Jeffrey, J.W. Harper, and N.P. Pavletich. 2003. Structure of a beta-TrCP1-Skp1-beta-catenin complex: destruction motif binding and lysine specificity of the SCF(beta-TrCP1) ubiquitin ligase. *Molecular cell*. 11:1445-1456.

Yang, C.H., C. Kasbek, and S. Majumder. 2010. Mps1 phosphorylation sites regulate the function of centrin 2 in centriole assembly. *Molecular biology of ….*

Yao, T., and R.E. Cohen. 2002. A cryptic protease couples deubiquitination and degradation by the proteasome. *Nature*.

Ye, Y., and M. Rape. 2009. Building ubiquitin chains: E2 enzymes at work. *Nature reviews Molecular cell biology*. 10:755-764.

Yu, Z.K., J.L. Gervais, and H. Zhang. 1998. Human CUL-1 associates with the SKP1/SKP2 complex and regulates p21(CIP1/WAF1) and cyclin D proteins. *Proceedings of the National Academy of Sciences of the United States of America*. 95:11324-11329.

Yuan, J., K. Luo, L. Zhang, J.C. Cheville, and Z. Lou. 2010. USP10 regulates p53 localization and stability by deubiquitinating p53. *Cell*. 140:384-396.

Zhou, M.-j.J., F.-z.Z. Chen, and H.-c.C. Chen. 2014. Ubiquitination involved enzymes and cancer. *Medical oncology (Northwood, London, England)*. 31:93.

Zhu, F., S. Lawo, A. Bird, D. Pinchev, A. Ralph, C. Richter, T. Müller-Reichert, R. Kittler, A.A. Hyman, and L. Pelletier. 2008. The mammalian SPD-2 ortholog Cep192 regulates centrosome biogenesis. *Current biology : CB*. 18:136-141.

Appendix

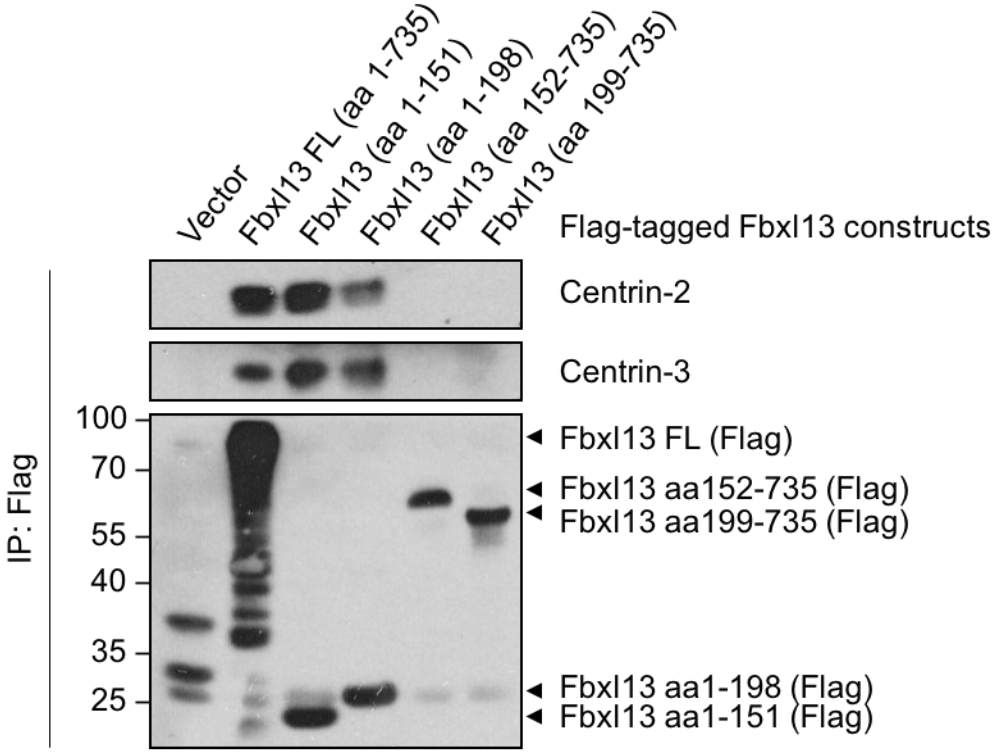

Appendix 1 Centrin-2 and Centrin-3 bind to the N terminal of FbxI13

Detection of Centrin-2 and Centrin-3 after immunoprecipitation of the indicated Flag-tagged FbxI13 truncation mutants in HEK293T cells. Full length FbxI13 (FL) and the N terminal of FbxI13 were able to bind Centrin-2 and Centrin-3 (aa1-151 and aa1-198). FbxI13 aa152-198 is the F-box region. An empty vector (Vector) was used as a negative control. HEK293T cells were treated with MLN4924 (2 μM) for 5 hours prior to collection. N=2 biological replicates.

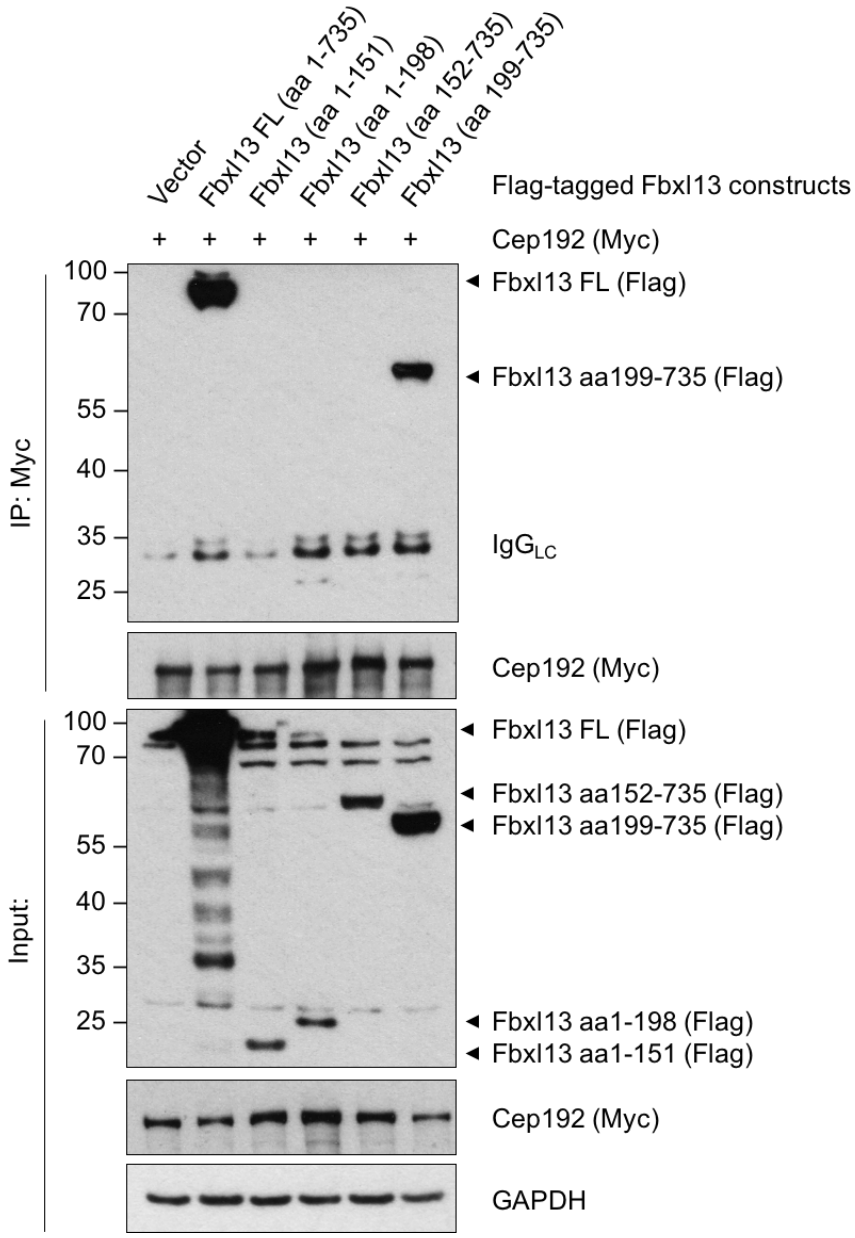

Appendix 2 Cep192 binds to the C terminal region of FbxI13

Detection of FbxI13 truncation mutants after immunoprecipitation of Cep192 (Myc) in HEK293T cells. Cep192 was able to pull down full length FbxI13 (FL) and the C terminal of FbxI13 lacking the F-box region (aa199-735). FbxI13 aa152-198 is the F-box region. An empty vector (Vector) was used as a negative control. HEK293T cells were treated with MLN4924 (2 μM) for 5 hours prior to collection. N=2 biological replicates.

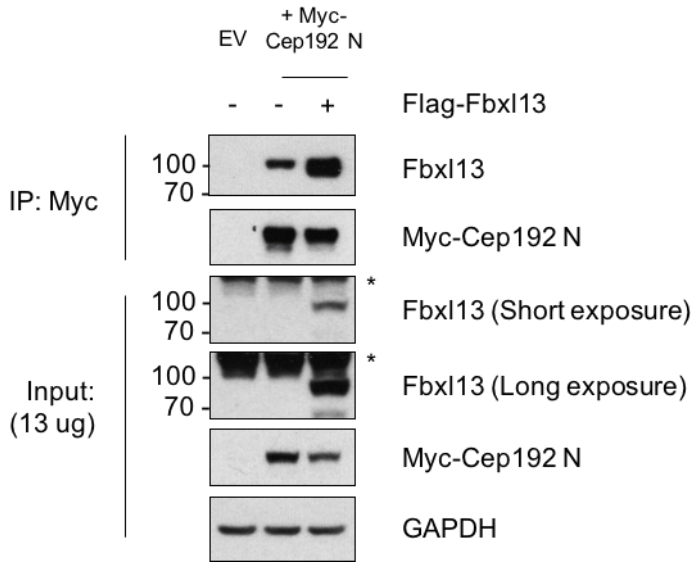

Appendix 3 Exogenous Cep192 binds endogenous Fbxl13

Detection of endogenous and Flag-tagged Fbxl13 after immunoprecipitation of Myc-tagged Cep192 in U2OS cells. An empty vector (EV) was used as a negative control. U2OS cells were treated with MLN4924 (2 μM) for 5 hours prior to collection. N=1 biological replicate.

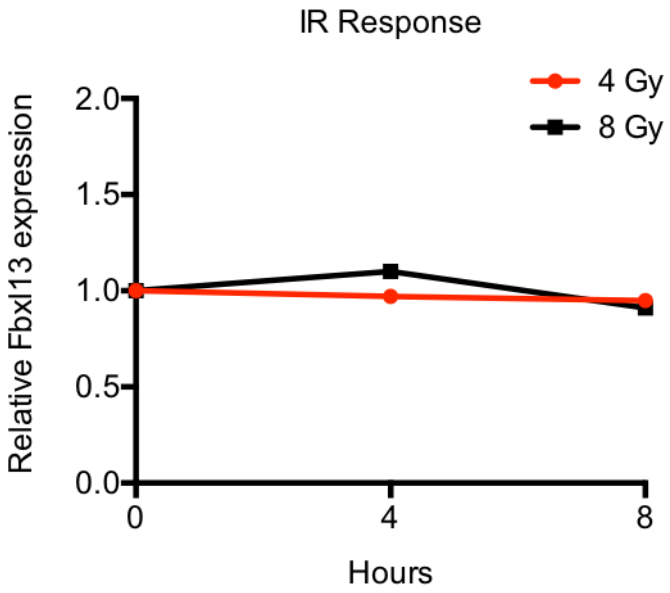

Appendix 4 Fbxl13 mRNA expression following irradiation

Fbxl13 mRNA expression levels were measured using quantitative real-time PCR (qPCR) following 4 Gy and 8 Gy irradiation (IR) at the given time points. N=1 biological replicate.

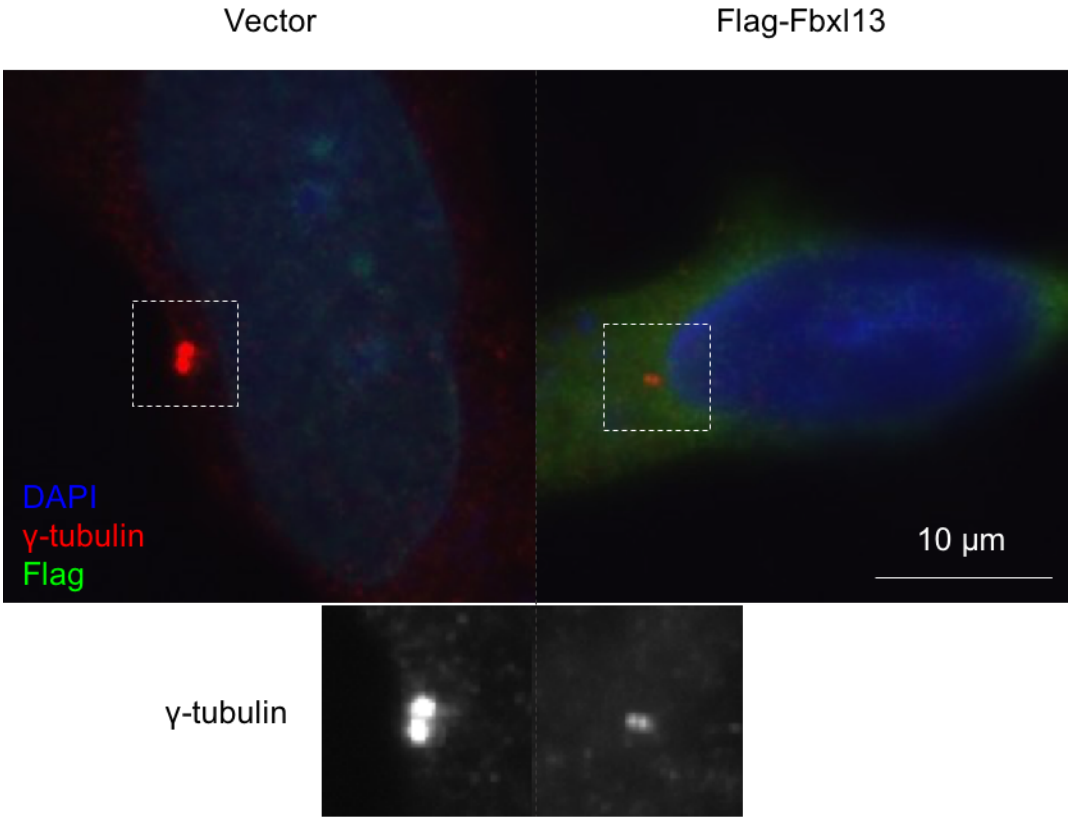

Appendix 5 Flag-Fbxl13 overexpression reduces γ-tubulin intensity in U2OS cells

U2OS cells transiently overexpressing Flag-Fbxl13 or an empty vector control were fixed and stained for DNA (blue), γ-tubulin (red), and Flag (green). In this experiment, cells had also been treated with 4 mM hydroxyurea for 72 hours to measure centrosome overduplication. Scale bar, 10 μm.

		Presence under different treatment samples in Tan et al. screen 2 = present in two replicates 1 = present in one replicate 0 = absent		
Accession	Description	Untreated	MLN4924	Bortezomib
Q8NEE6	F-box/LRR-repeat protein 13	2	2	2
P41208	Centrin-2	2	2	2
O15182	Centrin-3	2	2	2
E9PAV3	Nascent polypeptide-associated complex subunit alpha, muscle-specific form	1	1	1
Q9HBW1	Leucine-rich repeat-containing protein 4	1	1	1

Appendix 6 Intersection of LC-MS/MS data for Fbxl13 Isoform 1 with published data

Intersection of our LC-MS/MS data for Fbxl13 isoform 1 (Fbxl13-1) with published data by Tan et al. (2013). The presence of our interactors in the data of Tan et al. is indicated by 1 or 2 as the number of replicates the protein is present in. The three columns represent three published treatments: untreated, MLN4924, and Bortezomib.

Accession	Description	Presence under different treatment samples in Tan et al. screen 2 = present in two replicates 1 = present in one replicate 0 = absent Untreated	MLN4924	Bortezomib
Q8NEE6	F-box/LRR-repeat protein 13	2	2	2
P41208	Centrin-2	2	2	2
O15182	Centrin-3	2	2	2
Q9H078	Caseinolytic peptidase B protein homolog	0	0	2

Appendix 7 Intersection of LC-MS/MS data for Fbxl13 Isoform 3 with published data

Intersection of our LC-MS/MS data for Fbxl13 isoform 1 (Fbxl13-1) with published data by Tan et al. (2013). The presence of our interactors in the data of Tan et al. is indicated by 1 or 2 as the number of replicates the protein is present in. The three columns represent three published treatments: untreated, MLN4924, and Bortezomib.

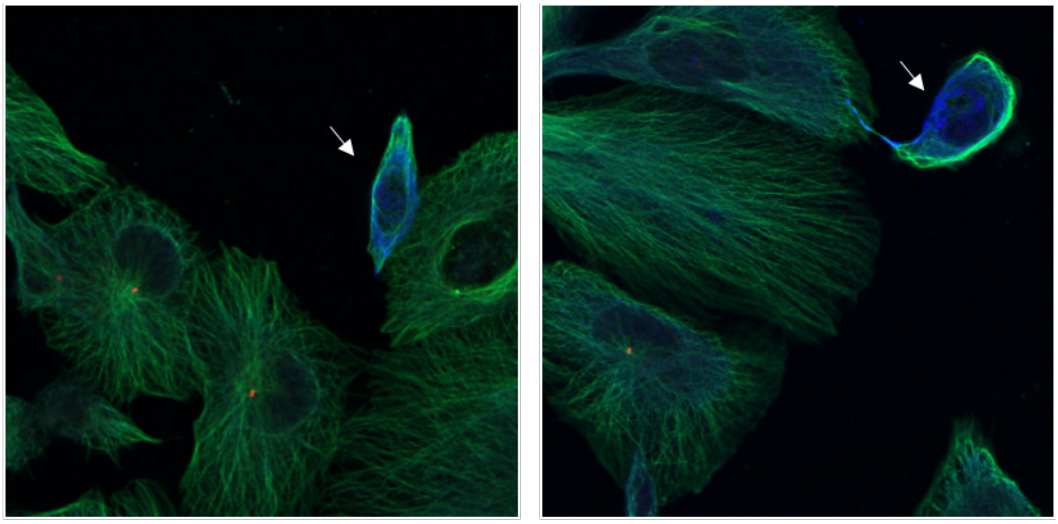

Appendix 8 U2OS cells overexpressing Fbxl13 show strong morphological phenotypes

U2OS cells overexpressing Flag-Fbxl13 were fixed and stained for microtubules (α-tubulin, green), Cep192 (red), and Fbxl13 (Flag, blue). Flag-Fbxl13 positive cells are indicated with a white arrow. Confocal images were acquired by Dr Hongbin Yang.

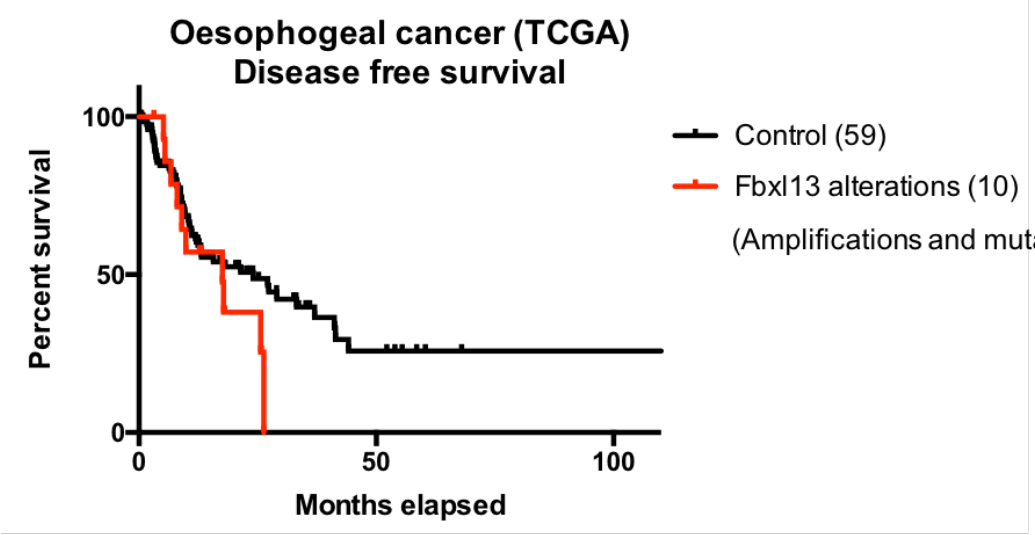

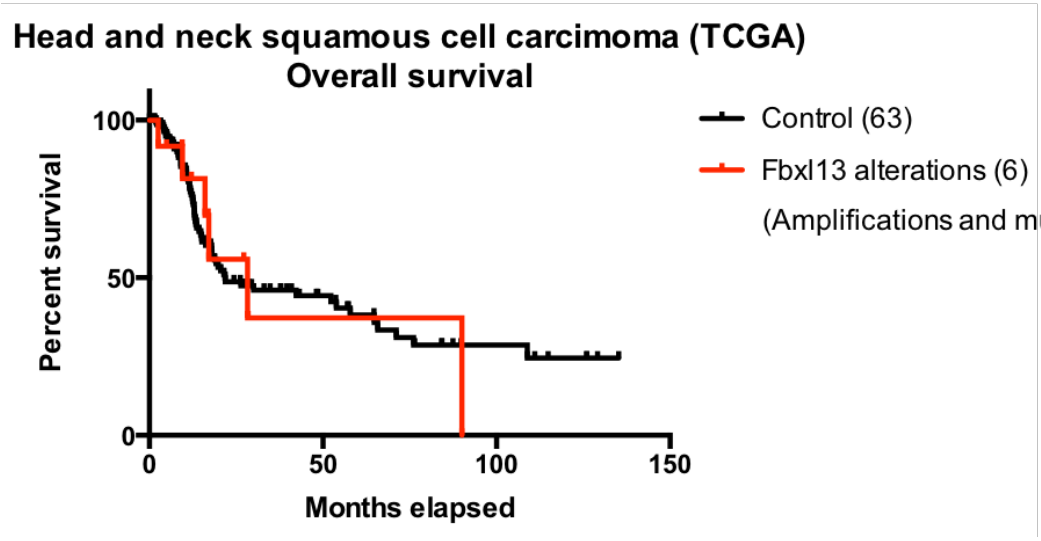

Appendix 9 TCGA Cancer patient prognosis data

Patient survival data in two cohorts, stratified by Fbxl13 amplifications and mutations versus wild-type. The number of patients in each group is indicated in the legend. In both cases, the cohorts are too small to reach statistical significance. Figure adapted from TCGA (TCGA Research Network, http://cancergenome.nih.gov/).

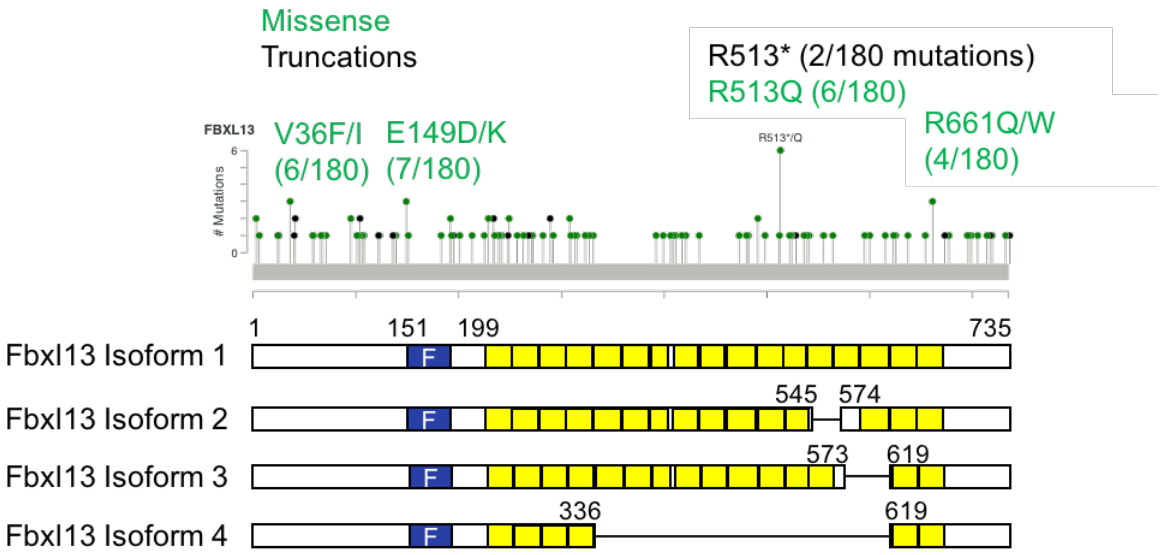

Appendix 10 Cancer patient mutations in Fbxl13

Patient mutations in Fbxl13. Figure adapted from TCGA (TCGA Research Network, http://cancergenome.nih.gov/).